

## A study on fully inkjet-printed chemiresistive gas sensor matrix

葛, 靈普

<https://hdl.handle.net/2324/5068236>

---

出版情報 : 九州大学, 2022, 博士 (工学), 課程博士  
バージョン :  
権利関係 :

**A study on fully inkjet-printed  
chemiresistive gas sensor matrix**

全印刷化学抵抗性ガスセンサマトリクスに  
関する研究

**Lingpu Ge**

Graduate School of Information Science and Electrical  
Engineering Kyushu University

June 2022

# Contents

|   |    |
|---|----|
| <b>Chapter 1 Introduction</b> .....   | 1  |
| 1.1 Application of gas detection .....  | 1  |
| 1.2 Gas detection methods.....  | 2  |
| 1.2.1 Semiconductor gas sensor.....   | 2  |
| 1.2.2 Electrochemical gas sensor .....  | 3  |
| 1.2.3 QCM gas sensor .....  | 4  |
| 1.2.4 Gas chromatography .....  | 5  |
| 1.2.5 E-nose.....   | 6  |
| 1.3 Sensing film fabrication methods.....   | 8  |
| 1.3.1 Drop casting.....   | 8  |
| 1.3.2 Spin coating.....   | 9  |
| 1.3.3 Screen printing.....  | 9  |
| 1.3.4 Inkjet printing.....  | 10 |
| 1.4 Inkjet printers and flexible substrates .....   | 11 |
| 1.4.1 DMP-2850.....   | 11 |
| 1.4.2 EPSON L310 and EPSON PX-105.....  | 11 |
| 1.4.3 PET film .....  | 13 |
| 1.4.4 Photo paper .....   | 14 |
| 1.5 Aim and novelty in this research.....   | 16 |
| 1.6 Thesis outline .....  | 16 |
| Reference.....  | 18 |
| <b>Chapter 2 A fully inkjet-printed gas sensor array with conductive polymer composites</b> ..... | 23 |
| 2.1 Introduction.....   | 23 |
| 2.2 Experimental .....  | 24 |
| 2.2.1 Fabrication of interdigitated electrode .....   | 24 |
| 2.2.2 Parameters of nozzles and droplet of inkjet printer .....                                   | 26 |
| 2.2.3 Fabrication of CB ink .....   | 28 |
| 2.2.3 Sensor measurement system .....   | 29 |
| 2.3 Results and discussion .....  | 31 |
| 2.3.1 Comparison of gas responses of different polymers.....                                      | 31 |
| 2.3.2 Characteristic comparison of sensors produced in different ways....                         | 35 |
| 2.3.3 Effects of different salts on sensor performance 1 .....                                    | 37 |

|   |    |
|---|----|
| 2.3.4 Effects of different salts on sensor performance 2 .....  | 38 |
| 2.4 Conclusion .....  | 40 |
| Reference.....  | 41 |
| <b>Chapter 3 Chemiresistor sensor matrix prepared by full-printing processes</b><br>.....                   | 42 |
| 3.1 Introduction.....   | 42 |
| 3.2 Materials and methods .....   | 44 |
| 3.2.1 Sensor matrix with multilayer structure .....   | 44 |
| 3.2.2 Materials and inkjet printer specifications .....   | 44 |
| 3.2.3 Fabrication of PEG-CB ink .....   | 45 |
| 3.2.4 Fabrication of the inkjet-printed sensor matrix .....   | 46 |
| 3.2.5 Sensor measurement system .....   | 47 |
| 3.3 Results and discussion .....  | 49 |
| 3.3.1 Method of dispersing CB in water .....  | 49 |
| 3.3.2 Measurement of the CB concentration .....   | 51 |
| 3.3.3 Morphology characterization of the insulating layer .....   | 54 |
| 3.3.4 The principle of PEG-CB layer responding to gas .....   | 55 |
| 3.3.5 Comparison of resistance stability of sensors produced in different<br>ways.....                      | 56 |
| 3.3.6 Characteristic comparison of sensors produced in different ways....                                   | 57 |
| 3.3.7 Comparison of different gas responses.....  | 59 |
| 3.4 Conclusion .....  | 60 |
| Reference.....  | 60 |
| <b>Chapter 4 Sensor matrix printed molecularly imprinted materials for<br/>organic acid detection</b> ..... | 63 |
| 4.1 Introduction .....  | 63 |
| 4.2 Materials and methods .....   | 65 |
| 4.2.1 Materials .....   | 65 |
| 4.2.2 Inkjet printer specifications .....   | 65 |
| 4.2.3 Prepatation of functional ink .....   | 66 |
| 4.2.4 Ink characterization .....  | 66 |
| 4.2.5 Optical microscopy and scanning electron microscopy (SEM) .....                                       | 67 |
| 4.2.6 Measurement system fabrication.....   | 67 |
| 4.2.7 Sensor matrix fabrication .....   | 69 |
| 4.2.8 Preparation of I&C layer by inkjet.....   | 70 |
| 4.3 Results and discussion .....  | 72 |

|  |           |
|--|-----------|
| 4.3.1 Morphology and performance analysis of I&C layer .....           | 72        |
| 4.3.2 The selectivity of MIP films to the template molecules .....     | 74        |
| 4.3.3 Gas-sensing performance of sensor matrix.....                    | 75        |
| 4.3.4 Response characteristics of sensor unit coated with PA-MIP ..... | 78        |
| 4.3.5 Mechanical stability of MIP-based sensor matrix .....            | 79        |
| 4.4 Conclusion .....   | 81        |
| Reference.....   | 81        |
| <b>Chapter 5 Conclusion.....</b>                                       | <b>85</b> |
| 5.1 Conclusion .....   | 85        |
| 5.2 Prospect.....  | 85        |
| 5.2.1 Smart mask and human activity monitoring.....                    | 85        |
| 5.2.2 Fabrication of multilayer sensor with heating electrode .....    | 90        |
| 5.2.3 Electronic nose based on sensor matrix .....                     | 91        |
| Reference.....   | 93        |
| <b>Acknowledgements.....</b>   | <b>94</b> |

## Figures list

|  |    |
|--|----|
| Fig.1.1 The structure of metal oxide semiconductor sensor.....   | 3  |
| Fig.1.2 The schematic graph of electrochemical gas sensor. ....  | 4  |
| Fig.1.3 The basic structure of QCM sensor.....   | 5  |
| Fig.1.4 Schematic diagram of gas chromatography. ....  | 6  |
| Fig.1.5 E-nose system. ....  | 7  |
| Fig.1.6 Schematic diagram of the drop casting process.....   | 8  |
| Fig.1.7 The main stages of spin coating. ....  | 9  |
| Fig.1.8 The screen-printing process. ....  | 10 |
| Fig.1.9 Schematic diagram of the inkjet printing system. ....  | 10 |
| Fig.1.10 Product of DMP-2850 and some main components.....   | 11 |
| Fig.1.11 Pictures of the internal structure and parts of EPSON L310. ....  | 12 |
| Fig.1.12 Pictures of the internal structure and parts of EPSON PX-105. ....  | 13 |
| Fig.1.13 Schematic diagram of the structure and ink-fixing process of swellable photo paper. ....                  | 14 |
| Fig.1.14 Schematic diagram of the structure and ink-fixing process of cast coating photo paper. ....               | 15 |
| Fig.1.15 Schematic diagram of the structure and ink-fixing process of micro-porous photo paper.....                | 15 |
| Fig.2.1 Schematic diagram of the formation process of the coffee ring. ....  | 23 |
| Fig.2.2 Common interdigital electrode shapes.....  | 24 |
| Fig.2.3 Structural parameters of IDEs. ....  | 24 |
| Fig.2.4 Design drawing and physical drawing of a single sensor. ....   | 25 |
| Fig.2.5 Design drawing and physical drawing of a sensor array. ....  | 25 |
| Fig.2.6 Overall view and partial microscope view of the nozzle of a home printer. ....                             | 26 |
| Fig.2.7 a. Micrograph after printing with black pigment ink. b. Micrograph after printing with silver ink. ....    | 27 |
| Fig.2.8 The dispersion effect of CB in different solvents.....   | 28 |
| Fig.2.9 A sample filter system was used to filter the CB ink. ....   | 29 |
| Fig.2.10 Photograph of the experiment setup.....   | 30 |
| Fig.2.11 Configuration of the experimental sensing apparatus and block diagram of the electrical measurement. .... | 30 |
| Fig.2.12 Three methods of fabricating sensor films.....  | 35 |
| Fig.2.13 The CB layer 50 um micrograph (A) made by inkjet printer and the CB                                       |    |

|  |    |
|--|----|
| layer 50 $\mu\text{m}$ micrograph by micropipette (B). .....   | 35 |
| Fig.2.14 Transient response of the sensors to acetic acid gas made by inkjet printer and the sensors made by micropipette.....   | 36 |
| Fig.2.15 Transient response of the sensors to ethanol gas made by inkjet printer and the sensors made by micropipette. ....  | 36 |
| Fig.3.1 Three views of one unit of a multilayer sensor matrix. ....  | 44 |
| Fig.3.2 Fabrication process of the gas sensor matrix. ....   | 46 |
| Fig.3.3 (A) Thirty gas sensor matrices printed with a home printer. (B) A sensor matrix containing 36 interdigitated electrodes that can be used to produce gas sensors. (C) Electrode dimensions. (D) An example of a PEG–CB composite printed sensor for reference. .... | 47 |
| Fig.3.4 (A) Configuration of the experimental sensing apparatus and block diagram of the electrical measurement. (B) Photograph of the experiment setup.....   | 48 |
| Fig.3.5 Principle of surfactant SDS dispersion of CB.....  | 49 |
| Fig.3.6 Micrographs of the PEG–CB layers (100 $\mu\text{m}$ scale) produced with an inkjet printer. ....   | 50 |
| Fig.3.7 Micrographs of the PEG–CB layers (100 $\mu\text{m}$ scale) produced with a micropipette. ....  | 50 |
| Fig.3.8 Relationship between the concentration of the CB solution and the absorbance. ....   | 51 |
| Fig.3.9 Relationship between the resistance and the CB concentration. ....   | 53 |
| Fig.3.10 Relationship between the resistance and the number of printing passes. ....   | 53 |
| Fig.3.11 (A)–(C) Schematic diagrams of the insulation layer. Micrographs of the pattern after the color pigment ink was printed (D) one and (E) three times. (F) SEM image of the silver electrode on the insulation layer.....  | 54 |
| Fig.3.12 The gas response principle. ....  | 56 |
| Fig.3.13 Resistance average and standard deviation of different sensor matrices. ....  | 56 |
| Fig.3.14 Transient response to ethanol gas of sensors produced with an inkjet printer and a micropipette. ....   | 57 |
| Fig.3.15 The response and recovery time to ethanol gas of sensors produced with an inkjet printer and a micropipette. ....   | 58 |
| Fig.3.16 Schematic of percolation effect in CB/polymer composites. ....  | 59 |
| Fig.3.17 Transient responses of the PEG–CB film to different gases. ....   | 59 |

|  |    |
|--|----|
| Fig. 4.1 Schematic diagram of the sensor matrix measurement system. ....   | 68 |
| Fig. 4.2 Printed electrode matrix and sensor matrix. a Schematic of the printed sensor matrix fabrication process. b Photograph of completed sensor matrix. c Schematic of the silver interdigital electrode with the pitch (P), gap (G) and width (W) parameters. d Microscope image of G=230 $\mu\text{m}$ silver interdigital electrodes. e Microscope image of G=180 $\mu\text{m}$ silver interdigital electrodes and interdigital gap showing evidence of silver ink micro-splashing (scale bar= 100 $\mu\text{m}$ ). ....  | 70 |
| Fig.4.3 Microstructure analysis of I&C layer. a Film formation from acrylic dispersions. b Principle of ink absorption on the polymer-type coating layer. c Cross-sectional scanning electron microscopy (SEM) images of the photographic paper and the I&C layer. Scale bars are 90 $\mu\text{m}$ (left panels) and 30 $\mu\text{m}$ (right panels). ....   | 71 |
| Fig.4.4 Insulation and ink fixing functions of I&C layer. a SEM images of top (column) silver electrode printing effects, a without adding other polymers, b with addition of polyethylene glycol (PEG), and c with addition of M-30 polymer to the insulating ink. d Change of resistance between row and column electrodes versus the number of times I&C layers are printed using insulating ink with added M-30. e Comparison of resistance values of top silver electrodes printed on three insulating layer types. f Comparison of resistance values of bottom (row) and top (column) silver electrodes of sensor matrix with I&C layers made from insulating ink with added M-30. Scale bars are 30 $\mu\text{m}$ for a-c. .... | 73 |
| Fig.4.5 a GC-MS result of the 4 kinds of MIPs exposed to PA vapors at 100 ppm. b SPME-GC-MS result of the 4 kinds of MIPs exposed to 4 kinds of fatty acid vapors (PA/HA/OA/HPA) at 100 ppm. ....  | 75 |
| Fig.4.6 Uniformity and selective performance of gas sensor matrix. a Resistance average and standard deviation of different sensor matrices. b Micrographs of the CB layer (50 $\mu\text{m}$ scale) produced with an inkjet printer and a micropipette. c The relationship between CB printing times and the average value of sensor matrix resistance and the response to PA at 6 ppm level. d Changes in PA sensing response with the number of PA-MIP layers. e Real-time responses of sensor unit coated with PA-MIP, HA-MIP, HPa-MIP, OA-MIP and NIP to PA vapor at 6 ppm level. f Sensitivity of MIP sensor matrix to same concentrations of PA, HA, HPa and OA vapor. ....  | 77 |
| Fig.4.7 Response characteristics of sensor unit coated with PA-MIP. a Real-time  |    |

|   |    |
|---|----|
| sensing response of sensor unit coated with PA-MIP upon PA exposure with concentrations ranging from 3 to 48 ppm. b Cycling performance of sensor unit coated with PA-MIP in response to PA at 3 ppm level. c Response and recovery times calculated for 3 ppm of PA. d Long-term stability of response over a month under 3 ppm of propionic acid for sensor unit coated with PA-MIP. .... | 79 |
| Fig.4.8 Characterization of the sensor matrix under bending tests. a Photograph of a flexible sensor matrix. b Changes in resistance as a function of bending cycles. ....  | 80 |
| Fig.5.1 A comparison is about sensor, sensor array, and sensor matrix.....  | 85 |
| Fig.5.2 The schematic of the smart mask. ....   | 86 |
| Fig.5.3 The schematic of the measurement circuitry. ....  | 87 |
| Fig.5.4 The process of data transfer.....   | 88 |
| Fig.5.5 Sensor array printing and PCB fabrication. ....   | 89 |
| Fig.5.6 The response of CO <sub>2</sub> , Temperature, and Relative Humidity includes three human activity states which use the green, grey and yellow blocks to show.....  | 89 |
| Fig.5.7 The response of the VOCs gas sensor includes three human activity states which use the green, grey, and yellow blocks to show.....  | 90 |
| Fig.5.8 Three views of the sensor with heater.....  | 91 |
| Fig.5.9 Schematic representation of the sensor matrix coated with different sensing materials and schematic diagram of the realization method of 3D gas sensor. ....  | 92 |

## Tables list

|   |    |
|---|----|
| Table.2.1 Comparison of parameters of three printers .....    | 26 |
| Table.2.2 Sensor's responses to acetic acid and ethanol ..... | 31 |
| Table.2.3 Sensor's responses to acetic acid and ethanol ..... | 33 |
| Table.2.4 Sensor's responses to acetic acid. ....             | 34 |
| Table.2.5 Sensor's responses to acetic acid and ethanol. .... | 37 |
| Table.2.6 Sensor's responses to acetic acid and ethanol. .... | 39 |
| Table.4.1 Properties of functional inks at 28°C.....          | 67 |

## Symbols and abbreviations list

|                |                                       |
|----------------|---------------------------------------|
| CB             | carbon black                          |
| DAQ            | Data acquisition                      |
| DNPH           | 2,4-Dinitrophenylhydrazine            |
| E-nose         | Electronic-nose                       |
| EC             | Ethyl cellulose                       |
| EG             | Ethylene glycol                       |
| IDEs           | Interdigitated electrodes             |
| I&C layer      | Insulating & Coating layer            |
| GC/MC          | Gas chromatography/mass spectrometer  |
| GLC            | Glycerol                              |
| HA             | Hexanoic acid                         |
| HpA            | Heptanoic acid                        |
| LCR meter      | Inductance-capacitor-resistance meter |
| LSPR           | Localized surface plasmon resonance   |
| MC             | Methyl cellulose                      |
| MIP            | Molecular imprinted polymer           |
| MFC            | Mass flow controller                  |
| MFFT           | Minimum film-forming temperature      |
| NIP            | Non-imprinted polymer                 |
| NMP            | N-Methyl-2-pyrrolidone                |
| OA             | Octanoic acid                         |
| PA             | Propanoic acid                        |
| PAA            | Polyacrylic acid                      |
| PEG            | Polyethylene glycol                   |
| PVA            | Polyvinyl alcohol                     |
| PVP            | Polyvinyl pyrrolidone                 |
| QCM            | Quartz crystal microbalance           |
| SEM            | Scanning electron microscopy          |
| SDS            | Sodium dodecyl sulfate                |
| TEG            | Triethylene glycol                    |
| T <sub>g</sub> | Glass transition temperature          |
| UV             | Ultraviolet                           |
| VOC            | Volatile organic compound             |

# Chapter 1 Introduction

## 1.1 Application of gas detection

The application of gas sensors has a long history<sup>1</sup>. Due to environmental concerns, gas sensors are becoming more and more widely used worldwide<sup>2</sup>. In petroleum<sup>3</sup>, chemical<sup>4</sup>, medical<sup>5</sup>, transportation, home security and other fields, gas sensors are often used to detect the presence of flammable and toxic gases and their corresponding concentrations<sup>6-8</sup>.

In many industrial production, toxic and harmful gases are often emitted, such as fluoride, chlorine, nitrogen oxides, mercury vapor and so on<sup>9</sup>. These gases are very harmful to people and may lead to chronic poisoning or pathological changes in some tissues of the body. Combustible gases such as carbon monoxide, methane, ethane and ethylene will also be produced in industrial production. When these gases are discharged into the atmosphere, they will not only waste energy, but also cause environmental pollution. There will be a lot of gas in the process of coal mining. The main component of the gas is alkane, in which methane accounts for the vast majority, and a small amount of ethane, propane and butane. The gas is flammable and explosive, which poses a serious threat to the safety of mining production. If it cannot be detected and ventilated in time, it will bring serious consequences. In addition, sulfur-containing gases are discharged from the process of refining oil, coking coal and non-ferrous metal refining, which will be discharged into the atmosphere to form acid rain. If these gases are detected in time and treated accordingly, environmental pollution, explosion, poisoning and other dangerous events can be prevented. This shows the important role of gas sensors in industrial production.

With the market competition and economic growth, agriculture in all countries is developing towards intelligence. Agricultural Internet of things is a new industry and an important means to realize intelligent control and scientific management of production and operation process<sup>10</sup>. Gas sensors play an important role in the Agricultural Internet of things<sup>11</sup>. Plants consume CO<sub>2</sub> in photosynthesis, so CO<sub>2</sub> concentration will have a very significant impact on plant growth and development. Many studies have shown that the increase of CO<sub>2</sub> concentration can promote the growth of vegetables, fruits and crops<sup>12</sup>. This is mainly because the increase of CO<sub>2</sub> concentration contributes to the increase of carbon assimilation rate and photosynthetic rate of plants. However, for livestock farms, too high CO<sub>2</sub>

concentration will make the oxygen content relatively insufficient, which has a very negative impact on livestock<sup>13</sup>. Due to the decomposition of animal feces, urine and feed, NH<sub>3</sub>, H<sub>2</sub>S and other toxic gases will be produced in the livestock farms, which are very harmful to livestock<sup>14</sup>. Therefore, the monitoring and analysis of CO<sub>2</sub> in the greenhouse and CO<sub>2</sub>, NH<sub>3</sub>, H<sub>2</sub>S and other gases in the livestock farm will be of great help to the realization of precision agriculture and smart agriculture.

Volatile organic compounds (VOCs), also known as solvents, are chemicals that evaporate easily at room temperature<sup>15</sup>. There are many sources of VOCs, such as industrial emissions, decoration materials, tobacco smoke, dry-cleaned clothing, moth repellents and air fresheners and breathing in animals<sup>16-19</sup>. Most VOCs have unpleasant special odor, toxicity, irritation, teratogenicity and carcinogenicity<sup>20</sup>. Therefore, the monitoring and early warning of VOCs in different environments has become a hot spot of research and development<sup>21,22</sup>. Humans also emit VOCs such as methanol, ethanol, ethers, acids and other VOCs during the process of exhalation<sup>23</sup>. These exhaled gas components can reflect a person's physiological state. At present, disease diagnosis by monitoring VOCs components in patients' breathing gas has attracted more and more attention as a non-invasive diagnostic technology<sup>24</sup>. Gas detection also has a wide range of applications in health and medical care.

## **1.2 Gas detection methods**

### **1.2.1 Semiconductor gas sensor**

Semiconductor gas sensors can be divided into resistive and non-resistive types. The principle of resistive gas sensor is that gas molecules cause changes in the resistance of sensitive materials. The resistance value will vary according to the concentration and type of gas being measured. Some metal oxides (SnO<sub>2</sub>, ZnO, Fe<sub>2</sub>O<sub>3</sub><sup>25</sup>, MgO<sup>26</sup>, NiO<sup>27</sup>, TiO<sub>2</sub><sup>28</sup>, etc.) are used as sensitive materials due to their simple preparation method, low cost, and responsiveness to various gases<sup>29</sup>. This type of sensor has the characteristics of fast response, high sensitivity, and insensitivity to temperature and humidity. However, the disadvantages of this type of sensor are also obvious. When the semiconductor gas sensor works, it can promote the speed of direct ion exchange between gas molecules and sensitive materials by heating<sup>30</sup>. Because of this feature, this kind of sensor works at a higher ambient temperature, resulting in high power consumption. The sensitive material made of these metal oxides has response to a variety of gases, so the selectivity of

this kind of sensor is poor. When the components of the tested gas contain hydrogen sulfide and other reducing sulfur compounds (carbon disulfide, trimethyl disulfide, nitro compounds, etc.), these components will be oxidized to mineral acids. These acidic substances will cause corrosion to the sensitive material, which can lead to sensor poisoning<sup>31</sup>.

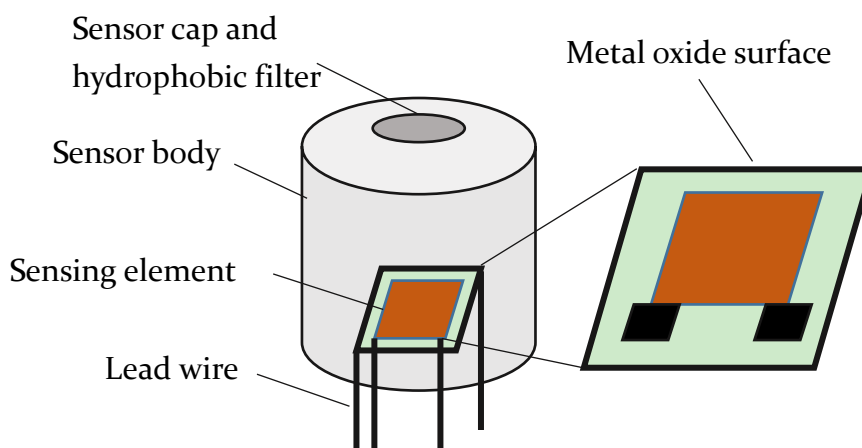


Fig.1.1 The structure of metal oxide semiconductor sensor.

Fig.1.1 shows the basic structure of a metal oxide semiconductor sensor. The sensing performance of the sensor is closely related to the heating electrode and gas sensing material. The selectivity of gas sensitive materials mainly refers to the recognition function of gas sensitive materials for target gas, which mainly depends on the ability of surface reaction or surface adsorption of materials. The selectivity of gas sensitive materials is determined by the type and microstructure of the materials. Therefore, the physical and chemical properties of the materials can be changed by such methods as compounding, doping and surface modification, so as to enhance the selectivity of the sensitive materials. Doping the gas sensing material is the main method to improve the selectivity of the sensor. The addition of Pt, Pd, Ir and other precious metals can not only effectively improve the sensitivity and response time of the element, but also improve the selectivity due to different adsorption tendencies caused by changes in the catalyst<sup>32</sup>.

### 1.2.2 Electrochemical gas sensor

Electrochemical gas sensor refers to a device that reacts with a specific sensing element to produce a sensing signal, and then converts this sensing signal into an

identifiable electrical signal proportional to the concentration of the target substance through a specific transducer, to achieve qualitative or quantitative analysis and detection of the target substance<sup>33,34</sup>. Due to its simple operation process, high selectivity, accurate and fast analysis, and low price, this gas sensor has been used in many fields, such as food industry, biomedical research and environmental detection. The basic structure of an electrochemical gas sensor is shown in Fig.1.2.

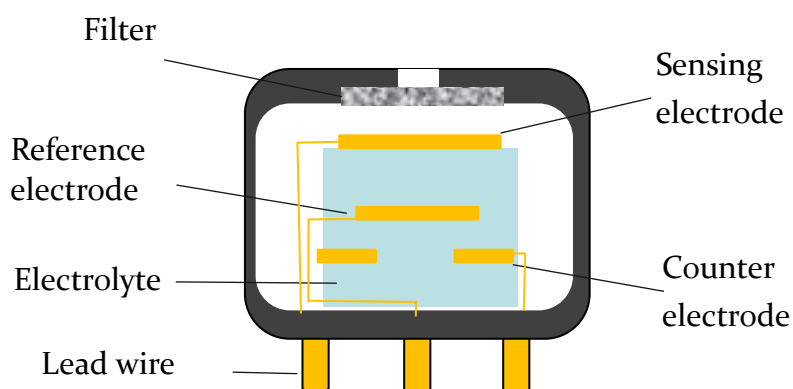


Fig.1.2 The schematic graph of electrochemical gas sensor.

Most electrochemical gas sensors are current type sensors, which produce a current that is linearly proportional to the gas concentration. The service life of current type electrochemical gas sensor is mainly related to electrolyte. Therefore, how to choose a suitable electrolyte to prolong the service life of the sensor is a common concern.

### 1.2.3 QCM gas sensor

Quartz crystal microbalance (QCM) is a device that is sensitive to mass changes, and has the advantages of high sensitivity, low cost, simple operation, and real-time online detection<sup>35</sup>. The sensitive material is the key component of the QCM gas sensor. The sensitive material interacts with the target gas molecules, so that the mass change signal is converted into a frequency change signal to achieve the purpose of detection. In order to make QCM gas sensors selective, organic polymers, supramolecular compounds, ionic liquids and nanomaterials are often used to modify QCM gas sensors.

QCM sensor modified by organic polymer sensitive materials uses the principle

of physical adsorption of polymer molecules on target gas molecules, including hydrogen bond and van der Waals force. Although organic polymers have high sensitivity and good reversibility, their selectivity is poor.

Supramolecules are molecular aggregates formed by intermolecular interactions. Some molecules are cages with hole structures, which can recognize organic gas molecules. According to the molecular properties of different target gases, the host compounds with different structures can be selected to synthesize sensitive films with high sensitivity. Such molecules include phthalocyanines, molecularly imprinted compounds, cyclodextrins, etc.

Although the selectivity of the modified QCM sensor has become better<sup>36</sup>, there are still many disadvantages, such as poor signal-to-noise performance due to surface interference and crystal size. The basic structure and gas response principle of the QCM gas sensor are shown in Fig.1.3.

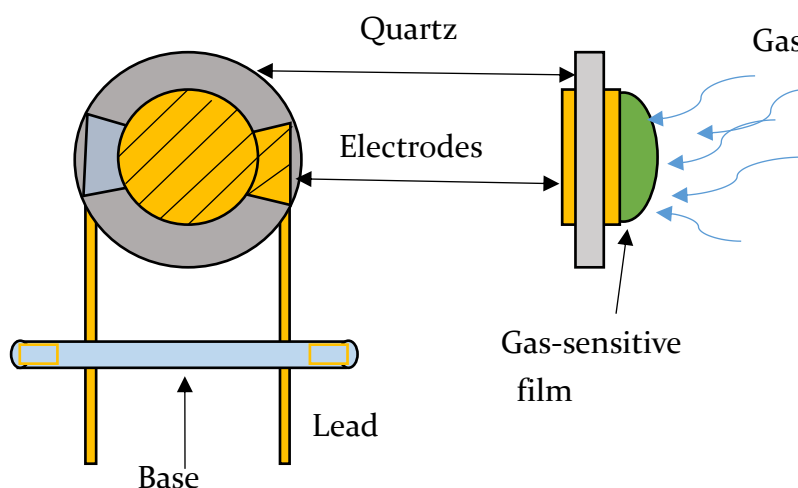


Fig.1.3 The basic structure of QCM sensor.

#### 1.2.4 Gas chromatography

Gas chromatography (GC) is a type of chromatography. Chromatography has two phases, one is the mobile phase, and the other is the stationary phase<sup>37</sup>. When a liquid is used as the mobile phase, it is called liquid chromatography. The use of gas as the mobile phase is called gas chromatography. Gas chromatography is a chromatographic separation and analysis method using gas as the mobile phase, which is widely used in the quantitative analysis of small molecular weight and complex components. A gas chromatograph is mainly composed of a gas system, a

sample injection system, a separation system (column), a detection and temperature control system, and a recording system, as shown in Fig.1.4.

The carrier gas of a gas chromatograph goes through a series of treatments and sends the sample gas to the column for separation. The separated components flow into the detector successively for detection. The detector converts the concentration or mass change of the component to be measured into an electrical signal, which is amplified and recorded on the recorder to obtain the chromatographic outflow curve. Qualitative analysis can be carried out according to the retention time on the chromatographic outflow curve. Quantitative analysis can be carried out according to the peak area or peak height.

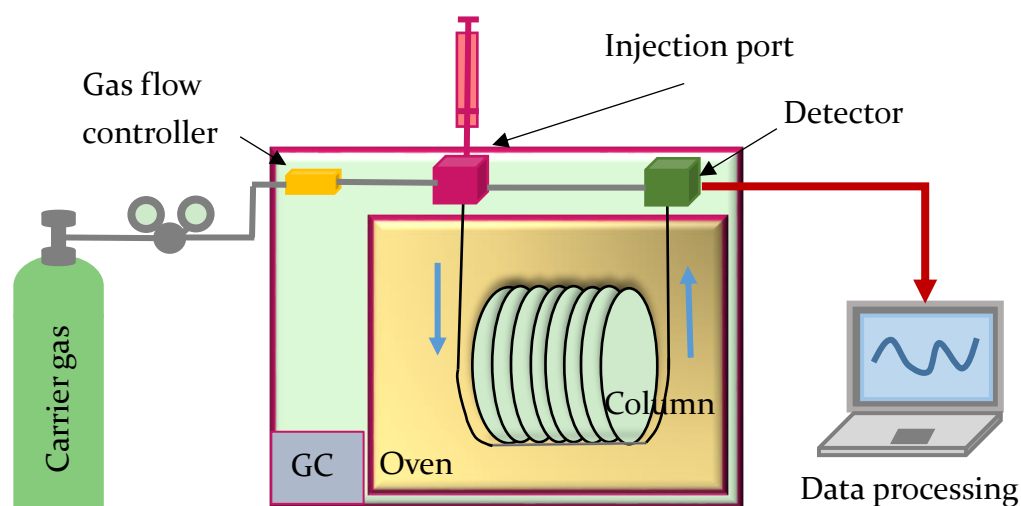


Fig.1.4 Schematic diagram of gas chromatography.

### 1.2.5 E-nose

Compared with other animals, human sense of smell is the least sensitive. But at present, in the process of food quality evaluation, people mainly rely on their sense of smell. Practitioners of this kind of work generally need some professional training, and the identification process cannot avoid a lot of subjective factors. There are considerable individual differences in the identification results with age, gender, identification ability and language expression ability. The manual identification time should not be too long, nor can it identify toxic and harmful gases, otherwise the olfactory sensitivity will be reduced or damaged. Therefore, an objective and accurate olfactory identification method to replace the human sense of smell to identify odor and volatiles has been the expectation of people for many

years.

An e-nose is an instrument that can identify simple or complex odors, consisting of a partially selective chemical sensor array and an appropriate pattern recognition system<sup>38</sup>. The electronic nose has attractive application prospects in the food industry<sup>39</sup>, environmental monitoring<sup>40</sup>, etc., and has many advantages compared to the human sense of smell. Therefore, this research field has received extensive attention.

The e-nose is mainly composed of three functional parts: odor sampling system, gas sensor array and appropriate pattern-classification system, as shown in Fig.1.5.

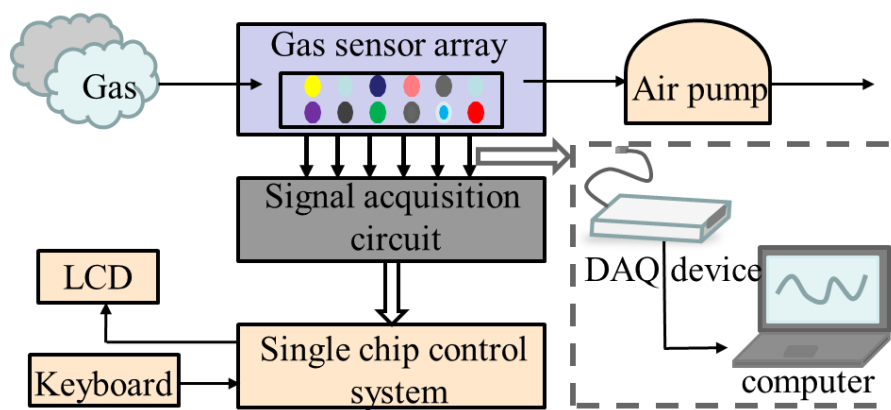


Fig.1.5 E-nose system.

The main mechanism of the electronic nose to identify odor is that each sensor in the array has different sensitivity to the measured gas, and the response curve of the entire sensor array to different gases is different. It is this distinction that allows the system to identify odors based on the sensor's response curve.

In addition to these devices and equipment, Photoionization detection<sup>41</sup> (PID) and plasmonic gas sensors<sup>42,43</sup> are also commonly used to detect VOCs.

A PID is a gas detector with extremely high sensitivity and can detect VOCs and some toxic gases from very low concentrations of 10 ppb<sup>44</sup> to higher concentrations of 10000 ppm<sup>45</sup>. Compared with traditional detection methods such as metal oxide gas sensors, it has the advantages of high accuracy, fast response and good real-time performance<sup>46</sup>, however, its low selectivity is an unavoidable problem<sup>47</sup>.

Plasmonic gas sensor can be divided into localized surface plasmon resonance (LSPR) gas sensor<sup>48,49</sup> and surface enhanced raman spectroscopy (SERS) gas sensor<sup>50</sup> depending on the principle. Both types of sensors use optical principles for gas detection and therefore have the advantage of fast response and high accuracy. This type of sensor can be made selective with a specific layer<sup>51-53</sup>.

## 1.3 Sensing film fabrication methods

In the field of sensors, it is often necessary to deposit nano particles and polymer materials on the substrate<sup>54,55</sup>. At present, there are many ways to make thin films. The type of solvent, the concentration of particles and temperature can affect the formation of the films. By adjusting these parameters, the thickness and morphology of the film can be further controlled<sup>56</sup>.

### 1.3.1 Drop casting

For small substrates, the drop casting method has the advantages of fast and easy operation. The thickness of the film can be adjusted by the volume of the dispersion used and the particle concentration. After the drop casting is completed on the substrate, it needs to be dried to form a film. A schematic diagram of the drop casting process is shown in Fig.1.6. By adjusting the pressure and temperature during drying, the time required for film formation can be changed, which also has a certain impact on the final morphology of the film. In addition, the degree of wetting the substrate with solvent, the rate of evaporation, capillary forces associated during drying, etc. can also have an effect on the morphology of the film.

However, the film prepared by drop casting method is greatly affected by the coffee ring effect, and the homogeneity of the film is poor. Even under ideal conditions, the difference of evaporation rate or concentration fluctuation of solvent will cause changes in the internal structure of the film.

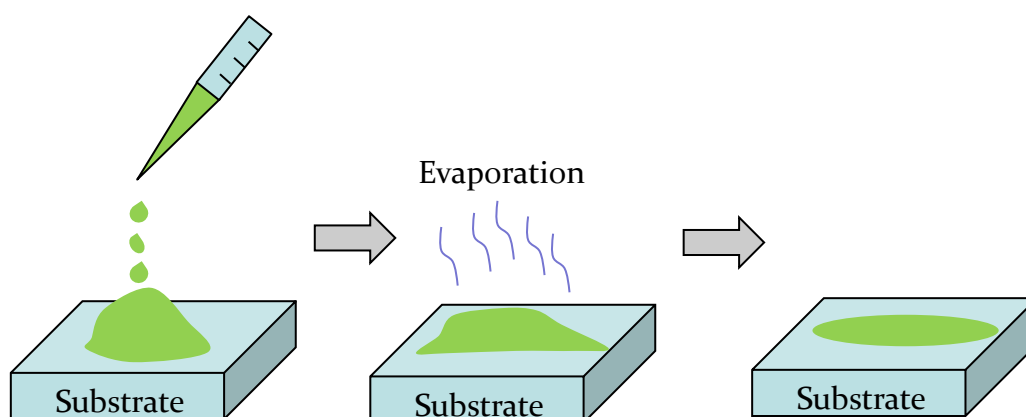


Fig.1.6 Schematic diagram of the drop casting process.

### 1.3.2 Spin coating

As one of the many thin film preparation methods, spin coating has the advantages of accurate and controllable film thickness, high-cost performance, energy saving and so on<sup>57</sup>. It has a broad application prospect in the fields of microelectronics<sup>58</sup>, biology, nanophotonics, medicine and so on. The spin coating method requires the use of a spin coater. Compared with drop casting, spin coating usually provides a more uniform film thickness on the substrate, and the film can be formed on a larger substrate using appropriate equipment. Three steps are required to prepare thin films by spin coating, as shown in Figure 1.7. First, drop a certain volume of solution into the center of the substrate, then set the rotation speed and rotation time of the spin coater, and finally dry the spin-coated substrate, and evaporate the solvent to produce a thin film. Centrifugal force causes the dispersion to be uniformly distributed on the substrate. The thickness of the film is related to the surface tension, viscosity of the solution and the rotation speed of the substrate. Actual material usage in spin coating methods is usually very low (about 10% or less) and the rest of the material is discarded. While discarded material is usually not a problem for the environment, it is a waste for mass production. Other than that, quantitative film cannot be produced, and it is difficult to make 2 to 3 times the thickness of the base film.

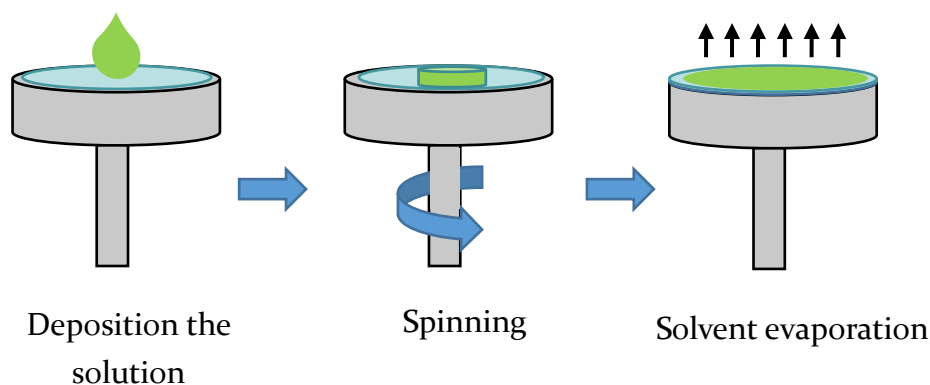


Fig.1.7 The main stages of spin coating.

### 1.3.3 Screen printing

Screen printing refers to the use of a screen as a plate base, and a screen-printing plate with a pattern is made by a photosensitive plate-making method. The screen-printing plate is printed based on the basic principle that the patterned part of the

mesh can pass through the ink, and the non-patterned part of the mesh cannot pass through the ink<sup>59</sup>. A schematic diagram of screen printing is shown in Fig.1.8. Compared with inkjet printing, screen printing requires less ink and requires relatively simple equipment. However, for different patterns, the screen needs to be remade, which will not only cause a certain amount of waste, but also make the experiment tedious.

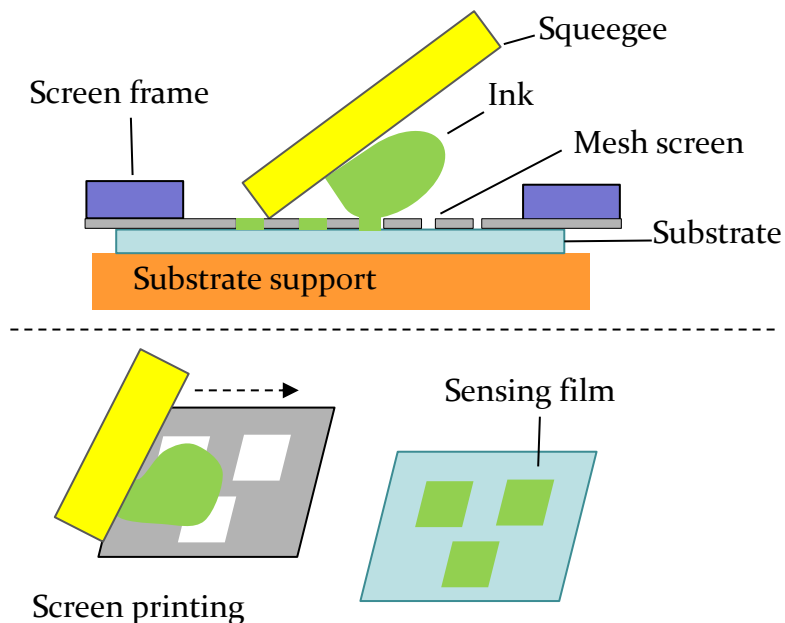


Fig.1.8 The screen-printing process.

### 1.3.4 Inkjet printing

Inkjet printing technology has rapidly developed in the field of organic electronic devices because of its advantages of low cost, simplicity, and reliability<sup>60</sup>.

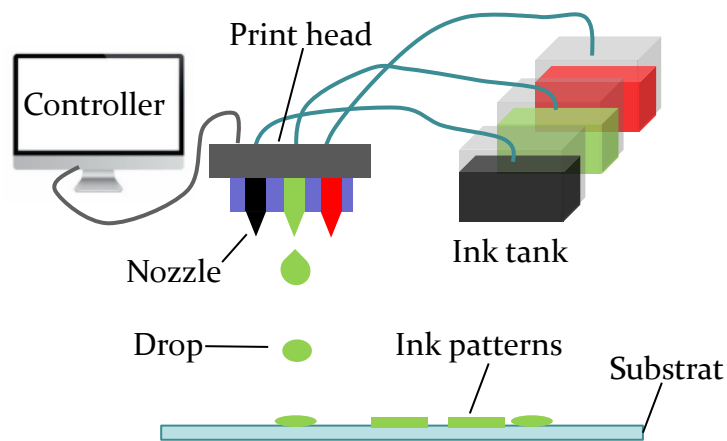


Fig.1.9 Schematic diagram of the inkjet printing system.

A schematic diagram of inkjet printing is shown in Fig.1.9. Current inkjet printing technology can control the printed droplets to the picometer level, and the droplet diameter formed on the substrate can be controlled to the micron level. Because of the extremely small droplets, the coffee ring effect on film uniformity can be reduced, thus improving the performance of organic electronics. Ink is the key to inkjet printing technology, however, making functional materials into inkjet printing inks is a complex problem.

## 1.4 Inkjet printers and flexible substrates

### 1.4.1 DMP-2850

The Dimatix Materials Printer (DMP-2850) is a desktop, laboratory inkjet printing device with micron-level accuracy that can print different functional materials on a variety of substrates. The printer has a viewing system for ink drop and a calibration camera for substrate alignment and measurement, which is very helpful for making films in the lab. Although the device has many advantages for experimental development, the price is very expensive, about 2000 times the price of an ordinary home printer EPSON PX-105.

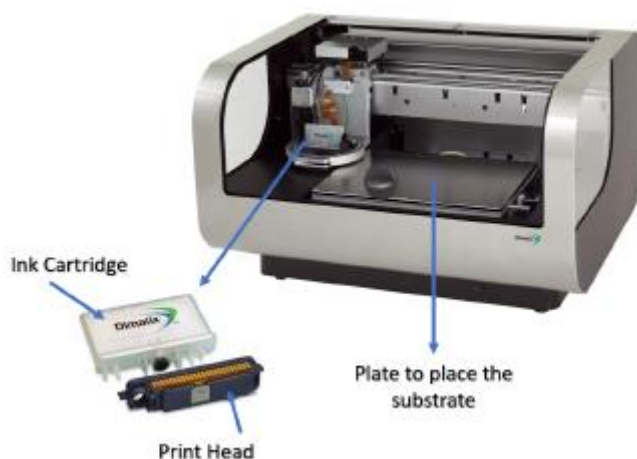


Fig.1.10 Product of DMP-2850 and some main components<sup>35</sup>.

### 1.4.2 EPSON L310 and EPSON PX-105

In this study, the printer model recommended by the commercial silver ink company is EPSON L310, so the first printer model we used is EPSON L310. The printer is not currently available in Japan and must be imported from the

Philippines or from China. If the printer imported from China is used in Japan, the power module must be replaced. By observing the original ink that comes with the printer, it can be found that it is a dye ink. Disassembling and observing the printheads of the printer show that the number of printheads for black ink is 180, and the number of printheads for yellow, magenta and cyan ink is 59. Compared with this experiment, the Epson L310 printer has the following advantages and disadvantages.

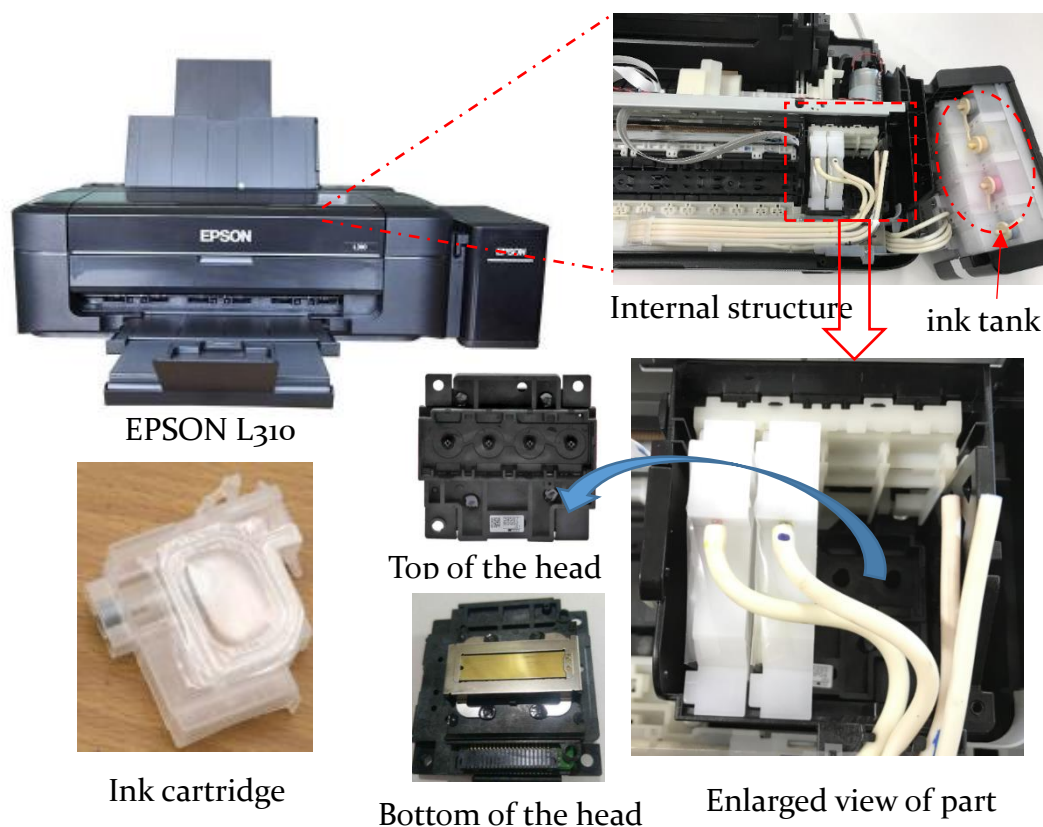


Fig.1.11 Pictures of the internal structure and parts of EPSON L310.

**Advantages:** 1. Although the original ink of the printer is dye ink, pigment ink can still be used. Since the functional inks in this experiment are mainly pigment inks, this feature is very important for this experiment.

2. Through the corresponding settings of the printout in Inkscape, a certain ink can be printed separately.

**Disadvantages:** Since this experiment requires frequent replacement of ink, it is necessary to clean the place containing ink in the printer. However, as shown in Fig.1.11, the parts containing ink in this model of printer include the ink tank, ink cartridge, ink flow path and print head, which is very difficult to clear and

completely replace the ink.

Epson PX-105 is a new printer to be found according to the experimental needs. The ink cartridge of the printer is not integrated with the printer, but independent. By using the unfilled ink cartridge corresponding to IC4CL69L, ink replacement becomes easier.

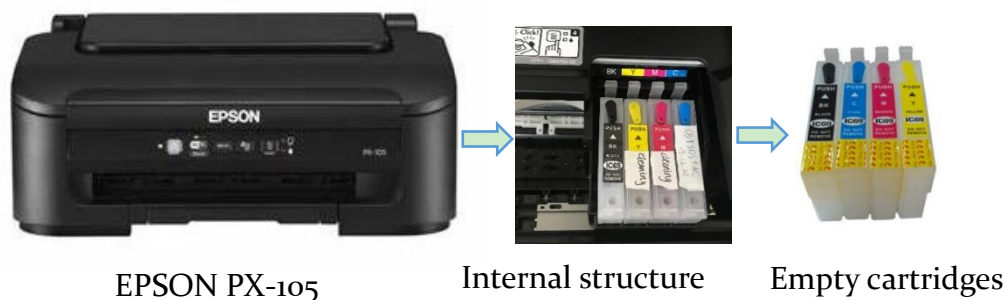


Fig.1.12 Pictures of the internal structure and parts of EPSON PX-105.

**Advantages:** In addition to being cheaper and more convenient to purchase, ink replacement is easier due to the unfilled ink cartridges. The original ink belongs to pigment ink, which is closer to the performance of the ink used in the experiment.

**Disadvantages:** When printing patterns, if standard printing is adopted, one of the four ink cartridges can be selected for printing by adjusting the CYMK value of the patterns. However, when setting the printing parameters, if the photo paper is selected as the printing paper and set as high-quality printing, the ink of any of the four ink cartridges cannot be printed separately. When setting photo paper to print, if a black pattern is printed, the ink is not from the black ink cartridge, but a mixture of three-color inks. When any color pattern is printed, the printed ink is also mixed with at least two inks. This is very unfavorable for the evaluation and discussion of thin film experiments.

### 1.4.3 PET film

Polyethylene terephthalate (PET) film has good mechanical properties and is widely used in food packaging, medical packaging, printing film, transformer insulating ink and flexible printed circuit. PET is a kind of plastics. Compared with other plastics, PET film has higher tensile strength, excellent dimensional stability, low moisture absorption and good physical properties in a wide temperature range. PET has a relatively high melting point, which makes it suitable for high-

temperature sterilization environment. However, compared with other cellulose products such as paper, PET is not easy to decompose, but biodegradable additives can be used to enhance the biodegradability of this plastic.

#### 1.4.4 Photo paper

The photo paper in the product can be divided into Photo Quality Glossy Film, Photo Quality Glossy Paper and Photo Paper in detail according to the use and surface characteristics of the photo paper. The photos printed with these three types of paper will be different in terms of color saturation, bright color, detail performance, etc.

According to different coating methods and coating materials, photo paper can be divided into Swellable Photo Paper, Cast Coating Photo Paper and Micro-porous Photo Paper. Since the formation of various functional films needs to be discussed in this study, the photo paper is discussed in detail from the perspective of coating methods and coating materials.

##### A. Swellable Paper

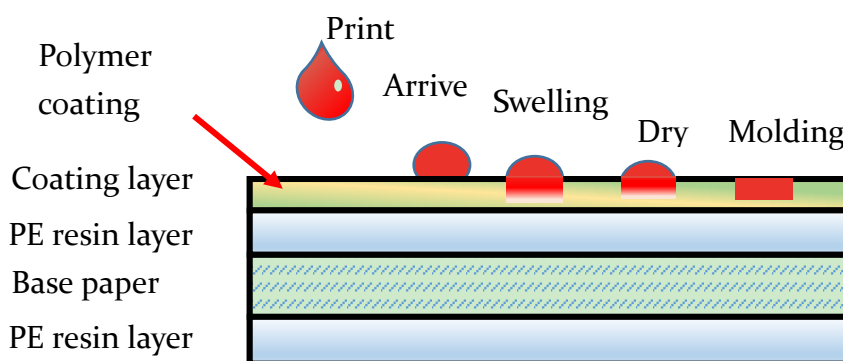


Fig.1.13 Schematic diagram of the structure and ink-fixing process of swellable photo paper.

The coating layer is also called ink absorbing layer. It uses polyvinyl alcohol (PVA) as the main film-forming material to form a bentonite coating on the base paper. Its surface is composed of gelatin, polyvinyl alcohol and other polymers to form an ink absorption layer.

### B. Cast Coating Photo Paper

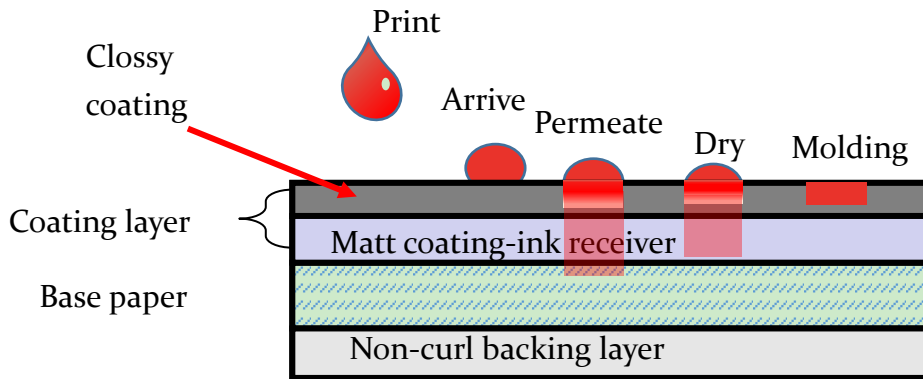


Fig.1.14 Schematic diagram of the structure and ink-fixing process of cast coating photo paper.

The coating is made of micron silicon dioxide. After special processing, the brightness and whiteness can reach the level of traditional photo paper. It has a waterproof coating, but the base paper is the same as the swellable photo paper, so the overall waterproof performance is poor.

### C. Micro-porous Paper

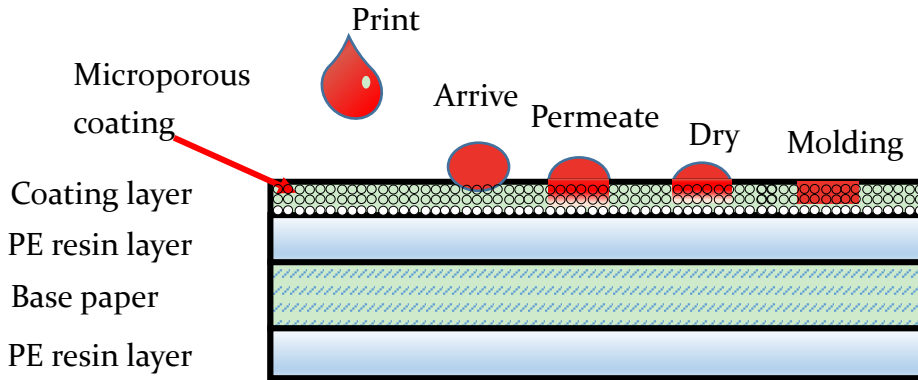


Fig.1.15 Schematic diagram of the structure and ink-fixing process of micro-porous photo paper.

Due to its special microporous structure, the coating has a strong ink absorption capacity, and can also express the layering effect well for the part with very dark tones; it dries quickly, and it can be directly touched when it comes out of the printer.

## 1.5 Aim and novelty in this research

Aim 1: Through the development of functional inks, a home printer can complete the production of sensors.

Aim 2: To develop an insulating layer that can be printed with a home inkjet printer, the insulating layer needs to have both insulating and ink-absorbing functions.

Novelty: 1. The fabrication of the fully printed sensor was realized.

2. A sensor matrix with a multilayer structure was developed.

## 1.6 Thesis outline

This research is mainly about the development of functional inks and the fabrication of fully printed gas sensor matrices using these functional inks.

In chapter 1, we introduce the application scenarios of gas sensors, existing gas sensing technologies, thin film fabrication methods and some common flexible substrates. The main object of this study is to realize the fabrication of large-scale sensor matrices on flexible substrates and further make the sensor matrices selective for VOCs.

Chapter 2 describes the dispersion effect of carbon black in different solvents with different dispersants. The preparation method of polymer carbon black ink that can be used for home inkjet printing is introduced in detail. Through a home printer, full inkjet printing of a sensor array containing 8 sensors was achieved. In addition, through experiments, it was found that some polymers and salts mixed with carbon black can be used to make gas sensing layers. This provides sufficient material for developing more sensors with different characteristics in the future.

In Chapter 3, we report a novel full printing process for fabricating chemiresistor gas sensor matrixes on photographic paper with an inkjet printer. Sensor matrices, which can increase the number of sensors significantly compared with a serial sensor array, were printed on one piece of A4 photographic paper. Each sensor matrix contains 36 interdigital electrodes in an area of less than 11 mm<sup>2</sup>, which greatly improves the density of the sensor. The basic architecture of the sensor matrix is electrodes that row and column intersecting. In order to insulate the row and column electrodes from meeting each other, an insulating layer needs to be fabricated at the point of intersection between the row and column electrodes. The insulation layer was produced by adjusting the number of printing passes and shape

of the printing pattern of color pigment ink. Carbon black was used to form conductive composites by changing its resistivity with a specific polymer for the preparation of sensing material. In order to make the sensing material can be printed, it is necessary to disperse carbon black first. Carbon black was dispersed in aqueous solution with sodium dodecyl sulfate added as a surfactant to lower the surface tension, which enabled printing of carbon black using an inkjet printer. Some polymers have certain adsorption characteristics for gases. According to the different gas properties, the adsorption characteristics are also different. By adding polyethylene glycol polymer to the carbon black layer, the response to four gases with different properties is improved. Compared with the drop coating, the full-printing sensors not only reduces the production time significantly, but also improves the gas response magnitude to ethanol by about 3 times. The results demonstrate that the developed sensor can be used as a low cost, disposable, and easily printable chemical sensor.

In chapter 4, a method was used to fabricate a fully inkjet-printed gas sensor matrix on photographic paper. An electrode matrix comprising 36 interdigital electrodes in a high-density layout that is easy to integrate has been fabricated using a combination of insulating ink and commercial silver ink. Molecular imprinted polymer (MIP) inks were then made using a simple solution mixing method, and these inks were printed together with carbon black ink on the electrode matrix to complete production of the sensor. Finally, experimental dynamic sensing of volatile organic compounds verifies that for detection of gases corresponding to the MIP template molecules, the MIP layer offers improvements in both sensitivity and selectivity when compared with non-imprinted polymer layers. The matrix can produce a response of more than 20% to 3 ppm propanoic acid gas through adjustment of the printing times for the carbon black layer and the MIP layer.

In the last chapter, the research is summarized, and the possible research prospect is proposed.

## Reference

1. Neri, G. First Fifty Years of Chemoresistive Gas Sensors. 1–20 (2015) doi:10.3390/chemosensors3010001.
2. Fine, G. F., Cavanagh, L. M., Afonja, A. & Binions, R. Metal Oxide Semiconductor Gas Sensors in Environmental Monitoring. 5469–5502 (2010) doi:10.3390/s100605469.
3. Darshane, S. L., Suryavanshi, S. S. & Mulla, I. S. Nanostructured nickel ferrite : A liquid petroleum gas sensor. **35**, 1793–1797 (2009).
4. Pandey, S., Goswami, G. K. & Nanda, K. K. Nanocomposite based flexible ultrasensitive resistive gas sensor for chemical reactions studies. 1–6 (2013) doi:10.1038/srep02082.
5. Kanazawa, E., Sakai, G., Shimano, K. & Kanmura, Y. Metal oxide semiconductor  $\text{NiO}$  sensor for medical use. **77**, 72–77 (2001).
6. Barreca, D. *et al.* Sensors and Actuators B : Chemical  $\text{ZnO}$  nano-assemblies by Plasma-CVD as chemical sensors for flammable and toxic gases. *Sensors & Actuators: B. Chemical* **149**, 1–7 (2010).
7. Zhou, R., Hu, G., Yu, R., Pan, C. & Lin, Z. Piezotronic effect enhanced detection of flammable / toxic gases by  $\text{ZnO}$  micro / nanowire sensors. *Nano Energy* **12**, 588–596 (2015).
8. Star, A. *et al.* Gas Sensor Array Based on Metal-Decorated Carbon Nanotubes. 21014–21020 (2006).
9. Habashi, F. Pollution problems in the metallurgical industry: A review. **2**, 17–26 (2011).
10. Hadipour, M., Farrokhi, J. & Aghazadeh, M. An experimental setup of multi-intelligent control system ( MICS ) of water management using the Internet of Things ( IoT ). *ISA Transactions* **96**, 309–326 (2020).
11. Gomes, B. A., Rodrigues, J. J. P. C., Rab, R. A. L., Kumar, N. & Kozlov, S. IoT-Enabled Gas Sensors : Technologies , Applications , and Opportunities.
12. Heckathorn, S. A. Effects of Elevated  $\text{CO}_2$  on Nutritional Quality of Vegetables : A Review. **9**, 1–11 (2018).
13. Cummins, E. P., Strowitzki, M. J. & Taylor, C. T. AND CARBON DIOXIDE SENSING IN MAMMALS GRAPHICAL ABSTRACT. 463–488 (2022) doi:10.1152/physrev.00003.2019.
14. Mackie, R. I., Stroot, P. G. & Varel, V. H. Biochemical Identification and Biological Origin of Key Odor Components in Livestock Waste 1

- ABSTRACT : 1331–1342 (1995).
15. Bennett, J. W. & Inamdar, A. A. Are Some Fungal Volatile Organic Compounds (VOCs) Mycotoxins. 3785–3804 (2015) doi:10.3390/toxins7093785.
  16. Sax, S. N., Bennett, D. H., Chillrud, S. N. & Kinney, L. Differences in source emission rates of volatile organic compounds in inner-city residences of New York City and Los Angeles. (2004) doi:10.1038/sj.jea.7500364.
  17. Sheu, R. *et al.* Human transport of thirdhand tobacco smoke : A prominent source of hazardous air pollutants into indoor nonsmoking environments. (2020).
  18. Wan-kuen, J. O., Jong-hyo, L. E. E., Ho-jin, L. I. M. & Woo-sik, J. Naphthalene emissions from moth repellents or toilet deodorant blocks determined using head-space and small-chamber tests. **20**, 1012–1017 (2008).
  19. Fischer, S. *et al.* Impact of food intake on in vivo VOC concentrations in exhaled breath assessed in a caprine animal model Impact of food intake on in vivo VOC concentrations in exhaled breath assessed in a caprine animal model. doi:10.1088/1752-7155/9/4/047113.
  20. Smeets, M. A. M. & Dalton, P. H. Evaluating the human response to chemicals : odor , irritation and non-sensory factors. **19**, 581–588 (2005).
  21. Cincinelli, A. *et al.* Science of the Total Environment Measurement of volatile organic compounds ( VOCs ) in libraries and archives in Florence ( Italy ). *Science of the Total Environment, The* **572**, 333–339 (2016).
  22. Dettenrieder, C., Raichlin, Y., Katzir, A. & Mizaiko, B. Toward the Required Detection Limits for Volatile Organic Constituents in Marine Environments with Infrared Evanescent Field Chemical Sensors. (2019).
  23. Tang, X., Misztal, P. K. & Goldstein, A. H. Volatile Organic Compound Emissions from Humans Indoors. (2016) doi:10.1021/acs.est.6b04415.
  24. Ma, P. *et al.* Non-invasive exhaled breath diagnostic and monitoring technologies. 1–14 (2021) doi:10.1002/mop.33133.
  25. Liu, L. *et al.* A Gas Sensor With Fe<sub>2</sub>O<sub>3</sub> Nanospheres Based on Trimethylamine Detection for the Rapid Assessment of Spoilage Degree in Fish. **8**, 1–9 (2020).
  26. Tao, Y., Cao, X., Peng, Y. & Liu, Y. Sensors and Actuators B : Chemical A novel cataluminescence gas sensor based on MgO thin film. *Sensors & Actuators: B. Chemical* **148**, 292–297 (2010).

27. Steinebach, H., Kannan, S., Rieth, L. & Solzbacher, F. Sensors and Actuators B : Chemical H<sub>2</sub> gas sensor performance of NiO at high temperatures in gas mixtures. *Sensors & Actuators: B. Chemical* **151**, 162–168 (2010).
28. Subramaniam, V. TiO<sub>2</sub> thin film gas sensor for monitoring ammonia. doi:10.1016/j.matchar.2006.11.007.
29. Li, T. *et al.* The Combination of Two-Dimensional Nanomaterials with Metal Oxide Nanoparticles for Gas Sensors : A Review. 1–40 (2022).
30. Raju, P. Review — Semiconductor Materials and Devices for Gas Sensors Review — Semiconductor Materials and Devices for Gas Sensors. (2022) doi:10.1149/1945-7111/ac6e0a.
31. Schultealbert, C., Uzun, I., Baur, T., Sauerwald, T. & Schütze, A. Siloxane treatment of metal oxide semiconductor gas sensors in temperature-cycled operation – sensitivity and selectivity. 283–292 (2020).
32. Reti, F., Kiss, G. & Perczel, I. V. Subjective Overview on Oxide Semiconductor Gas Sensors. **16**, 53–69 (2004).
33. Bakker, E. & Telting-diaz, M. Electrochemical Sensors. **74**, 2781–2800 (2002).
34. Toniolo, R., Pizzariello, A., Carrilho, E. & Piccin, E. Lab on a Chip An electrochemical gas sensor based on paper supported room temperature ionic liquids. 153–158 (2012) doi:10.1039/c1lc20663j.
35. Ark, H. J. P. & Ee, S. S. L. Strategic Approaches for Highly Selective and Sensitive Detection of Hg<sup>2+</sup> Ion Using Mass Sensitive Sensors. **35**, 883–888 (2019).
36. Yao, Y., Huang, X., Chen, Q., Zhang, Z. & Ling, W. High Sensitivity and High Stability QCM Humidity Sensors Based on Polydopamine Coated Cellulose Nanocrystals / Graphene Oxide Nanocomposite. 1–12 (2020).
37. Fountain, K. J. & Diehl, D. M. Influence of stationary phase chemistry and mobile-phase composition on retention , selectivity , and MS response in hydrophilic interaction chromatography. 740–751 (2010) doi:10.1002/jssc.200900660.
38. Wilson, A. D. & Baietto, M. Applications and Advances in Electronic-Nose Technologies. 5099–5148 (2009) doi:10.3390/s90705099.
39. Baldwin, E. A. *et al.* Electronic Noses and Tongues: Applications for the Food and Pharmaceutical Industries. 4744–4766 (2011) doi:10.3390/s110504744.
40. Capelli, L., Sironi, S. & Rosso, R. Del. Electronic Noses for Environmental

- Monitoring Applications. 19979–20007 (2014) doi:10.3390/s14119979.
41. Zhu, H. *et al.* Lab on a Chip. 3021–3029 (2015) doi:10.1039/c5lc00328h.
  42. Joy, N. A. *et al.* Selective Plasmonic Gas Sensing: H<sub>2</sub>, NO<sub>2</sub>, and CO Spectral Discrimination by a Single Au-CeO<sub>2</sub> Nanocomposite Film. (2012).
  43. Gaspera, E. Della & Martucci, A. Sol-Gel Thin Films for Plasmonic Gas Sensors. 16910–16928 (2015) doi:10.3390/s150716910.
  44. Macdonald, R. W., Griffiths, R. F. & Hall, D. J. A COMPARISON OF RESULTS FROM SCALED FIELD AND WIND TUNNEL MODELLING OF DISPERSION IN ARRAYS OF OBSTACLES. **32**, 3845–3862 (1998).
  45. Song, Y., Wu, S. & Yan, Y. Development of Self-Tuning Intelligent PID Controller Based on BPNN for Indoor Air Quality Control. **3**, (2013).
  46. Dequan, S. H. I., Guili, G. A. O., Zhiwei, G. A. O. & Peng, X. Procedia Engineering Application of Expert Fuzzy PID Method for Temperature Control of Heating Furnace. **29**, 257–261 (2012).
  47. Sauerwald, T. Review of Portable and Low-Cost Sensors for the Volatile Organic Compounds. (2017) doi:10.3390/s17071520.
  48. Yang, Z., Sassa, F. & Hayashi, K. A Robot Equipped with a High-Speed LSPR Gas Sensor Module for Collecting Spatial Odor Information from On-Ground Invisible Odor Sources. *ACS Sensors* **3**, 1174–1181 (2018).
  49. Chen, L. *et al.* A single-nanoparticle NO<sub>2</sub> gas sensor constructed using active molecular plasmonics †. 1326–1329 (2015) doi:10.1039/c4cc08395d.
  50. Rae, S. I. & Khan, I. Surface enhanced Raman spectroscopy ( SERS ) sensors for gas analysis. **44**, 1365–1369 (2010).
  51. Bin, C., Chuanjun, L. & Kenshi, H. Selective Terpene Vapor Detection Using Molecularly Imprinted Polymer Coated Au Nanoparticle LSPR Sensor. *Ieee Sensors Journal*, **14**, 3458–3464 (2014).
  52. Shang, L., Liu, C., Watanabe, M., Chen, B. & Hayashi, K. LSPR sensor array based on molecularly imprinted sol-gels for pattern recognition of volatile organic acids. *Sensors and Actuators, B: Chemical* **249**, 14–21 (2017).
  53. Kou, Y. *et al.* Recyclable Magnetic MIP-Based SERS Sensors for Selective, Sensitive, and Reliable Detection of Paclobutrazol Residues in Complex Environments. (2020) doi:10.1021/acssuschemeng.0c05065.
  54. Wackerlig, J. & Lieberzeit, P. A. Sensors and Actuators B : Chemical Molecularly imprinted polymer nanoparticles in chemical sensing – Synthesis , characterisation and application. *Sensors & Actuators: B. Chemical* **207**, 144–157 (2015).

55. Matsui, J. *et al.* Composite of Au Nanoparticles and Molecularly Imprinted Polymer as a Sensing Material. **76**, 1310–1315 (2004).
56. Tak, H., Lee, S. & Park, C. Controls of surface morphology on sol-gel derived ZnO films under isothermal treatment conditions. *Vacuum* **143**, 312–315 (2017).
57. Ortiz-lopez, J. undergraduate laboratory cost instrumentation for spin-coating deposition of thin films in an undergraduate. (2015).
58. Yonkoski, R. K. & Soane, D. S. Model for spin coating in microelectronic applications Advertisement : Model for spin coating in microelectronic. **725**, (1992).
59. Xiao, R. *et al.* Preparation of AlSb film by screen printing and sintering method. *Journal of Materials Science: Materials in Electronics* **30**, 13290–13296 (2019).
60. Yan, K. & Li, J. Inkjet printing for flexible and wearable electronics Inkjet printing for flexible and wearable electronics. **120705**, (2021).

# Chapter 2 A fully inkjet-printed gas sensor array with conductive polymer composites

## 2.1 Introduction

When a drop of liquid is spilled on a solid surface, and during drying, its suspended particulate matter is deposited in a ring-like fashion due to the migration of solution or particles to the edge of the drop<sup>1,2</sup>. The formation process of the coffee ring is shown in Fig.2.1, which is mainly divided into three steps.

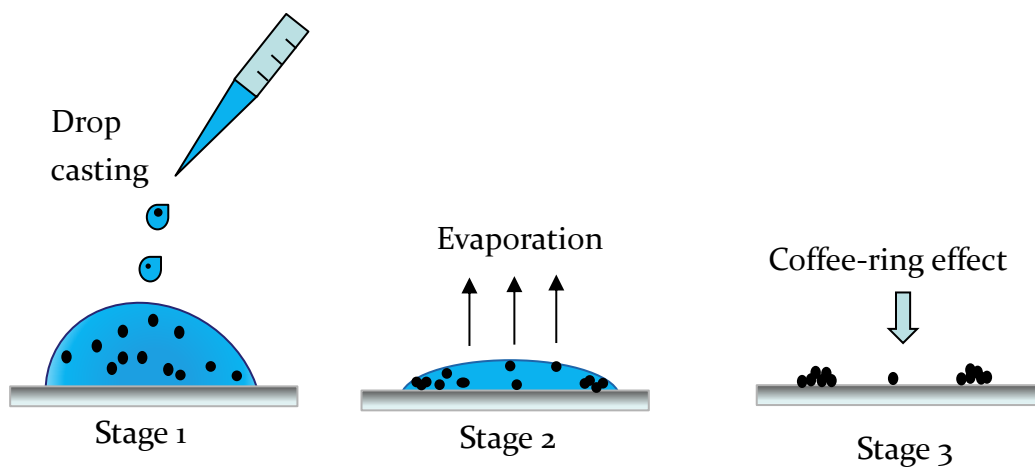


Fig.2.1 Schematic diagram of the formation process of the coffee ring.

Evaporation of water from a drying droplet does not take place evenly. It evaporates fastest from the boundary between liquid water, solid surface and air, which is the edge of the water droplet. This boundary is called the "three-phase boundary". As the water evaporates from the boundary, the water in the rest of the droplet moves to its position. This means that anything suspended in water - such as carbon black particles - will eventually be deposited on this outer ring. This effect can make the fabricated films very non-uniform and affect device performance. This effect is very harmful to the manufacture of solar cells, the manufacture of displays, and the manufacture of sensors.

There are many ways to suppress the coffee ring effect. The coffee ring effect can be suppressed by adding elongated particles (cellulose fiber) to the solution, mixing high-boiling point and low-boiling point solvents, controlling the substrate temperature, and controlling the wettability of the substrate surface. It was found that electrowetting can suppress the coffee ring effect of colloidal particles and DNA solutions of different sizes in the range of alternating current (AC) frequencies

from a few hertz to tens of kHz<sup>3,4</sup>.

In this study, through the improvement of the method of making the sensor film, the improvement of the properties of the solution, the mixing of solvents, etc., a more uniform sensing film was made and the performance of the gas sensor was improved.

## 2.2 Experimental

### 2.2.1 Fabrication of interdigitated electrode

An interdigitated electrode is an electrode with a periodic interdigitated pattern. Such electrodes are commonly used in the production of various types of sensors. Different application fields have different requirements for the shape of the interdigital electrode, the size of the die electrode, the processing technology, and the selection of materials. Therefore, different application scenarios will be designed separately<sup>5,6</sup>. Common interdigital electrodes are shown in the Fig.2.2 below.

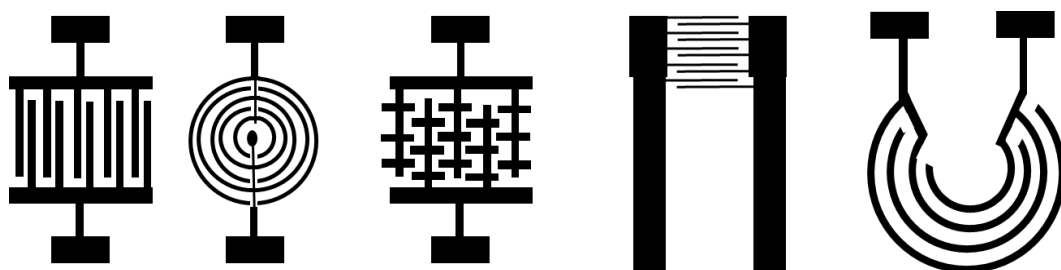


Fig.2.2 Common interdigital electrode shapes.

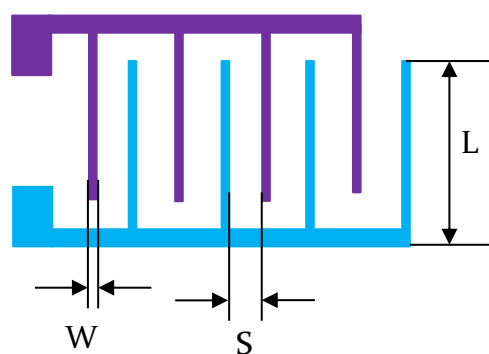


Fig.2.3 Structural parameters of IDEs.

The interdigital electrode sensor detects the concentration of the analysis object by reacting with the target analysis object to generate an electrical signal

proportional to the concentration of the target analysis object. The interdigital electrode sensor mainly includes four structural parameters<sup>7</sup>: number of fingers ( $N$ ), finger width ( $W$ ), finger length ( $L$ ), and finger spacing ( $S$ ), as shown in Fig.2.3. By analyzing the calculation formula of interdigital electrode resistance, the greater the aspect ratio of interdigital, the higher the density of interdigital, the smaller the initial resistance, and the higher the sensitivity and response speed of the sensor. It can be used as a gas sensor by dropping a gas response material on the interdigital electrode.

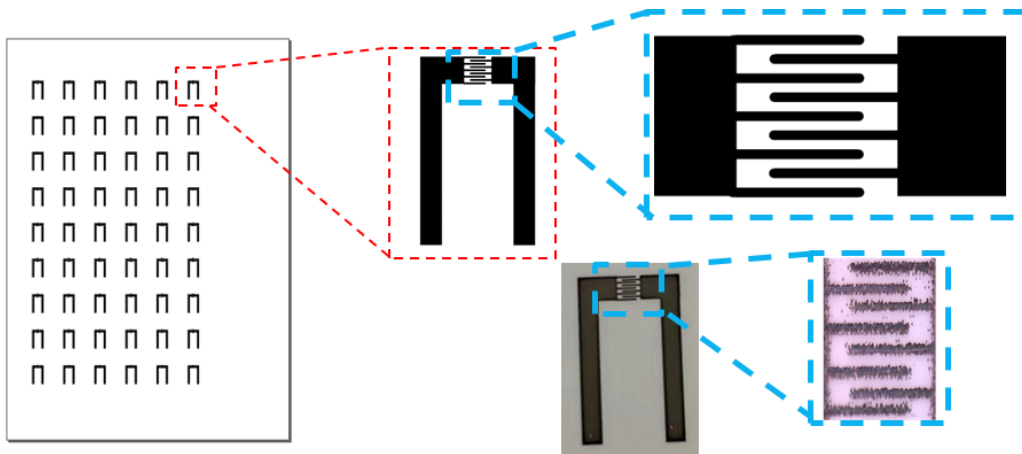


Fig.2.4 Design drawing and physical drawing of a single sensor.

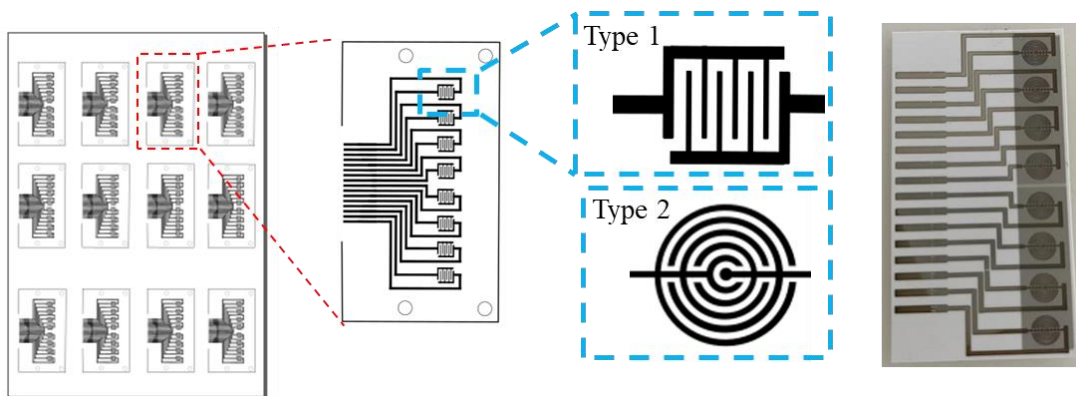


Fig.2.5 Design drawing and physical drawing of a sensor array.

We designed the sensor's interdigital electrodes and electrode array through Inkscape. In a single sensor, the number of pairs of fingers is 4, the width of the fingers is 0.1 mm, and the spacing of fingers is 0.1 mm. The reason why the interdigital width and spacing are set to 0.1 mm is because the printing accuracy of the used home inkjet printer is 0.1 mm.

### 2.2.2 Parameters of nozzles and droplet of inkjet printer

As shown in Table.2.1, the number of nozzles for the two home printers is the same, including 180 nozzles for black ink printing and 59 nozzles for three color ink printing.

Table.2.1 Comparison of parameters of three printers

| Printer model | Number of nozzles    | Drop volume |
|---------------|----------------------|-------------|
| EPSON L310    | BK: 180; C, M, Y: 59 | 3 pL        |
| EPSON PX-105  | BK: 180; C, M, Y: 59 | 3 pL        |
| DMP 2850      | 12                   | 2.4 pL      |

The number of DMP 2850 printer nozzles is limited, and the sensing layer cannot be produced by mixing multiple inks by controlling the color. Home printers and industrial printers can print about the same minimum droplet size.

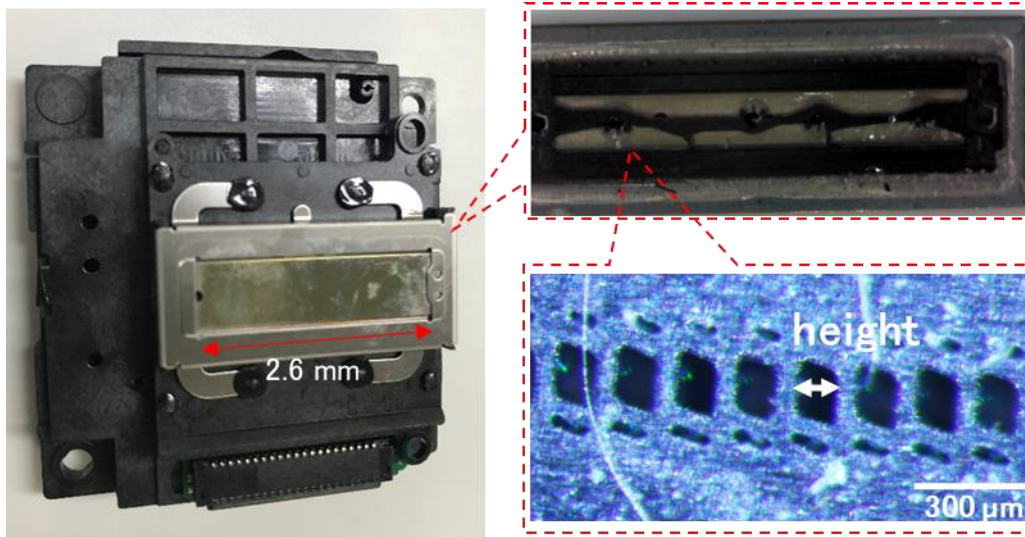


Fig.2.6 Overall view and partial microscope view of the nozzle of a home printer.

As shown in the microscope view in Figure 2.6, the nozzle shape of the printer is a diamond. The height of this diamond is about 100  $\mu\text{m}$ .

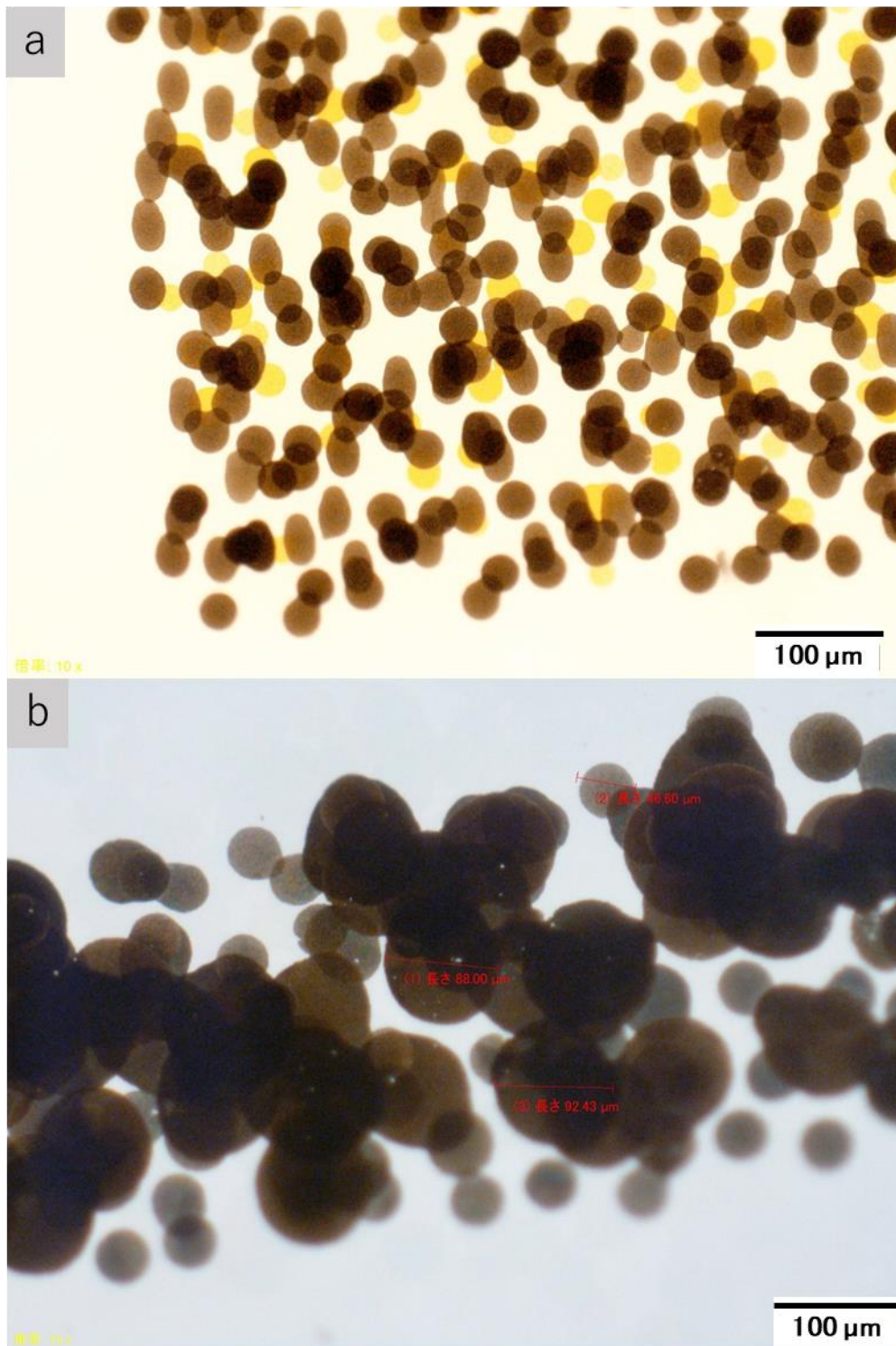


Fig.2.7 a. Micrograph after printing with black pigment ink. b. Micrograph after printing with silver ink.

The size of ink droplets formed after printing is related to the type of ink and the coating layer of the substrate. First, we printed on FUJIFILM Photo Paper Glossy

using black pigment ink as an example. The state after printing is shown in Fig. 2.7a, and the diameter of the ink droplet after drying is about 30  $\mu\text{m}$ . If silver ink is used for printing, the same substrate, but the diameter of the formed ink droplets is about 90  $\mu\text{m}$  as shown in Fig.2.7b. These parameters are of reference significance for our subsequent development of functional inks.

### 2.2.3 Fabrication of CB ink

As shown in Fig.2.8, carbon black can be directly dispersed in N-methyl-2-pyrrolidone (NMP) solution and THF solutions, but these two solutions are not suitable for producing inks for inkjet printing. Water and ethanol or their mixed solution is the best choice as ink solvent.

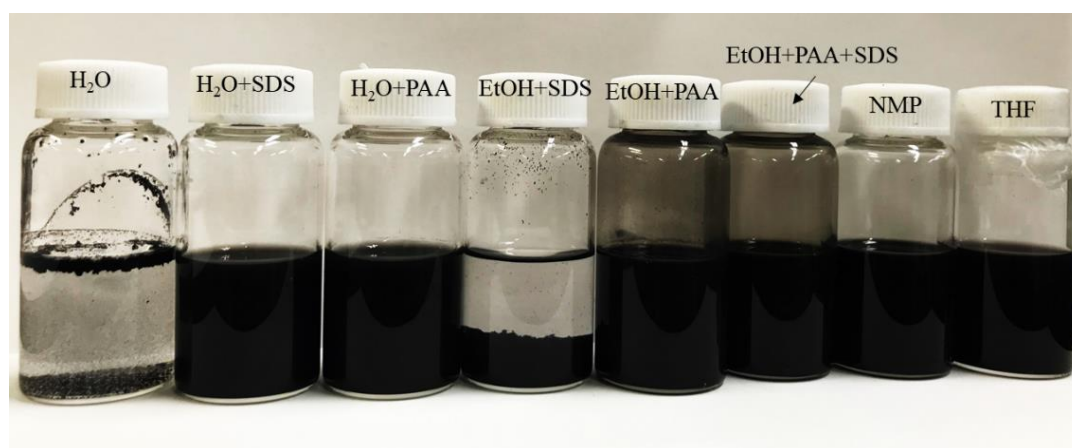


Fig.2.8 The dispersion effect of CB in different solvents.

Without the addition of a dispersing agent, carbon black can neither be dispersed directly in water nor in ethanol. Commonly used dispersants can be divided into anionic type (Poly acrylate, sodium dodecyl sulfate (SDS)), cationic type (Quaternary ammonium salts, amine salts) and non-ionic type (Nafion, triton X-100, polyarylic acid (PAA), polyethylene glycol (PEG)). Adding dispersants such as SDS or PAA to water can improve the dispersibility of carbon black in water. In this experiment, the ink production process that can be used for inkjet printing is divided into three steps.

#### Step 1: Preparation of primary carbon black solution

First, 10 mg of CB and 75 mg of SDS were added to 15 ml of water, then the mixed solution was subjected to ultrasonic treatment for 10 minutes, and finally centrifuged at 35 x 100 rpm for 10 minutes. After removing the precipitate, the primary CB solution was obtained.

#### Step 2: Addition of organic matter

**Humectant:** To keep the nozzle from drying out, a humectant needs to be added to the solution. In this experiment, glycerin or ethylene glycol was used as a humectant. The amount added is about 10%, which is 1.8 ml.

**Ethanol:** Ethanol has the effect of reducing the surface tension of the solution and increasing the volatility of ink droplets after printing. About 20 to 30 percent of ethanol was added in this experiment.

**Organic dispersant:** In order to further improve the dispersion effect of carbon black in solution, PAA or PVA (Polyvinyl alcohol) and other organic dispersants can be further added in this experiment.

**Other materials:** When producing a selective carbon black film that reacts with gas, various organic substances, salts, etc. can be added as functional materials for adjusting gas absorption.

After adding all the above materials, ultrasonic treatment was carried for 10 minutes.

**Step 3: Filter and observe**

The solution obtained in step 2 was further filtered through a 5-micron filter to obtain CB ink. The filtered ink will be left overnight for further observation to see if there is any coalescence of CB. If there is no carbon black coalescence it means that a stable CB ink has been obtained. A simple filter system is shown in Fig.2.9.

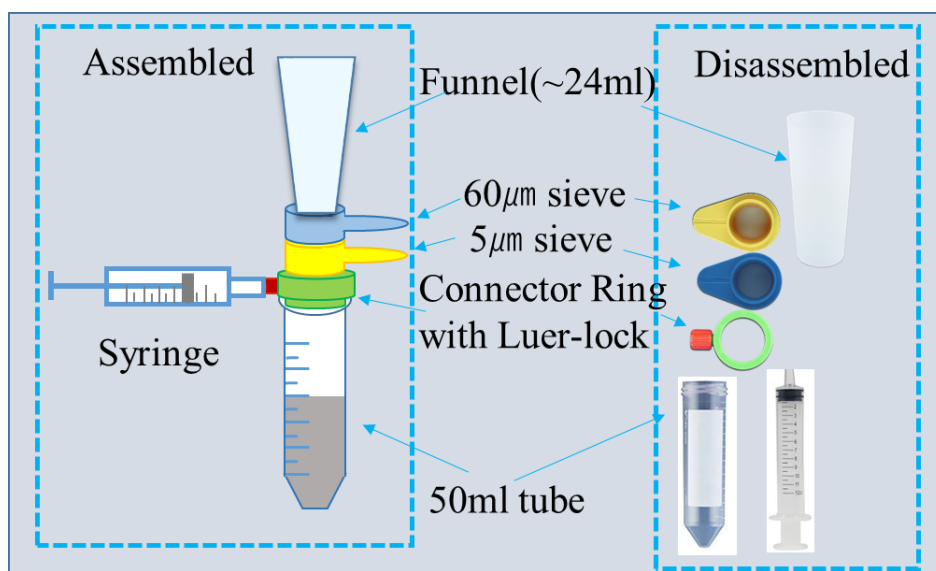


Fig.2.9 A sample filter system was used to filter the CB ink.

### 2.2.3 Sensor measurement system

A homemade multichannel sensing system can measure 8 individual sensors simultaneously or an array of sensor containing 8 units. The system (as shown in Fig. 2.10), consisting of eight sensor channels and six sample gas inlets, is equipped with a LCR meter and a custom LabView computer program<sup>8</sup>. The impedance variation of maximum 8 sensors upon exposure to maximum 6 gases can be recorded in one experimental batch. In the gas sensor response experiment, the voltage and frequency for the impedance measurement were set as 1.0 V and 500 Hz, respectively.

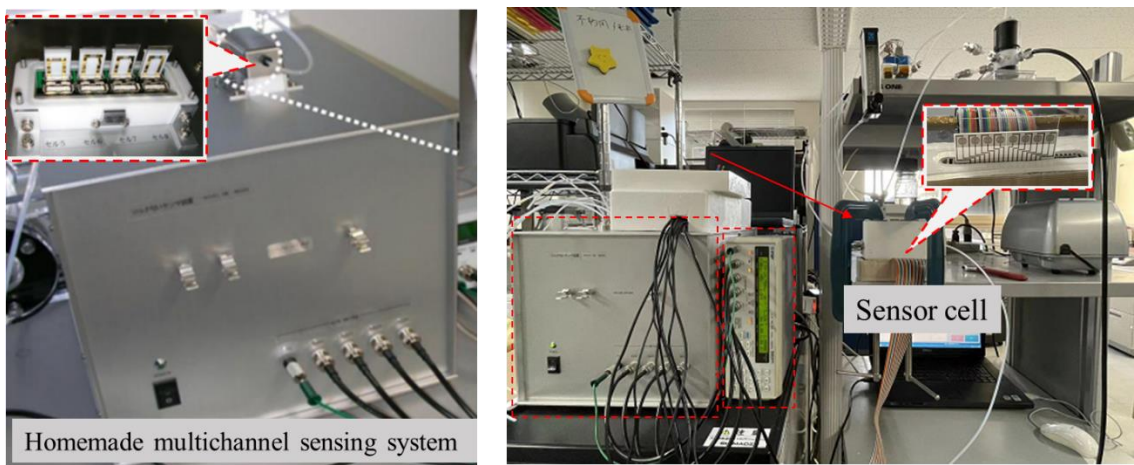


Fig.2.10 Photograph of the experiment setup.

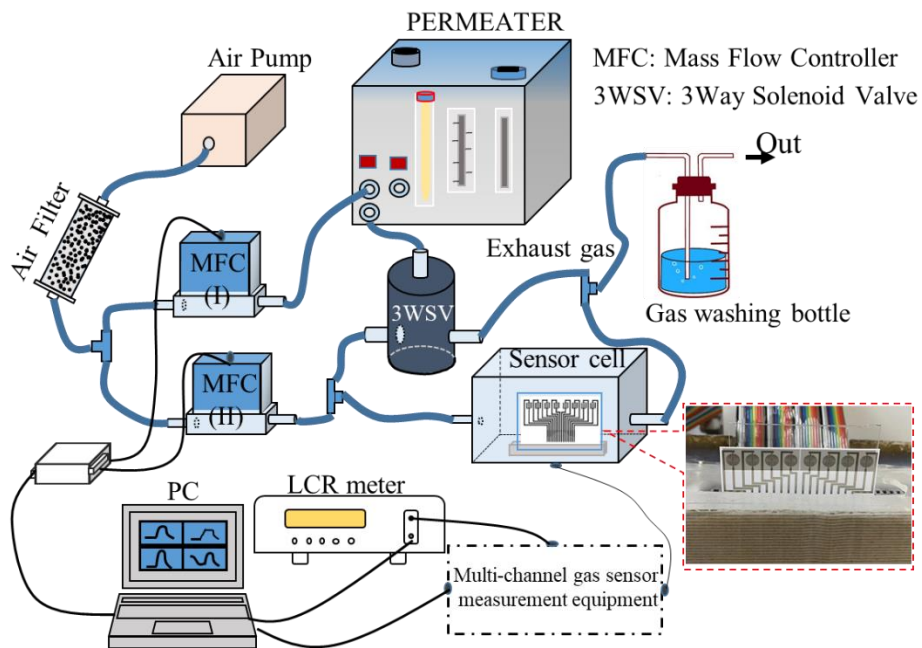


Fig.2.11 Configuration of the experimental sensing apparatus and block diagram of the electrical measurement.

Fig.2.11 shows the experimental set up for gas measurement and the block diagram of the signal processing. As shown in Fig.2.11, the system consisted of an air pump (LV-125A, Lincoln, Japan), an air-filtering tube filled with molecular sieves and activated carbon, two mass flow controllers (MFC) (3660, Kofloc, Japan), a three-way solenoid valve (3WSV) (FSM-0408Y, FLON Industry, Japan), a standard gas generator (PD-1B-2, GASTEC Corporation, Japan) and a self-made sensor chamber. By programming on LabView (National instruments, Austin, USA) and a data acquisition (DAQ), the velocity of gas and air and the concentration of gas can be controlled. The sensor resistance value of 8 channels can be measured at the same time through the multi-channel gas sensor measurement system and LCR meter (ZM2371, NF, Japan).

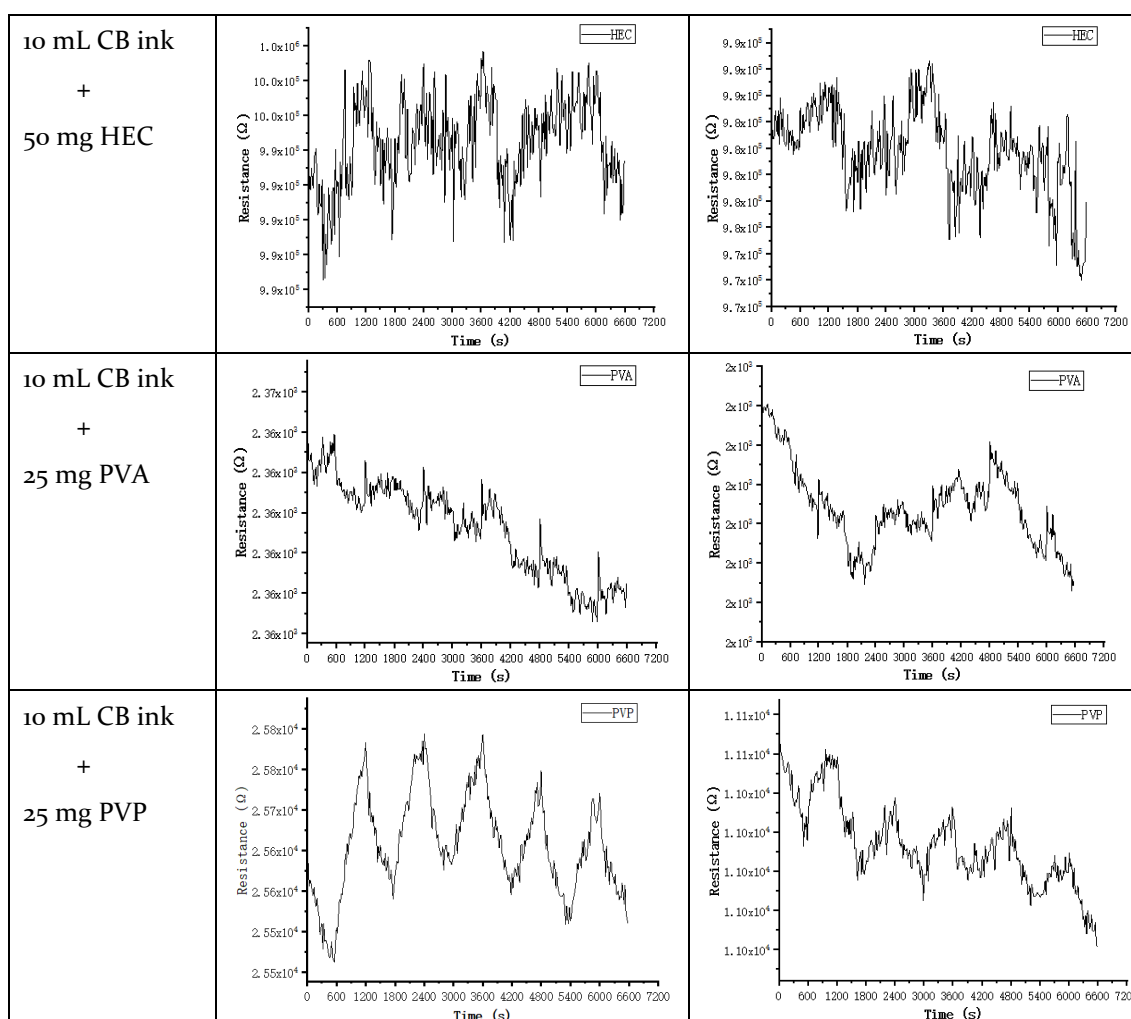
## 2.3 Results and discussion

### 2.3.1 Comparison of gas responses of different polymers

Different polymers have different adsorption effects on gases, resulting in different strength and speed of gas responses<sup>9,10</sup>. In order to select suitable polymers, I carried out gas response detection experiments from many polymeric materials and cellulosic materials. First, 150 mL of water was thoroughly mixed with 5 mg of CB and 75 mg of SDS and sonicated to obtain the simplest CB dispersion. Then different polymers were added to fabricate the sensing film by drop coating. The fabricated sensing films were heated and dried to obtain sensors, and two sensors for each polymer were fabricated. Finally, the air and gas were alternately passed through the air chamber, and the resistance change of the sensor was measured.

Table.2.2 Sensor's responses to acetic acid and ethanol

|                                 | Acetic acid | Ethanol |
|---------------------------------|-------------|---------|
| 10 mL CB ink<br>+<br>200 mg PAA |             |         |



It can be found from Table.2.2 that the sensor with PAA and HEC added did not respond to acetic acid and ethanol. The gas sensor with added PVA has a certain response to acetic acid and ethanol, but the response intensity is very low, and it may be necessary to adjust the amount of PVA to get a better response. The PVP polymer-added sensor responded to both acetic acid and ethanol, but the response to acetic acid was significantly better.

Ethyl cellulose (EC) is a type of cellulose that is soluble in ethanol and insoluble in water. I apply a certain concentration of EC solution to the surface of the PVP film to see if there is a certain selectivity for ethanol and acetic acid gas. From the gas response data in Table.2.3, it can be found that there is no good response effect. The other three polymers, PEG<sub>1450</sub>, PEG<sub>300</sub> and TEG, all had a certain response effect on acetic acid and ethanol gas. From the response graph, it can be found that the response effect of the three polymers to acetic acid is more obvious than that of ethanol. A phenomenon that can also be found is that the rise and fall of the baseline when the polymer responds to the gas is not consistent (PEG<sub>1450</sub> is rising,

others are falling), this interesting phenomenon also deserves further consideration.

Table.2.3 Sensor's responses to acetic acid and ethanol

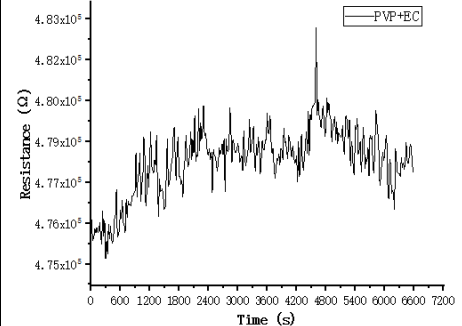
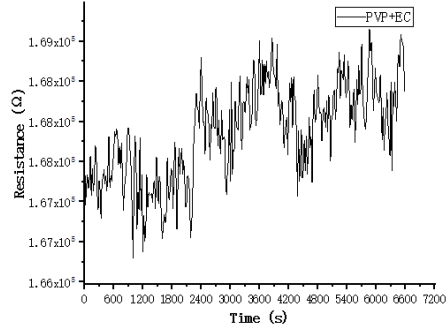
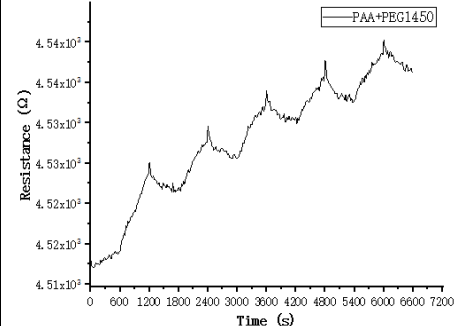
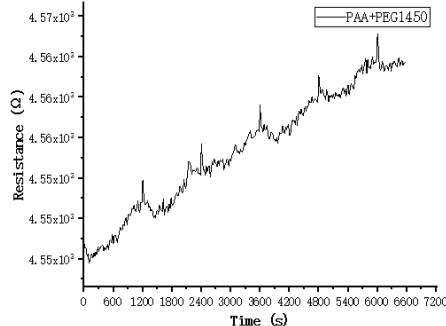
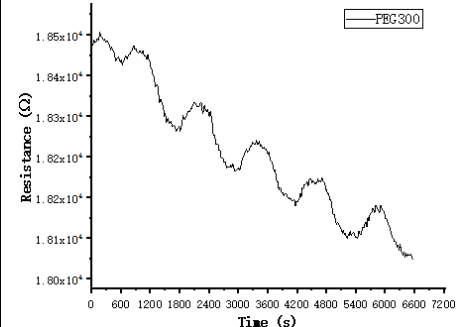
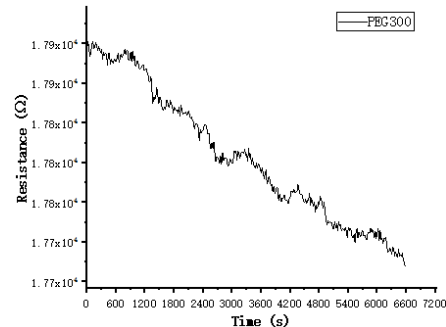
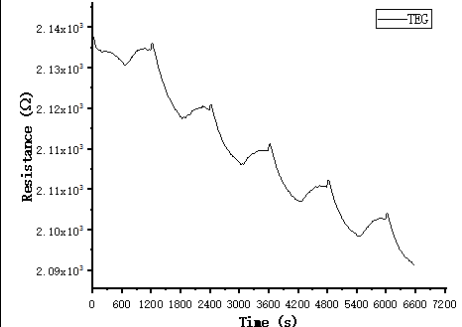
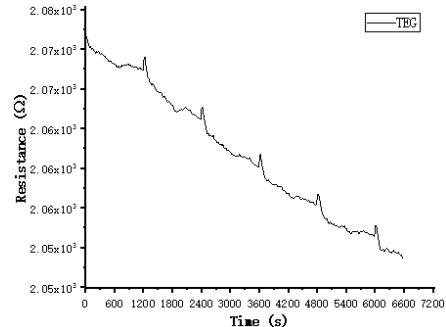
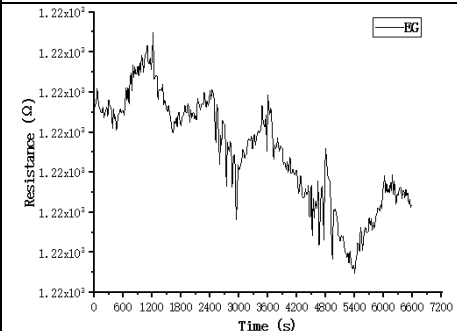
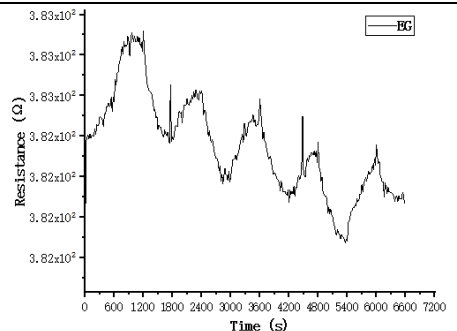
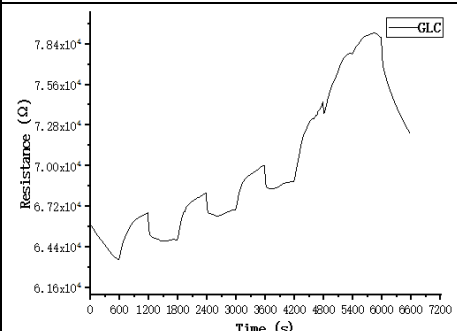
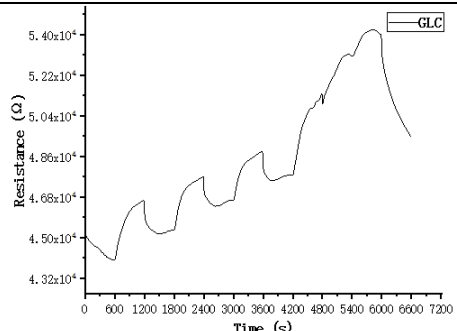
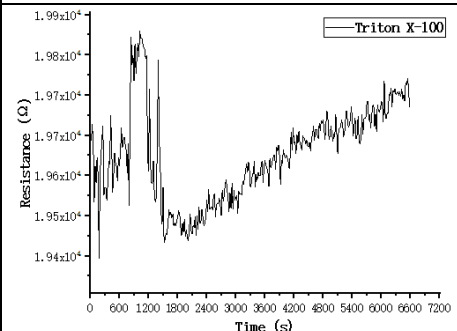
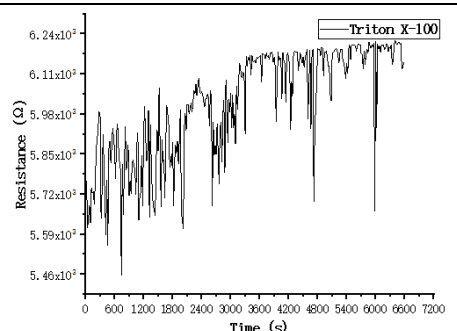
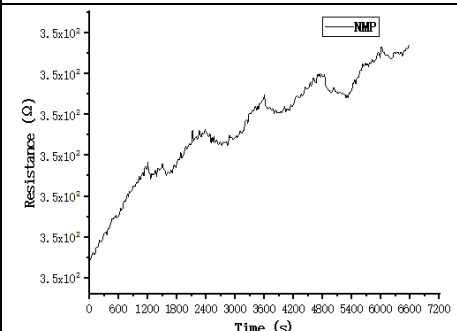
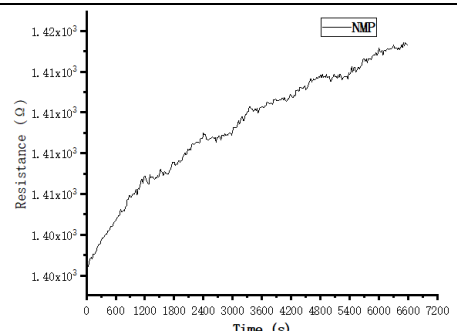
|   | Acetic acid   | Ethanol  |
|---|---|--|
| 10 mL CB ink<br>+<br>25 mg PVP+EC<br>(EC 50mg /10mL<br>ethanol) |    |    |
| 10 mL CB ink<br>+<br>PAA<br>+<br>PEG1450<br>(Not quantitative)  |   |   |
| 10 mL CB ink<br>+<br>3 mL PEG300                                |  |  |
| 10 mL CB ink<br>+<br>3 mL TEG                                   |  |  |

Table.2.4 Sensor's responses to acetic acid.

|  | Acetic acid (sensor 1)  | Acetic acid (sensor 2)   |
|--|---|--|
| 10 mL CB ink<br>+<br>3 mL EG   |    |    |
| 10 mL CB ink<br>+<br>3mL GLC   |   |   |
| 10 mL H <sub>2</sub> O<br>+<br>5mg CB<br>+<br>75 μL<br>Triton X- 100 |  |  |
| 15 mL NMP<br>+<br>10 mg CB   |  |  |

Two sensors of each polymer were fabricated using the same method for sensor 1 and sensor 2 respectively, and their response to acetic acid gas was measured. It can be found from Table.2.4 that if the carbon black solution contains ethylene glycol or glycerol (GLC), it will respond to acetic acid gas. Triton X-100 has no responsive properties to acetic acid gas. NMP solvent itself will have certain response

characteristics to acetic acid gas.

### 2.3.2 Characteristic comparison of sensors produced in different ways

In the past experiments in the laboratory, the drop coating method and the screen-printing method are often used to fabricate the sensing layer. After the improvement of the carbon black ink material, this experiment can further use the inkjet printing method to fabricate the sensing layer.

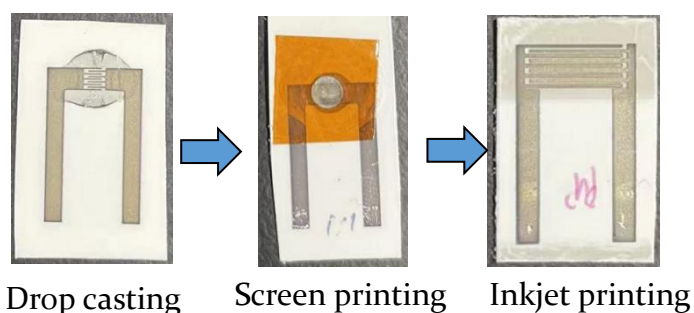


Fig.2.12 Three methods of fabricating sensor films.

The uniformity of the sensing layers fabricated by the three methods is shown in Fig.2.12, which gradually increases from left to right.

In this research, the sensing layers were fabricated in two different ways. One way is to use an inkjet printer to make the sensing layer, and the other is to use a micropipette to make the sensing layer.

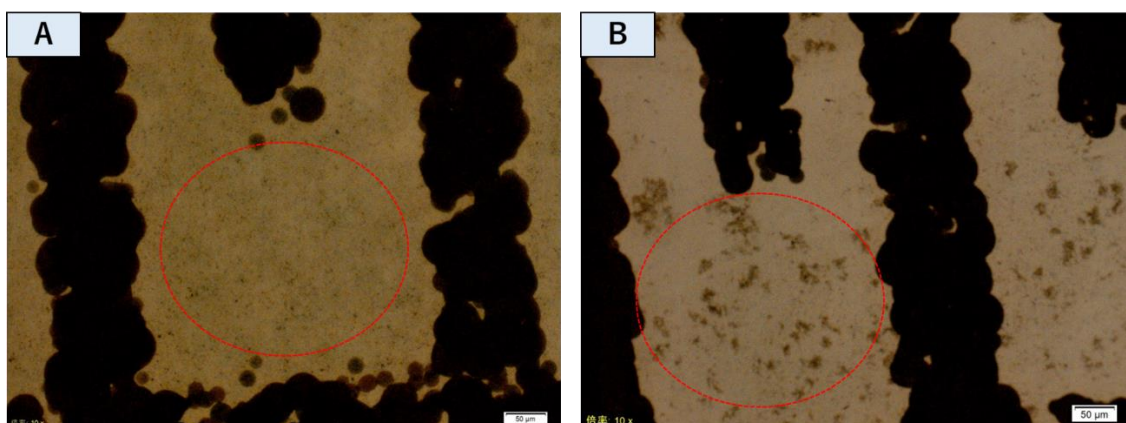


Fig.2.13 The CB layer 50 um micrograph (A) made by inkjet printer and the CB layer 50 um micrograph by micropipette (B).

As shown in Fig.2.13, the dispersion of carbon black in the sensor fabricated by the printer is more uniform, and the carbon black in the sensor fabricated by micrograph will cause aggregation.

In order to compare the sensing performance of sensors fabricated by different methods, I performed gas response experiments.

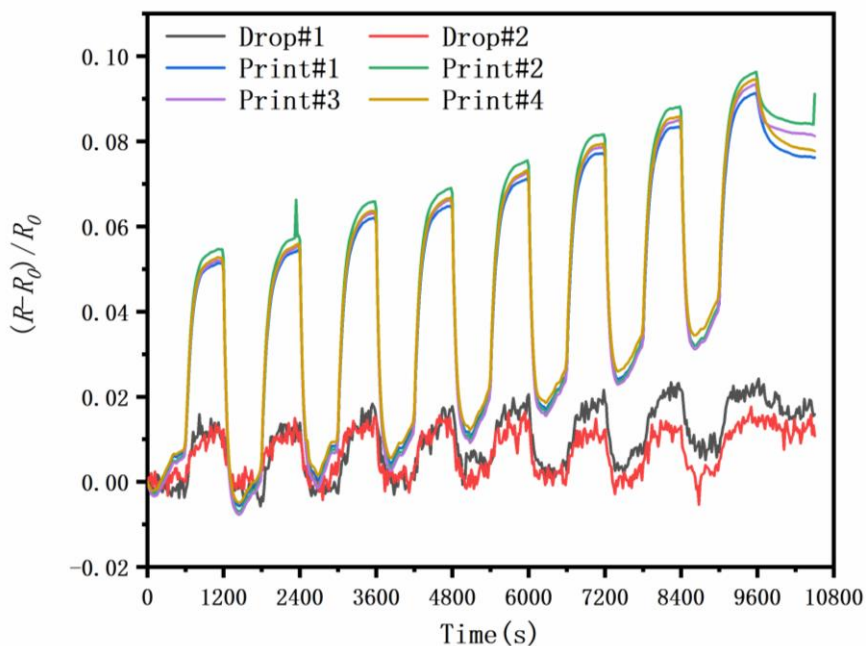


Fig.2.14 Transient response of the sensors to acetic acid gas made by inkjet printer and the sensors made by micropipette.

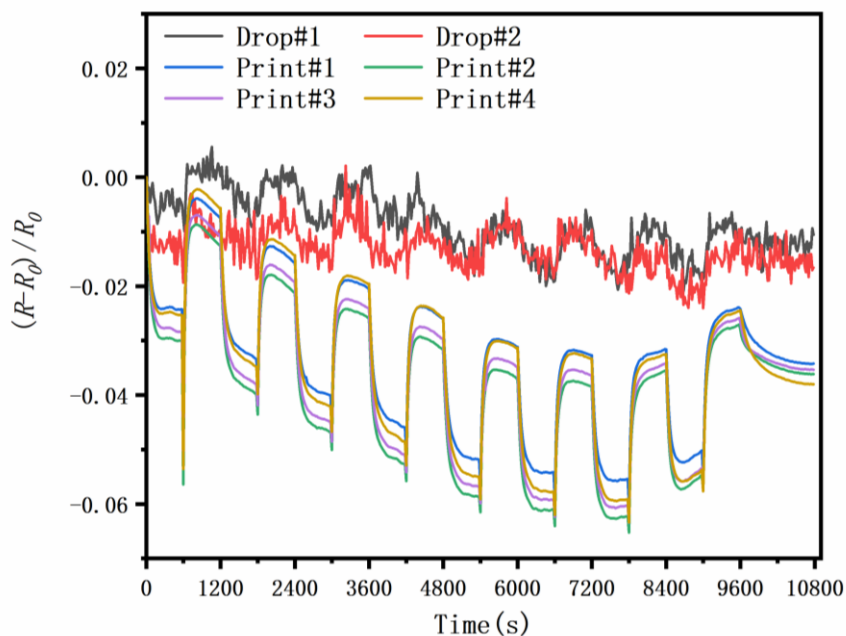


Fig.2.15 Transient response of the sensors to ethanol gas made by inkjet printer and the sensors made by micropipette.

It can be found from Fig.2.14 and Fig.2.15 that the gas response effect of the

sensing layer fabricated by inkjet printer is better. The sensor made by the inkjet printer not only has a greater response intensity, but also has better uniformity of the sensor and less noise in the gas response signal.

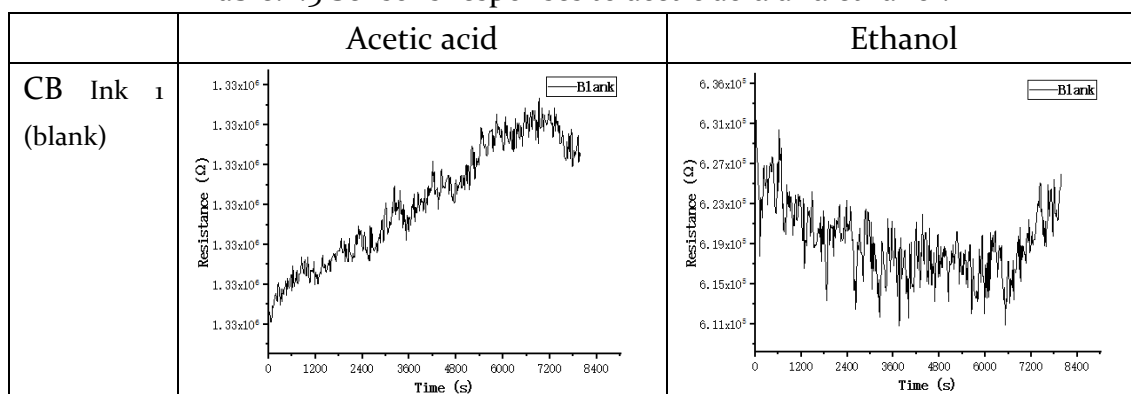
### 2.3.3 Effects of different salts on sensor performance 1

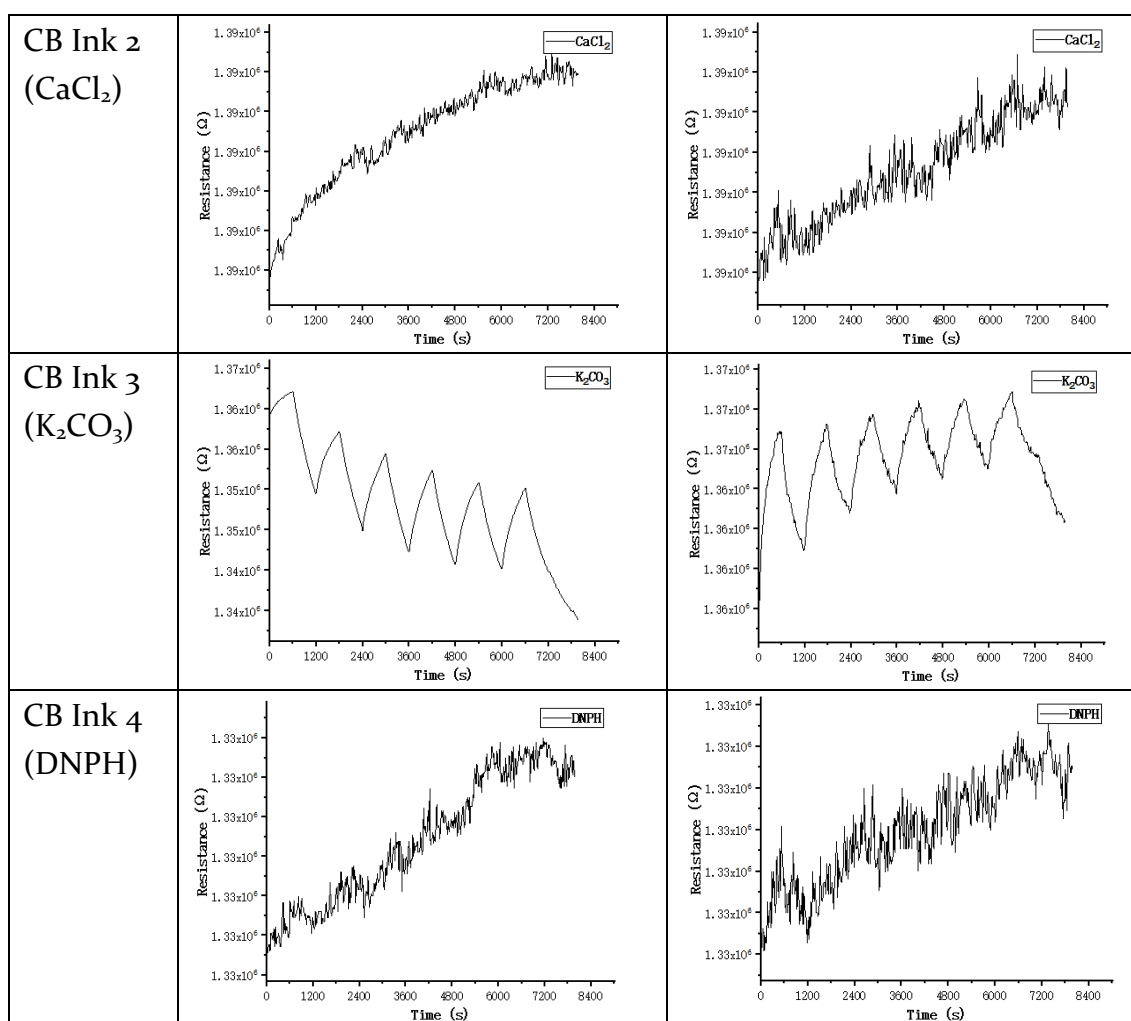
In order to explore the effect of salts on the sensor, I carried out the following experiments. Four kinds of CB inks were prepared in this experiment, and the basic composition of the inks is shown in the table below.

| Composition of the CB ink |           |              |
|---------------------------|-----------|--------------|
| Water                     | 10 mL     |              |
| CB                        | 0.0875 mg |              |
| Triton X-100              | 500 mg    | (Surfactant) |
| Salt                      | 500 mg    |              |

CB ink 1 is the ink used for the control experiment and does not contain salts. The salt in CB ink 2 is  $\text{CaCl}_2$ , that in CB ink 3 is  $\text{K}_2\text{CO}_3$ , and that in CB ink 4 is DNPH. Stirring and sonication were applied to the four solutions to make them well mixed. Finally, the sensors were made by drop coating method ( $5 \mu\text{L}$ ), and 2 sensors of each ink were made.

Table.2.5 Sensor's responses to acetic acid and ethanol.





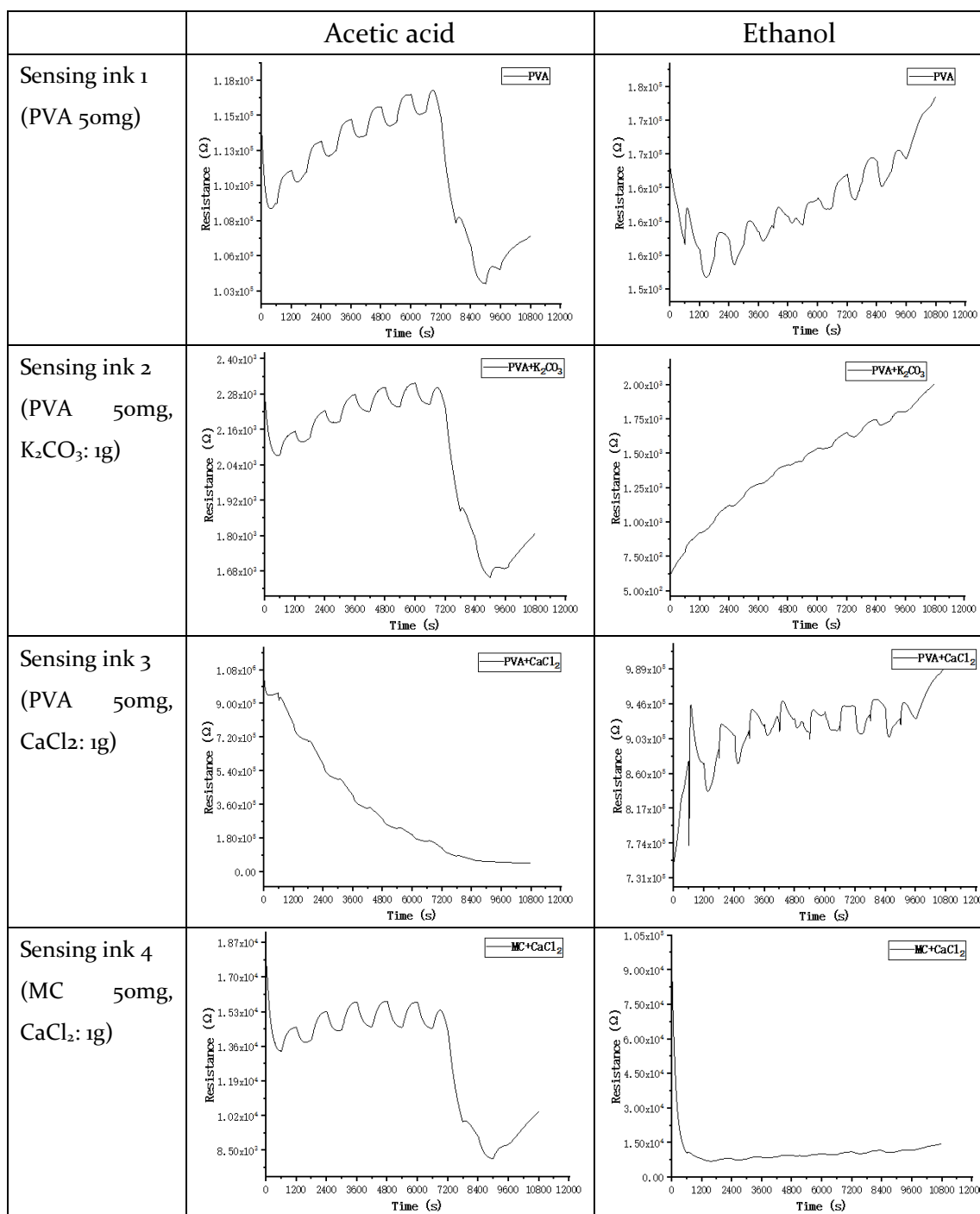
From Table.2.5, it can be found that only the sensing layer with K<sub>2</sub>CO<sub>3</sub> added responds to acetic acid or ethanol gas. After calculation, it can be found that the response intensity is relatively low with the addition of K<sub>2</sub>CO<sub>3</sub> compared to the addition of other polymers, which is about 0.1%.

### 2.3.4 Effects of different salts on sensor performance 2

In order to further explore the effect of salt solution on the response and selectivity of the sensor, in this experiment, the CB layer was first fabricated by the printing method, and then the mixed solution of salt and polymer was drop-coated on the CB layer. The polymers selected for this experiment were PVA and MC, and the salts selected were Na<sub>2</sub>CO<sub>3</sub>, K<sub>2</sub>CO<sub>3</sub> and CaCl<sub>2</sub>. Each ink includes 10 mL of water, 6 mL of ethanol, 50 mg of SDS, 50 mg of polymer, and 1 g of salt. When PVA is mixed with Na<sub>2</sub>CO<sub>3</sub> in proportion and added to the solution, there will be a lot of

PVA insoluble. When MC was mixed with  $\text{Na}_2\text{CO}_3$  or  $\text{K}_2\text{CO}_3$  in proportion and added to the solution, both precipitates were precipitated. Therefore, the above three mixing methods are not the appropriate mixing methods.

Table.2.6 Sensor's responses to acetic acid and ethanol.



A total of four inks were prepared for this experiment, of which ink 1 was used as a control and therefore contained only polymer and no salt. In the gas response experiment, air and the gas to be tested were alternately ventilated into the gas chamber for a total of 8 alternating rounds. The intervals between gas and air exchange during the experiment were all 10 minutes. The resistance of the sensor was measured every 20 seconds, and a total of 540 measurements were taken, and the effect of the sensor response is shown in Table .2.6.

From the Table .2.6, I can find that the solutions containing PVA and  $K_2CO_3$  have good response to acetic acid, but basically no response to ethanol. The response layer made from the solution containing PVA and  $CaCl_2$  responded to acetic acid in general but responded well to ethanol. Therefore, this experiment achieved a certain selectivity of the chemical sensor by mixing salt and polymer.

## 2.4 Conclusion

In this study, the adjustment of carbon black solution parameters made it possible to print carbon black with a home inkjet printer. Compared with drop coating, the carbon particles of the carbon black layer made by the printer are more uniformly dispersed, reducing the effect of the coffee ring effect on the carbon black layer, which is very beneficial for the fabrication of sensors.

There are many kinds of polymers, however, not all of them have certain responding effect to gas. Experiments on the gas responding characteristics of 12 organics were conducted by using drop coating method. Through the experiments, the organics with no response effect at all were excluded, and finally 7 organics were found to have good response effect to gas.

Salts can also influence on the performance of the sensor, and it was eventually found that by mixing salts such as  $K_2CO_3$  and  $CaCl_2$  with PVA or MC polymers, some selectivity for ethanol and acetic acid gases could be achieved. This provides a new idea for fabricated gas sensors with selectivity. This chapter is only a preliminary verification of the possibility of fabricating selective gas sensors by polymers or salts, and the ratio of the various components in the final sensing layer needs to be further adjusted.

## Reference

1. Tang, Y., He, W., Wang, S., Tao, Z. & Cheng, L. The superiority of silver nanoellipsoids synthesized via a new approach in suppressing the coffee-ring effect during drying and film formation processes. *Nanotechnology* **25**, (2014).
2. Malinowski, R., Volpe, G., Parkin, I. P. & Volpe, G. Dynamic Control of Particle Deposition in Evaporating Droplets by an External Point Source of Vapor. *Journal of Physical Chemistry Letters* **9**, 659–664 (2018).
3. Li, H. *et al.* Preventing the coffee-ring effect and aggregate sedimentation by: In situ gelation of monodisperse materials. *Chemical Science* **9**, 7596–7605 (2018).
4. Eral, H. B., Augustine, D. M., Duits, M. H. G. & Mugele, F. Suppressing the coffee stain effect: How to control colloidal self-assembly in evaporating drops using electrowetting. *Soft Matter* **7**, 4954–4958 (2011).
5. Kidner, N. J., Homrighaus, Z. J., Mason, T. O. & Garboczi, E. J. Modeling interdigital electrode structures for the dielectric characterization of electroceramic thin films. *Thin Solid Films* **496**, 539–545 (2006).
6. Kil Yun, B., Soo Kim, H., Joon Ko, Y., Murillo, G. & Hoon Jung, J. Interdigital electrode based triboelectric nanogenerator for effective energy harvesting from water. *Nano Energy* **36**, 233–240 (2017).
7. Ibrahim, M., Claudel, J., Kourtiche, D. & Nadi, M. Geometric parameters optimization of planar interdigitated electrodes for bioimpedance spectroscopy. *Journal of Electrical Bioimpedance* **4**, 13–22 (2013).
8. Liu, C., Hayashi, K. & Toko, K. Au nanoparticles decorated polyaniline nanofiber sensor for detecting volatile sulfur compounds in expired breath. *Sensors and Actuators, B: Chemical* **161**, 504–509 (2012).
9. Pang, H., Xu, L., Yan, D. X. & Li, Z. M. Conductive polymer composites with segregated structures. *Progress in Polymer Science* **39**, 1908–1933 (2014).
10. Pirsá, S. Chemiresistive gas sensors based on conducting polymers. *Materials Science and Engineering: Concepts, Methodologies, Tools, and Applications* **1–3**, 543–574 (2017).

## Chapter 3 Chemiresistor sensor matrix prepared by full-printing processes

### 3.1 Introduction

Organic electronics have received widespread attention because of their many advantages, such as mechanical flexibility, stretchability, and low fabrication cost<sup>1,2</sup>. They can be used in electronic skins, wearable devices, medical monitoring systems, solar cells, and other sensing applications<sup>3-6</sup>. In the process of fabricating organic electronic devices, the most important step is fabrication of films with different functions. For example, an insulating thin film layer is necessary when fabricating an organic field-effect transistor, a thin film for solar energy conversion is important when fabricating a solar cell, the carbon black (CB) film layer can be used to fabricate a pressure sensor<sup>7</sup>, and a gas sensing layer is necessary when fabricating a gas sensor<sup>8</sup>. There are many methods for fabricating thin organic films, such as spin coating<sup>9</sup>, spray coating<sup>10</sup>, drop casting<sup>11</sup>, screen printing<sup>12</sup>, and inkjet printing<sup>13</sup>. Among these methods, drop casting with a micropipette is the simplest method, but the repeatability of electronic device fabrication by the drop casting method is not good. Additionally, the films produced by drop casting easily form a “coffee ring” and then the films become uneven. A coffee ring is the pattern left after a puddle of particle-laden liquid evaporates<sup>14</sup>, and it is very detrimental to thin film production in the field of organic electronics.

Inkjet printing technology has rapidly developed in the field of organic electronic devices because of its advantages of low cost, convenience, simplicity, and reliability<sup>15</sup>. Current inkjet printing technology can control the printed droplets at the picoliter-level, and the diameter of the droplets formed on the substrate can be controlled at the micrometer level<sup>16</sup>, which for the same coffee ring effect at the macroscopic level smaller circles generate a more continuous surface. The films produced by inkjet technology have uniform texture and good repeatability, which improve the performance of organic electronics<sup>17</sup>. The ink is the core of inkjet printing technology<sup>18</sup>. However, it is a complex problem to make functional materials into inkjet printing ink. The chemical properties, evaporation characteristics, and electrical characteristics of the ink directly determine the resolution, number of defects, and adhesion of the organic film<sup>19,20</sup>.

When compared to single sensor, sensor array can add new dimensions to the

observation, helping to estimate more parameters and improve the estimation performance. However, when the number of sensors in the sensor array increases, the conductors used for the measurement also increases, which is inconvenient for measuring resistance. Sensor matrix with multilayer structure can reduce the number of conductors for the measurement, which would be helpful to simplify the sensor measurement system.

Insulating layer is necessary for the multilayer structure. Therefore, insulating inks are important and have many applications in the fields of organic electronics and flexible sensors<sup>21,22</sup>. Kassem et al.<sup>23</sup> proposed a method to prepare thermal curing type insulating ink using polyimide and other materials, and it has been applied to gas sensors. However, in the manufacturing process of the insulating layer, a high temperature heating of was required. This high temperature is destructive to many flexible materials like PET film and photo paper. Lei Xu et al.<sup>24</sup> fabricated a micro/nano gas sensing chip with a five-layer structure. The insulating layer of  $\text{Si}_3\text{N}_4$  was a key layer in the 5-layer structure and it was deposited on the supporting layer by plasma enhanced chemical vapor deposition (PECVD). However, although PECVD method can produce insulation layer at lower temperature, it needs large-scale equipment and high cost. In addition, harmful gas and metal vapor will be produced in the process of film production, which will cause environmental pollution. H.F. CASTRO et al.<sup>25</sup> proposed a method to manufacture the all-inkjet-printed organic thin-film transistors with silver electrodes by a silver ink and an ultraviolet (UV) curable dielectric. The UV curing type ink does not require heat treatment when producing the insulating layer, but it needs to be exposed to ultraviolet light for several seconds. In addition, the surface properties of the insulating layer need to be modified by corona treatment. Without the treatment, the insulating layer is too hydrophobic and does not allow the deposition of the silver ink in fine patterns on it. Therefore, the curing process of UV insulating ink is cumbersome and time-consuming for the present full-inkjet process.

In this study, I used color pigment ink to fabricate the insulating layer, which makes the stacked structure of the IDE possible. This structure makes it possible to reduce the number of conductors used for measurement. In the fabrication process of the insulation layer, there is no need for high temperature heating, UV curing, expensive equipment, only ordinary household-use inkjet printer is enough. As the main components of color ink are polymer and pigment particles, it has a certain function of fixing ink. As a result, silver electrodes can be printed on the surface of

the insulating layer without special treatment. I prepared water-based CB ink that can be printed by an inkjet printer through ultrasonic, filtration, and other steps. The gas sensing layer was fabricated by printing CB ink containing the polymer polyethylene glycol (PEG). By converting functional materials into ink, a flexible and fully printed gas sensor matrix on a photo paper substrate using an inkjet printer was realized. The uniformity and repeatability of the sensor matrix was improved by the fabrication process.

## 3.2 Materials and methods

### 3.2.1 Sensor matrix with multilayer structure

In this work, I propose a novel sensor structure which can flexibly expand sensor channels and can reduce the number of conductors for the measurement in a common sensor array. Thus, a sensor matrix with a multilayer structure was designed. The three views of one unit of a multilayer sensor matrix are shown in Fig.3.1.

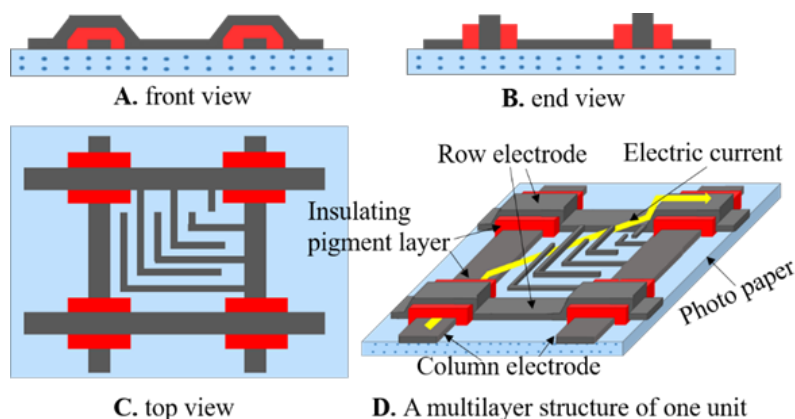


Fig.3.1 Three views of one unit of a multilayer sensor matrix.

### 3.2.2 Materials and inkjet printer specifications

Acetylene carbon black (50% compressed, averaged particle size 20 nm) was purchased from Strem Chemicals, Inc., USA. PEG 300, PAA, acetic acid, THF, acetone, and ethanol were purchased from FUJIFILM Wako Pure Chemical. Sodium dodecyl sulfate (SDS) was purchased from Sigma-Aldrich Chemistry. All the chemicals were used as received. Silver ink (AgIC ink#1000, AgIC, Japan) was poured directly into the cartridge for inkjet printing. Deionized water purified with a Direct-Q Water Purification System was used in all the experiments.

The printing process was performed with a commercially available inkjet printer (PX-105, EPSON, Japan), which was used as received without modification. A piece

of A4-sized photo paper was used as the gas sensor matrix substrate (WPA420PRM, FUJIFILM, Japan). This type of photo paper is suitable not only for dye ink, but also for pigment ink. Two full sets of refillable ink cartridges (IC4CL69 L, YZQ, Japan) for an EPSON PX-105 printer were used for loading the functional inks, including the conductive ink, insulation ink, and CB ink. One set of refillable ink cartridges contained four empty cartridges originally corresponding to black pigment ink, magenta pigment ink, yellow pigment ink, and cyan pigment ink. The print patterns were designed by a free open-source vector graphics editor called Inkscape (version 0.91). For the EPSON PX-105 printer, the print resolution of printouts can be changed through settings in the printer driver and there are four levels of print resolution of printouts can be selected. Higher resolution of printouts means the more dots (of ink) are printed per inch. In order to improve the detail and sharpness of the printed film, the highest print resolution ( $5760 \times 1440$  dpi) of printouts was chosen.

### **3.2.3 Fabrication of PEG-CB ink**

According to the results of our experiment, I found that CB is better dispersed in N-methyl-2-pyrrolidone (NMP) solution and THF solution than in water. However, because of the corrosive nature of NMP solution and the high volatility of THF solution, they are not suitable for an inkjet printer. Therefore, I choose water as the solution to disperse CB. The process of fabricating the CB ink was composed of three steps. First, 10 mg CB, 50 mg PAA and 70 mg SDS were dispersed in 15 mL deionized water and ultrasonication was then performed for 10 min to more uniformly disperse CB. Up to this step, the solution obtained is called CB solution. In the CB solution, the concentration of CB can be adjusted according to the requirements of the experiment, but the proportions of other materials remain unchanged. Finally, the CB ink was obtained by filtering. By adding SDS to the ink, not only can the CB be stably dispersed in water, but also the surface tension of the ink can be made sufficiently low so that the ink droplets can be discharged through the printer nozzle.

Some polymers have certain absorption properties for gases, and different polymers have different absorption properties for a particular gas. The sensing layer for detecting gases was produced by adding 3 mL PEG 300 and 9 mL ethanol to 15 mL CB ink, which is called PEG-CB ink. Ethanol was added to reduce the surface tension of the ink and increase the evaporation rate of the solvent after printing the ink. The specific gravity of the polymer was adjusted by taking into account the

viscosity, surface tension of the ink, and response effect of the gases.

### 3.2.4 Fabrication of the inkjet-printed sensor matrix

The sensor matrix was designed and printed in the multilayer configuration to produce all of the elements of the sensor on the top face of the photo paper. The process steps are shown in Fig.3.2.

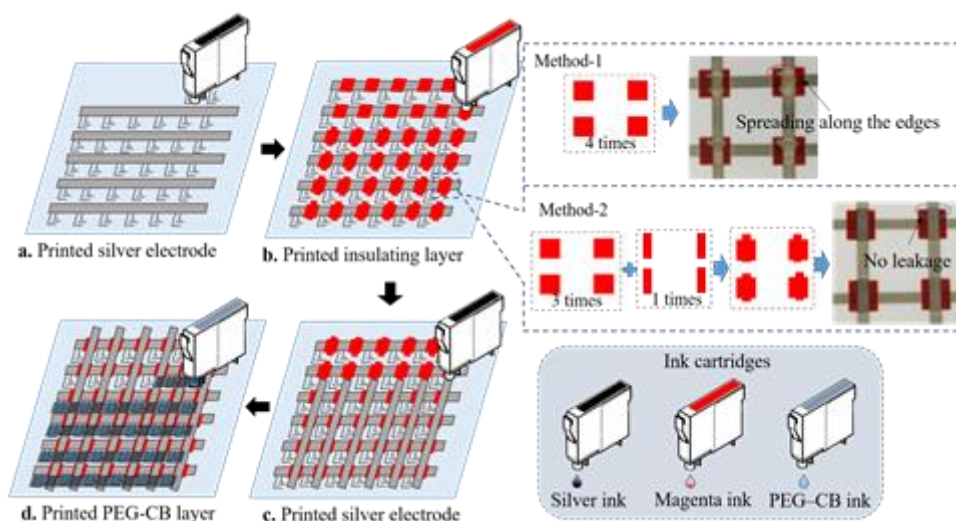


Fig.3.2 Fabrication process of the gas sensor matrix.

The row electrodes and IDEs were printed with an inkjet printer (PX-105, EPSON) using commercially available silver ink (Fig.3.2 a). The width of each IDE was 0.076 mm, and the width of the gap was 0.4 mm. The width of each row electrode or column electrode was 0.8 mm. An insulating layer was added between the row electrodes and column electrodes. The insulating layer was produced by printing commercially available color pigment ink four times (Fig.3.2 b). In the first method, the insulating layer was obtained by printing a square pattern with a side length of 1.6 mm for four times. However, when the silver ink was printed on the insulating layer, the silver ink would be in a liquid state for few seconds before the solvent of the silver ink was completely discharged and it leads to flow along the edge of the insulating layer as shown in Fig.3.2 Method-1. In order to solve this problem, two different sizes of printed patterns were used to make the insulating layer. In the process of printing pigment ink four times, a square pattern with a side length of 1.6 mm was printed three times at first, and a rectangular pattern with dimensions of 1.1 mm × 2.16 mm was printed the fourth time. Then the top silver electrodes can be printed well without spreading at the edges as shown in Fig.3.2 Method-2. Next,

the column electrodes were simultaneously printed over the insulating layer and on the photo paper (Fig.3.2 c). I fabricated the gas sensing layer by combining the CB with PEG polymer. I produced the gas sensing (PEG-CB) layer by printing the PEG-CB ink multiple times (Fig.3.2 d). The number of printing passes of the PEG-CB ink can be adjusted according to the requirement of the IDE resistance value. In this work, I printed the PEG-CB ink eight times. In the printing process, if a nozzle is used to print a different ink, it is necessary to clean the last ink contained in the nozzle with cleaning ink when replacing the ink cartridge. During the cleaning process, the printer's head cleaning program can be used.

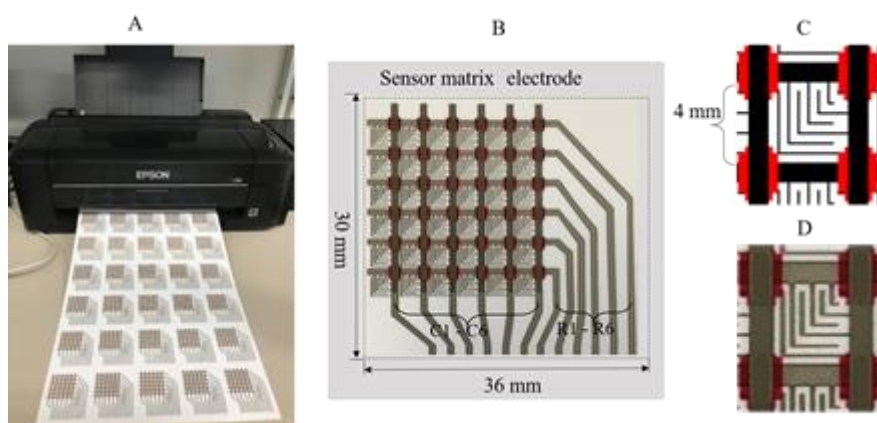


Fig.3.3 (A) Thirty gas sensor matrices printed with a home printer. (B) A sensor matrix containing 36 interdigitated electrodes that can be used to produce gas sensors. (C) Electrode dimensions. (D) An example of a PEG-CB composite printed sensor for reference.

The 30 sensor matrices printed on a piece of A4-sized photo paper with an inkjet printer are shown in Fig.3.3 A. The length and width of a sensor matrix were 36 mm and 30 mm, respectively. Each sensor matrix contained 36 units that can be used as sensors: six row electrodes (C<sub>1</sub>-C<sub>6</sub>) and six column electrodes (R<sub>1</sub>-R<sub>6</sub>) (Fig.3.3 B). I can see that a sensor matrix with multilayer structure can be produced just with 12 electrodes for the measurement and is enough to measure 36 sensors, while at least 37 are needed for a sensor array. To more clearly show the details of the sensor matrix, a design drawing and a photograph of one unit of the sensor matrix are shown in Fig.3.3 C and Fig.3.3 D. The actual sensor was largely consistent with the design objectives.

### 3.2.5 Sensor measurement system

An experimental system for detecting volatile organic compounds was used to

evaluate the performance of the CB-polymer materials for application in chemical gas sensors. The configuration of the system for gas sensing measurement is shown at the top of Fig.3.4 A. I produced dry air with an air pump (LV-125A, Lincoln, Japan) and an air filter containing activated carbon. The flow rate of the dry air was modulated by using two mass flow controllers (MFCs) (3660, Kofloc, Japan) to adjust the flow rate of the carrier gas. A three-way solenoid valve (FSM-0408Y, FLON Industry, Japan) was used to control the flow direction of the carrier gas. A standard gas generator (PD-1B-2, GASTEC Corporation, Japan) was used to generate a specified concentration of gas. A gas washing bottle was used to collect the exhausted gas to not pollute the environment. The system enables effective recovery of gases dissolved in water or ethanol.

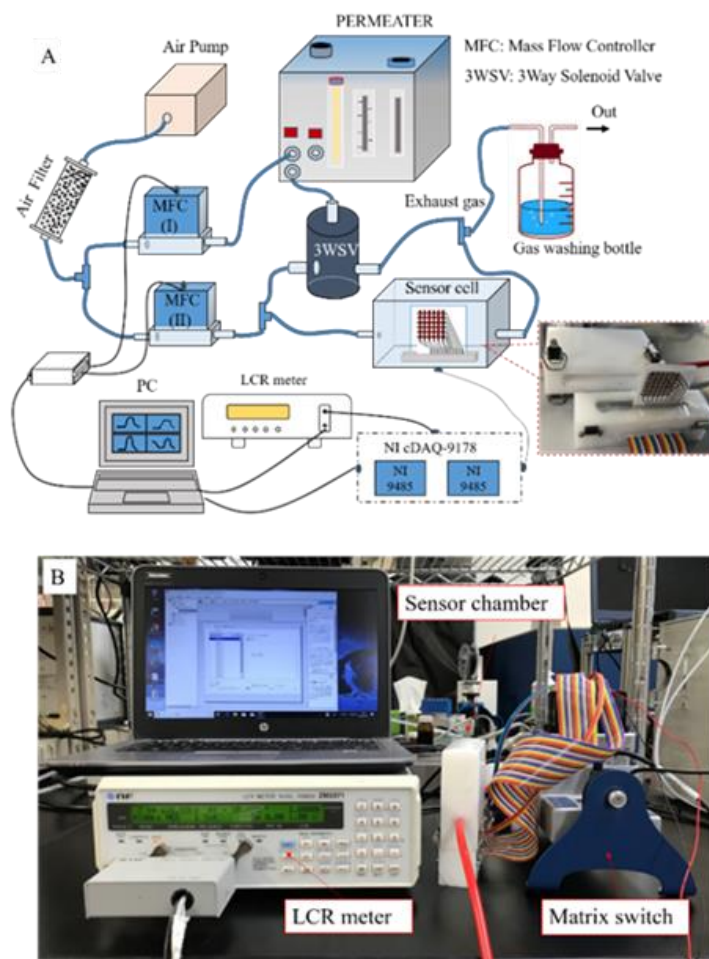


Fig.3.4 (A) Configuration of the experimental sensing apparatus and block diagram of the electrical measurement. (B) Photograph of the experiment setup.

A block diagram of the electrical measurement and a photograph of the sensor interface inside the gas chamber are shown at the bottom of Fig.3.4 A. A DAQ card

(USB-6009, National Instruments, USA) was used to control the MFC to provide an accurate flow rate. An inductance-capacitor-resistance (LCR) meter (ZM2371, NF, Japan) was used to measure the resistance of each channel of the sensor matrix. In order to determine the gas sensing properties, the electrical resistance of the sensor was measured using LCR-meter at frequency of 1 kHz and applied amplitude of 1 V. A NI cDAQ-9178 chassis and two C series relay output modules (NI 9485) were used to switch channels in the sensor matrix. Each NI 9485 module contained eight SSR relays. Therefore, through two NI 9485 modules, a sensor array containing at most 64 units can be measured. The home-made sensor chamber contained a connector to connect the sensor matrix.

A photograph of the system is shown in Fig.3.4 B. Through the LabVIEW software of the computer, the real time change in the resistance of the sensor after flow of the different gases could be observed.

### 3.3 Results and discussion

#### 3.3.1 Method of dispersing CB in water

To disperse CB in water, a dispersant must be added. The dispersant uniformly disperses solid particles that are difficult to dissolve in liquids, and it also prevents settling and coalescence of the particles to form a stable suspension. I found that CB can be dispersed by adding the surfactant SDS or the PAA to water.

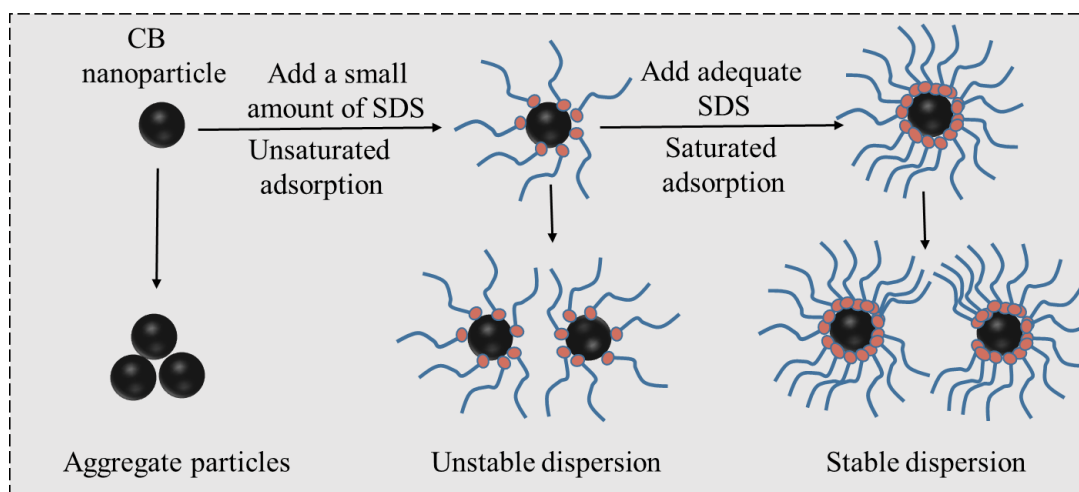


Fig.3.5 Principle of surfactant SDS dispersion of CB.

The principle of surfactant SDS dispersion of CB is shown in Fig.3.5. CB is hydrophobic, and when a surfactant is added, the hydrophobic group binds to the CB surface and the hydrophilic group binds to water, thus helping the CB to disperse. From Fig.3.5, the correct amount of surfactant must be added for CB to be stably

dispersed in water.

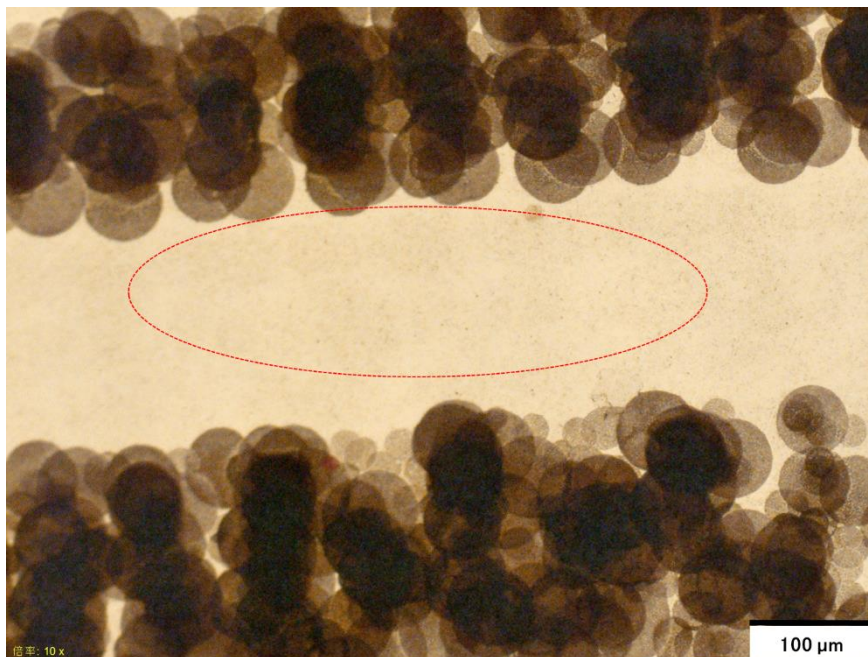


Fig.3.6 Micrographs of the PEG-CB layers (100 μm scale) produced with an inkjet printer.



Fig.3.7 Micrographs of the PEG-CB layers (100 μm scale) produced with a micropipette.

The PAA also has good ability to disperse CB. In the principle of polymer dispersion, not only is electrostatic repulsion between particles included, but the

steric effects generated by the polymer are also exploited. Through experiments, it was found that PAA did not respond to gas. To better disperse CB, the CB for this experiment was dispersed in water using the surfactant SDS and the PAA.

In order to compare the characteristics and gas response effects of the PEG–CB layer produced by the inkjet printing process and the PEG–CB layer produced by the drop coating, I used these two ways to produce it. The first way was with the printer, and the second way was with a micropipette. Micrographs of the PEG–CB layers produced with the printer and a micropipette are shown in Fig.3.6 and Fig.3.7, respectively. The PEG–CB layer produced with the inkjet printer was more uniform than that produced with a micropipette.

### 3.3.2 Measurement of the CB concentration

In order to facilitate the calculation of CB concentration, I define the concentration of CB as the mass ratio of CB to water without other substances. The measurement of the CB concentration needs to be completed before adding the PEG polymer. The absorbance values of CB solutions with known CB concentrations were measured with a spectrophotometer (UV-1800, Shimadzu, Japan).

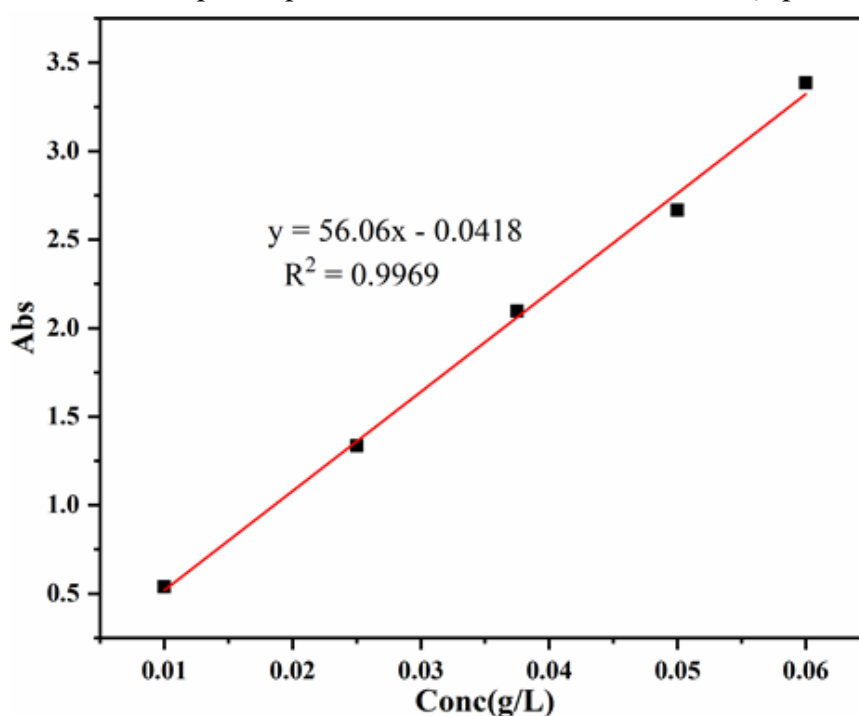


Fig.3.8 Relationship between the concentration of the CB solution and the absorbance.

The relationship between the absorbance and the CB concentration is shown in Fig.3.8. There is a good linear relationship between the concentration of the CB

solution and the absorbance. According to the relationship between the CB concentration and the absorbance in Fig.3.8, the CB concentration of the solution can be calculated by measuring the absorbance of the CB solution after filtration.

Considering the detection capability of the LCR meter and performance of the sensor, the resistance of the IDE containing the PEG-CB layer should be between 1 k $\Omega$  and 100 k $\Omega$ . To simplify the experiment, I used a single interdigitated electrode. Each interdigitated electrode consisted of nine fingers. The dimensions of each finger were 1.622 mm  $\times$  0.108 mm, and the gap between each finger was 0.11 mm. Then five kinds of PEG-CB solution were obtained by adding 3 mL PEG and 9 mL ethanol into 0.02%, 0.035%, 0.05%, 0.075%, and 0.1% CB solutions. The percentage is weight% of CB. The difference between PEG-CB solution and PEG-CB ink was that the CB solution of PEG-CB ink was filtered to ensure that it can be printed. When dispersing carbon black in a solvent, there is a small amount of aggregated carbon black or impurities that cannot be dispersed. The amount of these undispersed substances is very small and hardly has an impact in the drop formation and coffee ring effect. However, due to the large particle size of these undispersed substances, it is destructive to the nozzle of an inkjet printer. Therefore, the filtration is just to prevent the nozzle from being clogged. Forty-eight individual electrodes were divided into six groups, and the eight electrodes in each group were drip coated with 5  $\mu$ L of the corresponding concentration of PEG-CB solution using a micropipette and then dried. The resistance of each group of electrodes was then measured and the average and standard deviation were determined. The relationship between the resistance of the IDE and the PEG-CB concentration was obtained. From Fig.3.9, when the PEG-CB concentration is 0.02%–0.08%, the resistance value is between 1 k $\Omega$  and 100 k $\Omega$ . In this concentration range, the change rate of the resistance value is the highest with a small change in the concentration. Therefore, the concentration of the PEG-CB solution needs to be between 0.02% and 0.08%.

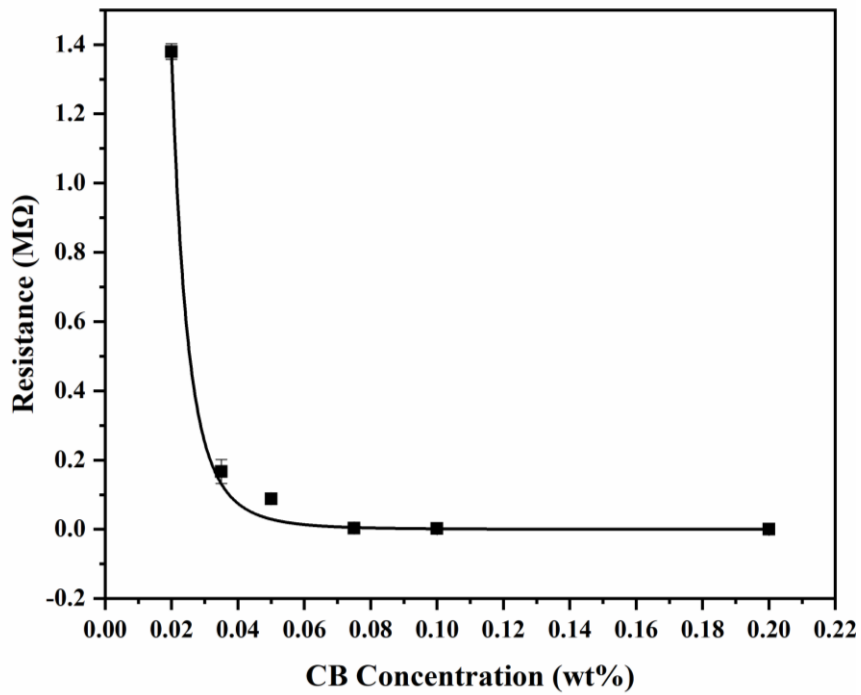


Fig.3.9 Relationship between the resistance and the CB concentration.

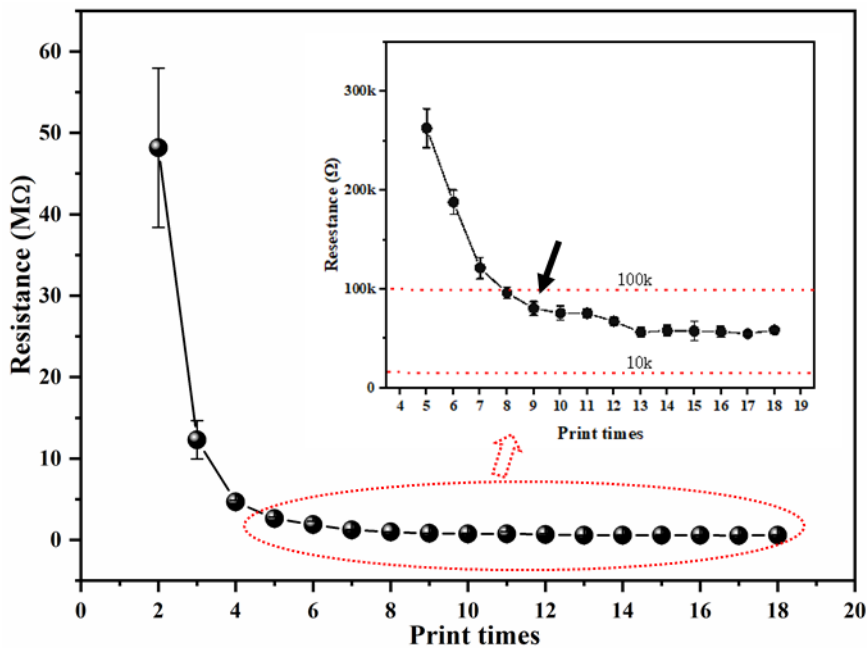


Fig.3.10 Relationship between the resistance and the number of printing passes.

After the PEG-CB solution was treated by filtration, the CB concentration of the solution determined by the above method was approximately 0.05%. The relationship between the number of printing passes of the PEG-CB layer and the

resistance for a large number of single electrodes is shown in Fig.3.10. From Fig.3.10, the PEG-CB ink with this concentration needs to be printed at least nine times before the resistance value of the IDE meets our requirement (1 k $\Omega$  - 100 k $\Omega$ ).

### 3.3.3 Morphology characterization of the insulating layer

To realize the double-layer structure of the silver electrode, an insulating layer needs to be printed on the overlapping portion of the bottom silver electrode and top silver electrode before printing the bottom silver electrode. This insulating layer is required not only to provide an insulating function, but also to be able to continue printing silver electrodes on the insulating layer. Whether color dye ink and color pigment ink can form an insulating layer was tested. Depending on the nature of the ink, the dye ink will penetrate into the photo paper after printing, while the pigment ink will remain on the photo paper surface (Fig.3.11A). When I printed the dye ink on the bottom silver electrode, the ink penetrated under the bottom silver electrode. When the top silver electrode was printed, it directly contacted the bottom silver electrode, causing the double-layer silver electrode structure to fail (Fig.3.11B). By observing the effect of pigment ink printing, it was found that the pigment ink can remain on the surface of the silver electrode and function as an insulating layer (Fig.3.11C).

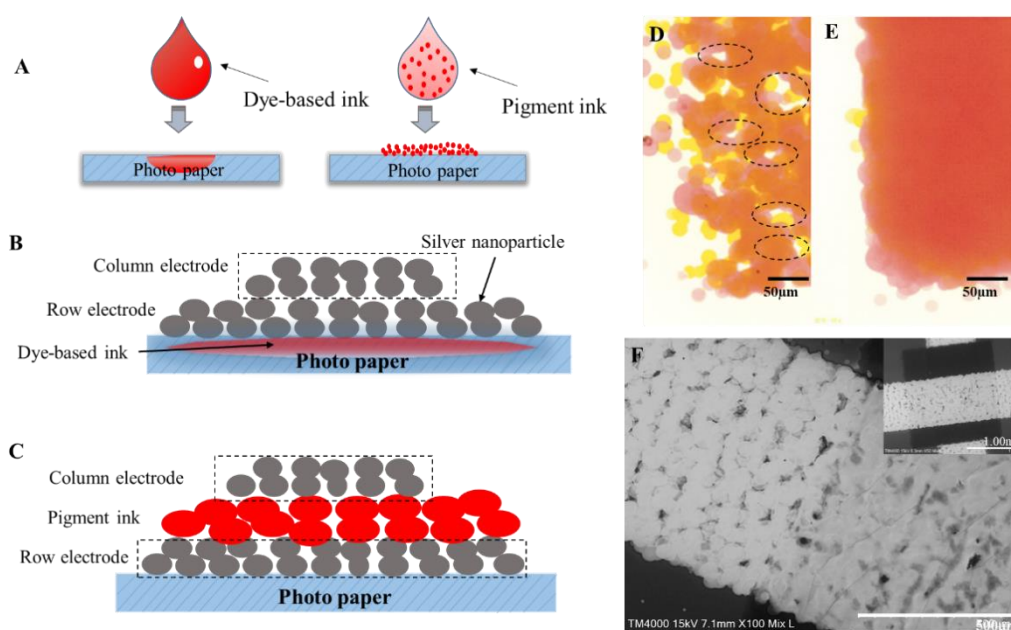


Fig.3.11 (A)–(C) Schematic diagrams of the insulation layer. Micrographs of the pattern after the color pigment ink was printed (D) one and (E) three times. (F) SEM image of the silver electrode on the insulation layer.

After the color pigment ink was printed once, there were a lot of “white pattern” areas not covered by the pigment ink, which are circled by black dashed lines in Fig.3.11D. These areas that are not covered with color pigment ink can lead to failure in insulating layer production. When the color pigment ink was printed three times, white pattern areas were no longer observed (Fig.3.11E). By weighing the insulation effect of the insulation layer and the sensor production efficiency, I chose to print the color pigment ink pattern four times to produce the insulation layer. Black pigment ink, however, contains carbon black, so it is not suitable for insulating layer and in this experiment, the magenta pigment ink was taken as an example to make the insulating layer.

A scanning electron microscopy (SEM) image of the silver electrode on the insulation layer is shown in Fig.3.11F. From the SEM image, the silver ink can be printed on the insulating layer uniformly with the rich solid pattern.

The resistance values of the bottom silver electrodes, the top silver electrodes, and between the top and bottom silver electrodes of the sensor matrix were measured with a digital universal meter (U1273A, Agilent Technologies, American). The resistance of each of the bottom silver electrodes was around  $3\ \Omega$ , the resistance of each of the top silver electrodes was around  $7\ \Omega$ , and the resistance between the top and bottom electrodes was above  $10\ M\Omega$ . An electrical insulator is a material with very little electric current will flow through it under the influence of an electric field. Therefore, according to the definition of the insulator and the results of the experiment, an insulating layer was successfully produced with color pigment ink.

### **3.3.4 The principle of PEG-CB layer responding to gas**

In this experiment, carbon black was used to form conductive composite with PEG in order to prepare sensing material. PEG is a kind of polymer that expands in volume after absorbing gas. As shown in Fig.3.12, when the corresponding gas is introduced, the PEG polymer region absorbs the gas and expands, causing the distance between the carbon black particles to increase. When the direct distance of carbon black increases, the conductivity of the PEG-CB layer decreases and the resistance increases. Since the volume change process is reversible, the PEG-CB layer can be used as a sensing layer for gas detection.

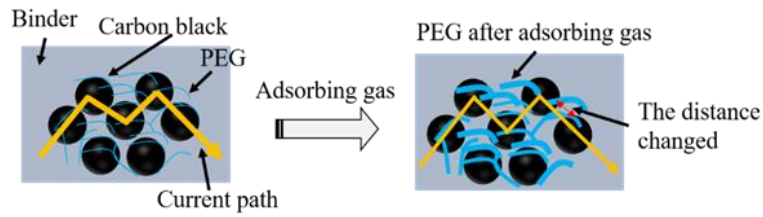


Fig.3.12 The gas response principle.

### 3.3.5 Comparison of resistance stability of sensors produced in different ways

In order to observe the reproducibility and uniformity about sensor matrix to sensor matrix, I made 15 sensor matrices and divided them into 3 groups. In the first group, there are five sensor matrices without PEG-CB layer, which are labeled from S<sub>1</sub> to S<sub>5</sub>. In the second group, there are five sensor matrices with the PEG-CB layer produced with a printer, which are labeled from P<sub>1</sub> to P<sub>5</sub>. In the third group, there are five sensor matrices with the PEG-CB layer produced with a micropipette, which are labeled from M<sub>1</sub> to M<sub>5</sub>. Then the average and standard deviation of the 36 units of each sensor matrix are measured, as shown in Figure 13.

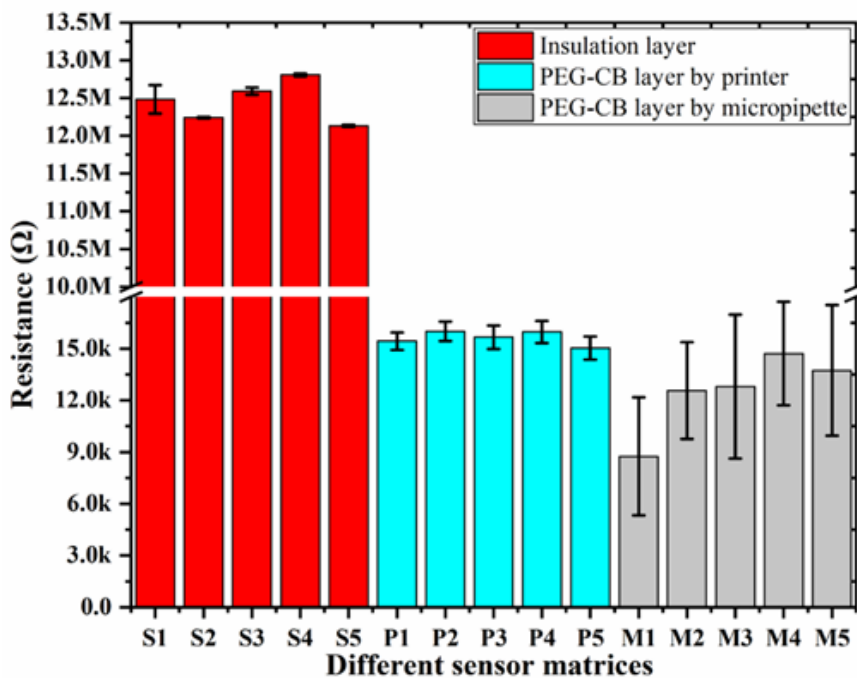


Fig.3.13 Resistance average and standard deviation of different sensor matrices.

As can be seen from Fig.3.13, the standard deviation of the resistance of the PEG-CB layer made by printer is smaller than that of drop coating. This shows that the sensor made by printer is more uniform and has better repeatability.

### 3.3.6 Characteristic comparison of sensors produced in different ways

A control experiment was performed to compare the gas responses of PEG–CB layers produced with the printer and a micropipette. By adjusting the number of printing passes and size of the droplet dropped by the micropipette, the resistance values of the sensing layers produced by the two methods can be made as close as possible. I used these two methods to fabricate two sensors in the sensor matrix to detect the response to ethanol gas. The resistance change was expressed as  $(R-R_0)/R_0$ , where  $R$  is the electrical resistance measured during the test, and  $R_0$  is the initial resistance.

The transient responses of the sensors produced with an inkjet printer and a micropipette to ethanol are shown in Fig.3.14. The sensors fabricated by inkjet printing showed better response strength than those produced with a micropipette.

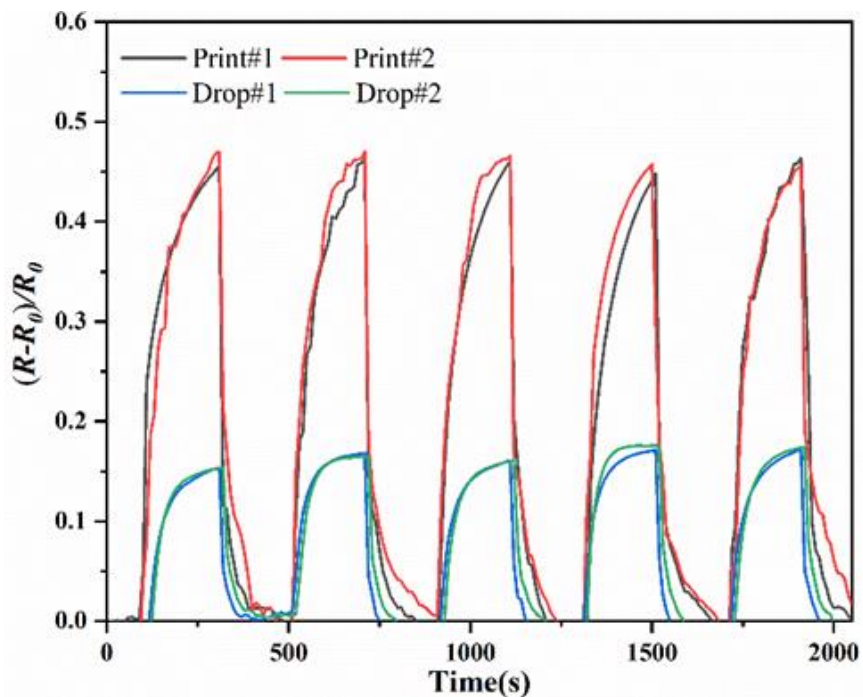


Fig.3.14 Transient response to ethanol gas of sensors produced with an inkjet printer and a micropipette.

The response time and recovery time were defined as the time to reach 80% of the total resistance change<sup>26</sup>.  $T_{80\%p}$  and  $T_{80\%m}$  are the response time to ethanol of gas sensors produced with an inkjet printer and a micropipette, respectively.  $T'_{80\%p}$  and  $T'_{80\%m}$  are the recovery time to ethanol of gas sensors produced with an inkjet printer and a micropipette, respectively. The response and recovery time to ethanol gas of sensors produced with an inkjet printer and a micropipette are shown in

Fig.3.15. Through calculation, the response time  $T_{80\%p}$  and  $T_{80\%m}$  to ethanol gas of sensors produced with an inkjet printer, a micropipette are 184s and 148s respectively with the recovery time  $T'_{80\%p}$  and  $T'_{80\%m}$  are 106s and 84s.

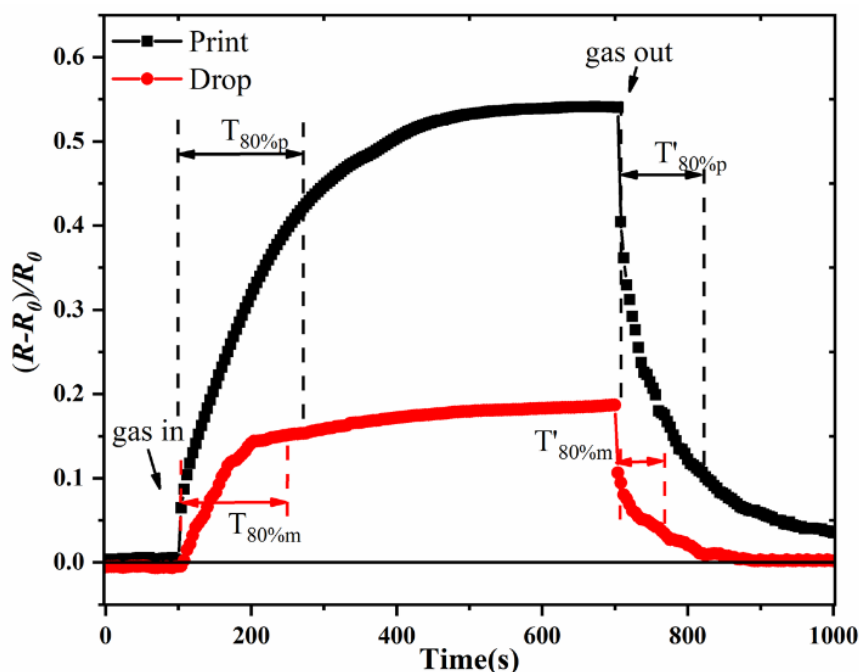


Fig.3.15 The response and recovery time to ethanol gas of sensors produced with an inkjet printer and a micropipette.

Although the response time and recovery time become slower of the sensors fabricated by inkjet printing, the response intensity of the sensors has increased by about three times is shown in Fig.3.14 and Fig.3.15. The reason can be explained by the percolation effect<sup>27,28</sup> and coffee ring effect. According to the percolation effect, in the conductive polymer formed by CB and polymer, the conductivity of the conductive polymer can be divided into three conditions according to the content of CB, as shown in Fig.3.16. There is a percolation condition between the conductive and insulating conditions. In this condition, a small change in the CB content will cause a significant change in the resistivity of the conductive polymer. Therefore, in order to obtain change of conductive path more significantly, the CB content of the PEG-CB layer is controlled in the percolation condition.

However, when the PEG-CB layer is produced with a micropipette, an obvious coffee ring effect will be produced, resulting in uneven CB content in the polymer. The resistance value of the edge area of the PEG-CB layer is too small and enters a conductive condition, losing the ability to respond to gas. The PEG-CB layer produced by inkjet printing can effectively slow down the coffee ring effect due to

the extremely small droplets from the nozzle. Therefore, the area in the percolation condition of the PEG-CB layer produced by inkjet printing is larger than that produced with a micropipette, so the response magnitude is better.

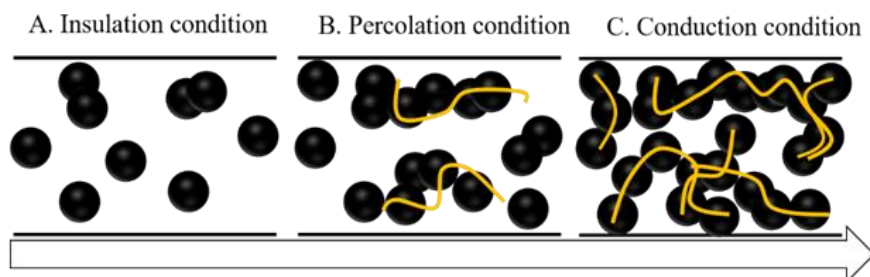


Fig.3.16 Schematic of percolation effect in CB/polymer composites.

According to the response principle of the sensor, the response speed of the sensor is related to the thickness of the PEG-CB layer. The thicker the PEG-CB layer, the longer it takes for the gas to penetrate to the bottom of the PEG-CB layer, and the longer it takes for the gas response to reach the maximum. In this experiment, the resistance values of the sensors produced with an inkjet printer and a micropipette were controlled in the same range. This makes the thickness of the PEG-CB layer produced by the inkjet printing thicker than the thickness of the effective part of that produced with a micropipette, so the gas response becomes slower.

### 3.3.7 Comparison of different gas responses

The responses of the PEG-CB layer to different gases (acetic acid, ethanol, acetone, and THF) were measured at approximately the same gas concentrations. The results are shown in Fig.3.17.

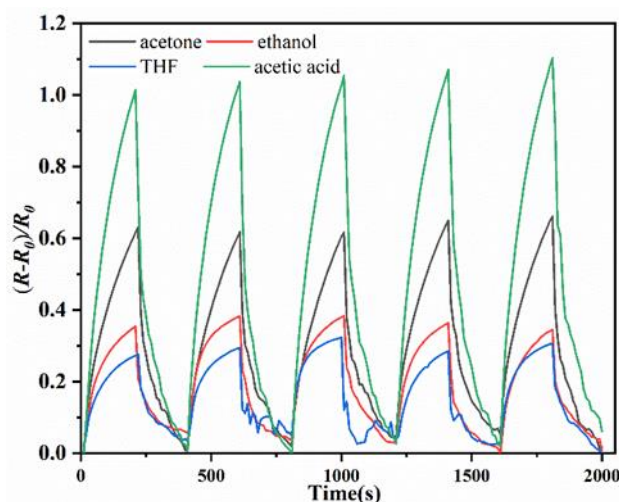


Fig.3.17 Transient responses of the PEG-CB film to different gases.

From Fig.3.17, the PEG–CB film showed good responsiveness to acetic acid, with a rate of change in resistance value of 1. The responses of the PEG–CB film to ethanol and THF were similar, with a rate of change in resistance value of about 0.3. The response of the PEG–CB film to acetone is lower than that of acetic acid, and the rate of change of resistance value is above 0.6. Therefore, I can conclude that the same film has selectivity for different gases.

### 3.4 Conclusion

A flexible gas sensor matrix has been successfully fabricated with an inkjet printer. An insulation layer was fabricated using commercial color pigment ink. I also fabricated the insulating layer with ink based on the composition of commercial color pigment ink. However, it needed to be printed more times to have an insulation effect, so this needs to be further investigated. CB ink containing the polymer PEG was not only uniformly printed on the interdigitated electrode, but it also responded well to gases. From the results of gas response experiments, the printed PEG–CB layer had a more uniform particle distribution and better gas response than the drop-coated PEG–CB layer produced with a micropipette.

### Reference

1. Tehrani, Z. *et al.* Ultra-thin flexible screen printed rechargeable polymer battery for wearable electronic applications. *Org. Electron.* **26**, 386–394 (2015).
2. Chen, Y., Carmichael, R. S. & Carmichael, T. B. Patterned, Flexible, and Stretchable Silver Nanowire/Polymer Composite Films As Transparent Conductive Electrodes. *ACS Appl. Mater. Interfaces* **11**, 31210–31219 (2019).
3. Liu, Y., Pharr, M. & Salvatore, G. A. Lab-on-Skin: A Review of Flexible and Stretchable Electronics for Wearable Health Monitoring. *ACS Nano* **11**, 9614–9635 (2017).
4. Boutry, C. M. *et al.* Biodegradable and flexible arterial-pulse sensor for the wireless monitoring of blood flow. *Nat. Biomed. Eng.* **3**, 47–57 (2019).
5. Lipomi, D. J. & Bao, Z. Stretchable, elastic materials and devices for solar energy conversion. *Energy Environ. Sci.* **4**, 3314–3328 (2011).
6. Hong, S. *et al.* Highly Stretchable and Transparent Metal Nanowire Heater for Wearable Electronics Applications. *Adv. Mater.* **27**, 4744–4751 (2015).
7. Han, Z. *et al.* Ultralow-Cost, Highly Sensitive, and Flexible Pressure Sensors

- Based on Carbon Black and Airlaid Paper for Wearable Electronics. *ACS Appl. Mater. Interfaces* **11**, 33370–33379 (2019).
8. Li, W. *et al.* Sprayed, Scalable, Wearable, and Portable NO<sub>2</sub> Sensor Array Using Fully Flexible AgNPs-All-Carbon Nanostructures. *ACS Appl. Mater. Interfaces* **10**, 34485–34493 (2018).
  9. Abdul Hadi, S. *et al.* Bipolar Cu/HfO<sub>2</sub>/p++ Si Memristors by Sol-Gel Spin Coating Method and Their Application to Environmental Sensing. *Sci. Rep.* **9**, 1–15 (2019).
  10. Ding, J. & Liu, J. An anode-supported solid oxide fuel cell with spray-coated yttria-stabilized zirconia (YSZ) electrolyte film. *Solid State Ionics* **179**, 1246–1249 (2008).
  11. Crenshaw, B. R. & Weder, C. Phase separation of excimer-forming fluorescent dyes and amorphous polymers: A versatile mechanism for sensor applications. *Adv. Mater.* **17**, 1471–1476 (2005).
  12. Dungchai, W., Chailapakul, O. & Henry, C. S. A low-cost, simple, and rapid fabrication method for paper-based microfluidics using wax screen-printing. *Analyst* **136**, 77–82 (2011).
  13. Denneulin, A., Bras, J., Carcone, F., Neuman, C. & Blayo, A. Impact of ink formulation on carbon nanotube network organization within inkjet printed conductive films. *Carbon N. Y.* **49**, 2603–2614 (2011).
  14. Cai, Y. *et al.* Inkjet printing of particle-free silver conductive ink with low sintering temperature on flexible substrates. *Chem. Phys. Lett.* **737**, 136857 (2019).
  15. Secor, E. B., Prabhumirashi, P. L., Puntambekar, K., Geier, M. L. & Hersam, M. C. Inkjet printing of high conductivity, flexible graphene patterns. *J. Phys. Chem. Lett.* **4**, 1347–1351 (2013).
  16. Aminayi, P., Young, B. R., Young, T. L., Sprowl, L. H. & Joyce, M. K. Inkjet printing and surface treatment of an optimized polyurethane-based ink formulation as a suitable insulator over silver for contact with aqueous-based fluids in low-voltage applications. *J. Coatings Technol. Res.* **14**, 641–649 (2017).
  17. Sekitani, T., Noguchi, Y., Zschieschang, U., Klauk, H. & Someya, T. Organic transistors manufactured using inkjet technology with subfemtoliter accuracy. *Proc. Natl. Acad. Sci. U. S. A.* **105**, 4976–4980 (2008).
  18. Dang, M. C., Dung Dang, T. M. & Fribourg-Blanc, E. Inkjet printing technology and conductive inks synthesis for microfabrication techniques.

- Adv. Nat. Sci. Nanosci. Nanotechnol.* **4**, (2013).
19. Gamerith, S. *et al.* Direct ink-jet printing of Ag-Cu nanoparticle and Ag-precursor based electrodes for OFET applications. *Adv. Funct. Mater.* **17**, 3111–3118 (2007).
  20. Doggart, J., Wu, Y. & Zhu, S. Inkjet printing narrow electrodes with <50  $\mu\text{m}$  line width and channel length for organic thin-film transistors. *Appl. Phys. Lett.* **94**, 18–21 (2009).
  21. Kumashiro, Y. *et al.* Novel materials for electronic device fabrication using ink-jet printing technology. *Appl. Surf. Sci.* **256**, 1019–1022 (2009).
  22. Matsui, K. *et al.* Multi-color organic light emitting panels using self-aligned ink-jet printing technology. *Mol. Cryst. Liq. Cryst.* **471**, 261–268 (2007).
  23. Kassem, O., Saadaoui, M., Rieu, M. & Viricelle, J. P. A novel approach to a fully inkjet printed SnO<sub>2</sub>-based gas sensor on a flexible foil. *J. Mater. Chem. C* **7**, 12343–12353 (2019).
  24. Xu, L. *et al.* Micro/nano gas sensors: A new strategy towards in-situ wafer-level fabrication of high-performance gas sensing chips. *Sci. Rep.* **5**, 1–12 (2015).
  25. Castro, H. F. *et al.* All-inkjet-printed bottom-gate thin-film transistors using UV curable dielectric for well-defined source-drain electrodes. *J. Electron. Mater.* **43**, 2631–2636 (2014).
  26. Hsieh, J. C., Liu, C. J. & Ju, Y. H. Response characteristics of lead phthalocyanine gas sensor: Effects of film thickness and crystal morphology. *Thin Solid Films* **322**, 98–103 (1998).
  27. Xu, S. & Rezvanian, O. Related content Percolation Threshold of Carbon Black- Polyethylene Composites. (1997).
  28. Choi, H. J., Kim, M. S., Ahn, D., Yeo, S. Y. & Lee, S. Electrical percolation threshold of carbon black in a polymer matrix and its application to antistatic fibre. *Sci. Rep.* **9**, 1–12 (2019).

# Chapter 4 Sensor matrix printed molecularly imprinted materials for organic acid detection

## 4.1 Introduction

Volatile organic compounds (VOCs) exist in the air in indoor and outdoor environments<sup>1</sup>. Long term exposure to air containing VOCs will have adverse effects on human health and may cause so-called sick building syndrome<sup>2,3</sup>. In addition, the skin and parts of the human body also produce some VOCs<sup>4</sup>. The production of these VOCs is related to gender, age, genetics, physiological state and eating habits<sup>5,6</sup>. Therefore, simple but effective VOC monitoring method development, particularly for room temperature VOC monitoring, is important for fields including air quality monitoring, human health monitoring and medical diagnosis. Traditionally, VOCs have been analyzed via the gas chromatography-mass spectrometry (GC-MS) method<sup>7</sup>. However, because of the disadvantages of GC-MS, e.g., high cost, large volume and non-real-time analysis, it is necessary to develop new sensors to detect organic compounds. Recently, sensors including localized surface plasmon resonance (LSPR) sensors<sup>8</sup>, quartz crystal microbalance (QCM) sensors<sup>9</sup>, surface acoustic wave sensors<sup>10</sup> and metal oxide sensors<sup>11</sup>, were developed for VOC detection.

Chemiresistor-type gas sensors have been widely investigated and used to detect VOCs because of unique advantages that include cost effectiveness, a simple sensing mechanism and easy integration<sup>12</sup>. Their working principle is that when the target gas exists, it can then interact with the sensing material through covalent bonding, hydrogen bonds or molecular recognition, causing the sensing material's resistance to change<sup>13</sup>. The gas can then be detected by measuring the sensing material resistance. A basic chemiresistor gas sensor comprises a set of interdigital electrodes and a sensing layer that covers the electrodes<sup>14,15</sup>. Common sensing layer fabrication methods include drop coating<sup>16</sup>, spin coating<sup>17</sup>, screen printing<sup>18</sup> and inkjet printing<sup>19</sup>. Among these methods, development of chemiresistor gas sensors on flexible substrates using inkjet printing is becoming an important research area<sup>20,21</sup>. This method has attracted extensive attention because this sensor type's advantages include high monitoring sensitivity, light weight, good flexibility and designability<sup>22,23</sup>.

However, VOCs are composed of a complex matrix of chemicals, regardless of

whether these VOCs come from air pollutants<sup>24</sup> or various human body parts<sup>25</sup>, including low molecular weight fatty acids, aldehydes, alcohols, ketones, ethers, and esters. A single chemiresistor gas sensor is a nonspecific sensor and cannot perform more accurate analyses of VOCs with complex compositions. Use of a molecularly imprinted polymer (MIP) sensitive layer combined with the sensor matrix can solve this problem effectively<sup>26</sup>. This technology can realize selective gas molecule recognition. Molecular imprinting represents an effective approach to create recognition patterns with diverse shapes and sizes for target molecules<sup>27</sup>. MIPs are three-dimensional polymer networks obtained by copolymerization of functional monomers with crosslinkers in the presence of target molecules<sup>28</sup>. When the template molecules are removed from a polymer network by washing or heating, nanoscale cavities similar to the template molecules are generated<sup>29,30</sup>. Using these highly specific cavities, MIPs have been applied as highly selective sensing layers in some gas sensors<sup>31</sup>. When the target molecule exists in the cavity within the three-dimensional polymer structure, it will cause the material's resistance to change; the changes are then measured and converted into observable electrical signals. MIPs are used widely in chemiresistor gas sensors because of their low cost, easy synthesis, stable performance and reusability<sup>32</sup>.

In our work, a new stable insulating ink, carbon black (CB) ink and four MIP inks were formulated and were suitable for home printer use. Subsequently, a fully printed flexible gas sensor matrix was fabricated on photographic paper using a home printer. The sensor matrix comprises the following elements:

1. 36 interdigital electrodes that are used to form sensors with sensing layers.
2. 12 silver-based electrodes that connect the interdigital electrodes to the electrical characterization bench; these electrodes are divided into six row electrodes and six column electrodes.
3. An acrylic resin insulating layer that electrically insulates the row electrodes from the column electrodes, which are used to perform the measurements.
4. An MIP-based gas-sensitive layer.

This stacked structure reduces the number of electrodes required for the measurements significantly and leads to easier sensor integration into an electronic data acquisition card. Additionally, in printed electronics, this stacked structure greatly increases the sensor density per unit area when compared with a single-layer sensor array structure.

In this work, I printed acrylic dispersions to produce the insulating layer; this layer can also be used as an ink-absorbing layer by adjusting the film's wettability.

Inkjet printing provides a low-cost MIP thin film fabrication method. I prepared four MIP inks using PAA and four template VOCs (propenoic acid, hexanoic acid, heptanoic acid and octanoic acid). The CB ink and MIP inks were printed on the surfaces of interdigital electrodes as sensing layers. I studied the printability of these inks and performed physical and electrical characterizations.

Finally, I investigated the responses and sensitivity of the sensor matrix to four gases: propenoic acid, hexanoic acid, heptanoic acid and octanoic acid. The optimal CB layer and MIP layer printing times were selected via a control variable method. In addition, I also characterize the stability, repeatability and flexibility of the sensor matrix.

## **4.2 Materials and methods**

### **4.2.1 Materials**

Acetylene CB with diameter of approximately 20 nm was used (STREM CHEMICALS, USA). Ethylene glycol, glycerol, polyoxyethylene(10) octylphenyl ether, PAA, propenoic acid, hexanoic acid, heptanoic acid, octanoic acid, and ethanol were purchased from FUJIFILM Wako Pure Chemical. Sodium dodecyl sulfate (SDS) and hydrochloric acid were purchased from Sigma-Aldrich Chemistry. Ethyl cellulose was purchased from Tokyo Chemical Industry. Vinyblan 735 is a copolymerized resin consisting of vinyl chloride with acrylic acid ester and vinyl acetate. It was received from Nissin Chemical Industry. MYX-2252 is a kind of acrylic resin aqueous dispersion received from Takamatsu Oil & Fat Co., Ltd. M-30 is styrene-maleic acid resin received from SEIKO PMC Corporation. Silver ink (AgIC ink#1000, AgIC, Japan) was poured directly into the cartridge for inkjet printing. All of the chemicals were used as received.

### **4.2.2 Inkjet printer specifications**

To perform inkjet printing, I used a commercially available inkjet printer (PX-105, EPSON, Japan) that was equipped with two full sets of refillable ink cartridges (IC4CL69 L, YZQ, Japan). One set of refillable ink cartridges corresponds to four empty cartridges, and these four empty cartridges correspond to the print heads for four colors of ink (black pigment ink, magenta pigment ink, yellow pigment ink and cyan pigment ink). These refillable ink cartridges were filled with homemade functional inks with adjusted parameters, e.g. viscosity, surface tension and pH value adjustments, to fabricate the sensor matrix. I used a sheet of A4-sized photographic paper (WPA420PRM, Fujifilm, Japan) to act as a flexible substrate for

the sensor and designed the required print patterns using a free vector graphics editor called Inkscape (version 0.91). With regard to the printer's print settings, the paper type and paper quality are the two parameters that must be set. To print out the designed pattern clearly using the corresponding ink, I selected the paper type as *EPSON Photo Matte Paper* and set the quality to *High*.

#### **4.2.3 Preparation of functional ink**

Classified by function, there are three types of functional inks that need to be made by ourselves in our research, namely, CB ink, insulating ink and MIP inks. For the preparation of the CB ink, 5 mg of CB and 100 mg of PAA were added to 9 mL of ethanol. CB can be more evenly dispersed in ethanol solution due to the addition of PAA. In order to prevent the nozzle from being blocked due to too fast ethanol volatilization in the printing process, I added 0.5 mL ethylene glycol and 0.5 mL glycerol to the CB dispersion. 0.1 mL vinyblan 735 was added to prevent any delamination of the CB layer from the paper. After ultrasonic water bath treatment for 20 minutes and filtration through a 5  $\mu\text{m}$  filter, the preparation of CB ink was completed. To formulate the insulating ink, I prepared a solution including 4 mL water, 2 mL ethanol, 6 mL MYX-2252, 50  $\mu\text{L}$  polyoxyethylene (10) octylphenyl ether and 300  $\mu\text{L}$  M-30. Polyoxyethylene (10) octylphenyl ether was used to reduce the surface tension of the ink, and M-30 was used to improve the wettability of the ink. Molecular imprinted polymer inks were prepared by using a simple approach in following four steps: Firstly, four solutions of polymer were prepared by dissolving each 1 g of PAA in 30 mL ethanol. Secondly, 100  $\mu\text{L}$  of template molecules were added in four solutions separately. Here, propanoic acid, hexanoic acid, heptanoic acid, and octanoic acid were selected as the template molecules. Thirdly, 300  $\mu\text{L}$  of hydrochloric acid, 80 mg of SDS, and 50 mg of ethyl cellulose were also added in each solution. Finally, the final solutions needed to be stirred for 4 hours to ensure uniform mixing. Non-imprinted polymer ink (NIP ink) was prepared by the same procedure but without addition of template molecules.

#### **4.2.4 Ink characterization**

Viscosity and surface tension are important parameters to ensure that the ink can be printed by the printer. The viscosity of the ink was measured with a tuning fork vibration viscometer (SV-10, A&D Company, Japan). The surface tension was measured using the wilhelmy plate method (DY-300, Kyowa Interface Science, Japan). The basic principle of this method is that when the wilhelmy plate touches

the liquid surface, the liquid will wet the plate. At this time, surface tension acts along the periphery of the plate and tries to pull the plate into the liquid. Therefore, the measurement of the ink surface tension can be completed by measuring the pulling force. The basic parameters of all functional inks are shown in Table.4.1.

Table.4.1 Properties of functional inks at 28°C.

|                                       | CB ink  | Insulation ink | MIP ink | NIP ink |
|---------------------------------------|---------|----------------|---------|---------|
| Viscosity [mPa s]                     | 1.03    | 3.5            | 1.89    | 1.85    |
| Surface tension [mN m <sup>-1</sup> ] | 22.43   | 29.2           | 25.3    | 24.9    |
| Solid content [wt%]                   | 0.06    | -              | -       | -       |
| Particle size [nm]                    | 20      | -              | -       | -       |
| Solvents                              | Ethanol | Water, Ethanol | Ethanol | Ethanol |

#### 4.2.5 Optical microscopy and scanning electron microscopy (SEM)

Micrographs of the CB layers were acquired via optical microscopy (BX53, Olympus, Japan). The surface morphologies of the silver electrodes on the insulating layers were observed via SEM (TM4000Plus, Hitachi, Japan) at an accelerating voltage of 5 kV, a gun current of 6.4 pA and a working distance of 5.6 mm. Cross-sectional images of the photographic paper substrate and the cross-sections of the silver electrodes were acquired using the same SEM. The field emission gun was operated at an accelerating voltage of 5 kV, a gun current of 6.6 pA and a working distance of 6.6 mm in this case. When the cross-sectional observations were performed, the samples were mounted on a 90° aluminum mount using conductive carbon adhesive tape.

#### 4.2.6 Measurement system fabrication

Gas-sensing measurements were performed in a homemade sensor matrix testing system (Fig. 4.1). The system can be divided into two parts, one is the vapor generation system, and the other is the measurement system in which the sensor matrix responds to the gas. The vapor generation system consists of an air pump (LV-125A, Lincoln, Japan), an air filter, two mass flow controllers (MFCs) (3660, Kofloc, Japan), a standard gas generator (PD-1B-2, GASTEC Corporation, Japan), a three-way solenoid valve (FSM-0408Y, FLON Industry, Japan), and a gas flow meter (Model RK 1450, Kofloc, Japan). The air filter is filled with activated carbon, which can be used to dry the air and then eliminate the influence of water vapor on the

gas response. In this study, MFCs were used to control the flow rate of the carrier gas, and the three-way solenoid valve was used to complete the alternate flow of air and organic gas. MFCs and three-way valve were linked to the computer through a NI DAQ (USB-6009, National instruments, USA) card, and then controlled by LabVIEW software. By adding the liquid corresponding to the VOC analytes into the diffusion tube in the standard gas generator and setting at a controlled temperature to maintain a stable vapor pressure, the standard concentration of gas can be continuously and stably produced.

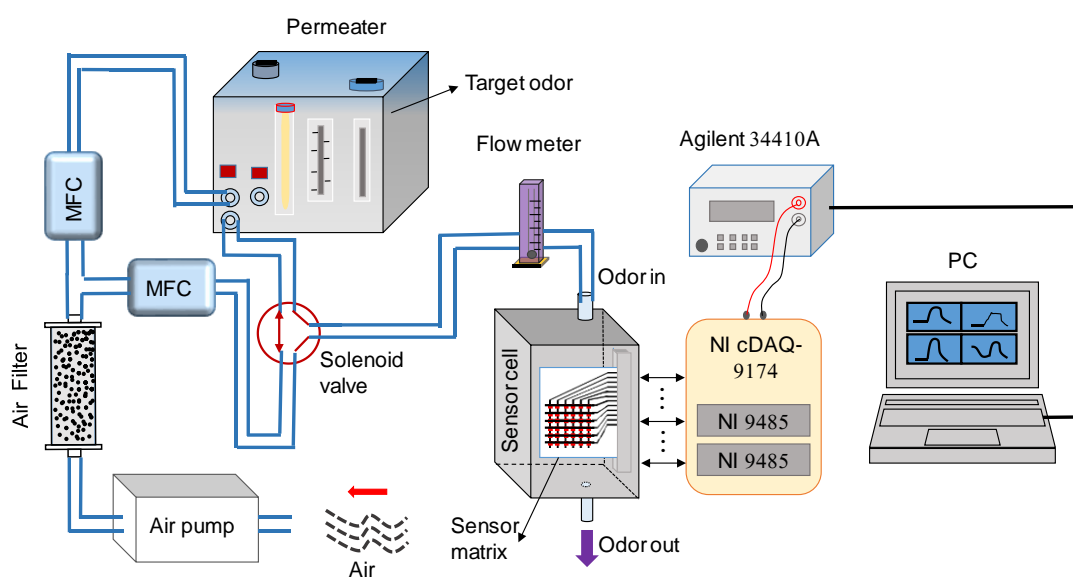


Fig. 4.1 Schematic diagram of the sensor matrix measurement system.

The measurement system consists of a homemade sensor cell, a NI cDAQ-9178 chassis with two C series relay output modules (NI 9485) and a digital multimeter (34110A, Agilent, USA). The sensor matrix was placed in a 3D printed sensor cell with gas inlet and outlet pipelines. Two C series relay output modules were used to select the sensor units of the sensor matrix that need to be measured. The digital multimeter was used to measure and record the resistance change signal of the sensor unit to be tested in the sensor matrix.

The response of the sensor matrix is defined as:

$$\text{Response}(\%) = \frac{(R - R_0)}{R_0} * 100\% \quad (1)$$

where R is the resistance of the sensor matrix in the presence of VOC analytes, and R<sub>0</sub> is the initial resistance.

#### 4.2.7 Sensor matrix fabrication

The sensor matrix was designed and printed in multilayer configuration to embed all the elements of the sensor on the photo paper. The size of a 6×6 sensor matrix with 36 sensor units is 36 mm × 42 mm. A piece of A4 photo paper can produce 30 sensor matrices of this specification. The sensor matrix was fabricated in the following 6 steps, as shown in Fig. 4.2. (a) the row electrodes and interdigital electrodes (IDEs) were printed by using inject printer with commercially available silver ink; (b) A layer with insulation and coating properties is needed between the row electrodes and column electrodes, which is named I&C layer. The I&C layer was produced by printing a square pattern with a side length of 1.6 mm six times using homemade insulating ink; (c) the column electrodes were simultaneously printed over the insulating layer and on the photo paper; (d) the CB layer was produced by printing CB ink multiple times. The printing times of the CB layer can be adjusted according to the needs of the sensor matrix; (e) the MIP layer was produced on the CB layer using MIP ink; (f) After all printing was completed, the sensor matrix needed to be vacuum heated at 40 ° C for half an hour. Through this step, the template molecules in the MIP layer can be removed. A photograph of a completed sensor matrix was shown in Fig. 1b. The key parameters of the interdigital electrode were shown in Fig. 1c. The pitch, gap and width were 0.3 mm, 0.23 mm, and 0.07 mm respectively. Studies have shown that the sensitivity of the sensor can be improved by increasing the electrode density of the IDEs<sup>33</sup>. However, when the distance between the electrodes is too close, the micro-splatter of the ink during printing will create a microscopic electrical path between the printed interdigital electrodes and cause a short circuit. Under the condition that the width of the interdigital electrode is unchanged, the printed interdigitating electrodes with gap G of 230 μm and 180 μm are shown in Fig. 1d and Fig. 1e, respectively. Obviously, it is more appropriate for the gap in the interdigital electrode to be set to 230 μm.

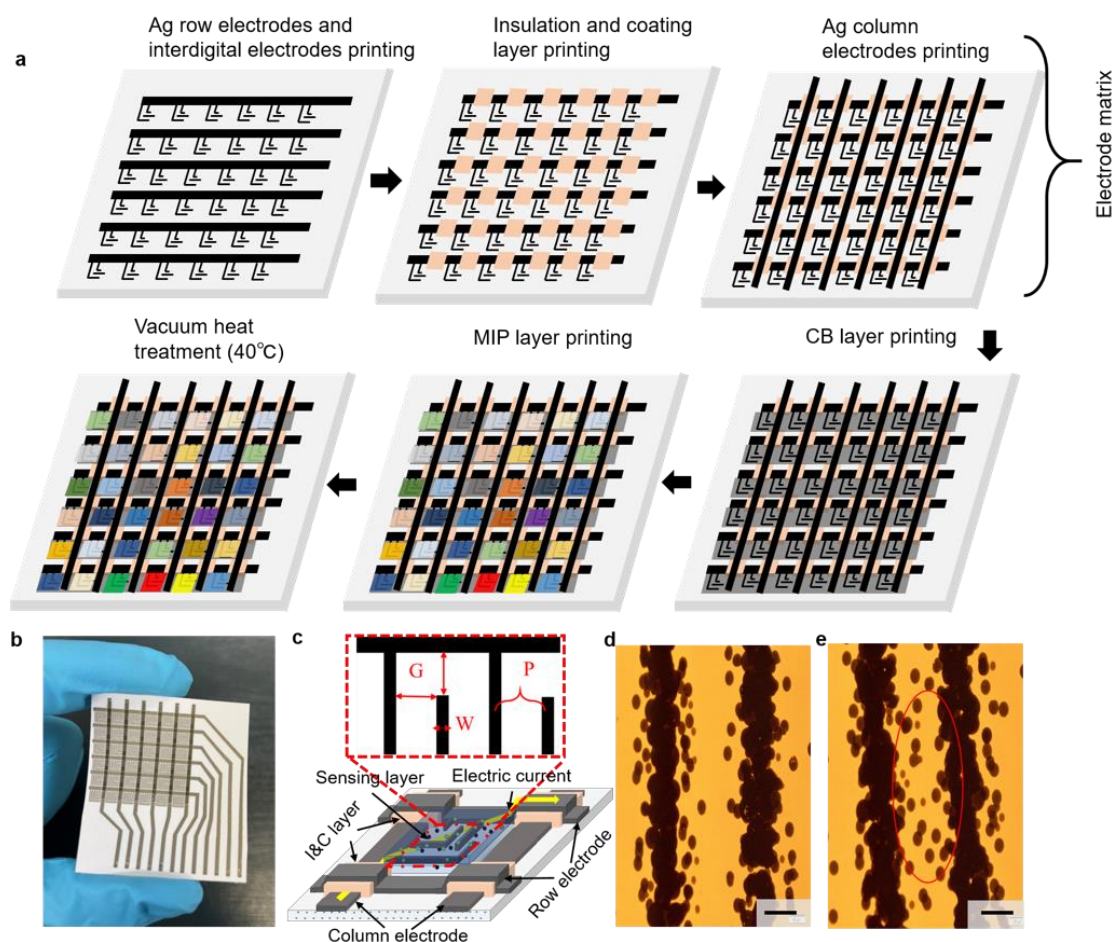


Fig. 4.2 Printed electrode matrix and sensor matrix. a Schematic of the printed sensor matrix fabrication process. b Photograph of completed sensor matrix. c Schematic of the silver interdigital electrode with the pitch (P), gap (G) and width (W) parameters. d Microscope image of  $G=230\ \mu\text{m}$  silver interdigital electrodes. e Microscope image of  $G=180\ \mu\text{m}$  silver interdigital electrodes and interdigital gap showing evidence of silver ink micro-splashing (scale bar=  $100\ \mu\text{m}$ ).

#### 4.2.8 Preparation of I&C layer by inkjet

In this study, the main component of the insulating ink is an acrylic dispersion. The microscopic I&C layer formation process is also the process of thin film formation from the acrylic dispersion liquid. Acrylic dispersions generally have high molecular weight, which aids in high-quality film formation. Formation of the acrylic film is mainly divided into four stages<sup>34</sup>. First, the aqueous acrylic dispersion solution is diluted by adding water and ethanol to produce a solution with a viscosity that can be printed. The state of the acrylic dispersion in water is shown in stage 1 in Fig.4.3a. After the insulating ink is printed on the paper, evaporation of

the water causes the latex solids to be locked together, as shown in state 2 in Fig.4.3a. When the external temperature  $T$  exceeds the minimum film-forming temperature (MFFT), the acrylic solid particles will become closer together until they generate sufficient deformation pressure to form a hexagonal deformation. When  $T$  exceeds the glass transition temperature ( $T_g$ ), the acrylic particles lose their original form completely and form a more coherent film, as shown in state 4 in Fig.4.3a. The coating layer (I&C layer) produced by the insulating ink is a polymer-type layer. After silver ink is printed on this type of layer, it will experience three states, as illustrated in Fig.4.3b. First, the silver ink falls on the coating layer, which will then absorb the solvent from the silver ink and swell. Finally, a dry and stable column electrode layer will form when the solvent volatilizes completely. When a cross-section of the photographic paper is observed via scanning electron microscopy (SEM), the photographic paper is found to be divided into four layers. The paper layer is sandwiched between two PET layers, and a coating layer is formed on top of the PET layer to fix the ink. Further enlarged observation of the coating layer on the photographic paper shows that I have fabricated a double-layer silver electrode structure. In this structure, an I&C layer with insulation and ink fixing functions is sandwiched between the silver row and column electrodes, as shown in Fig.4.3c. The figure shows that the thicknesses of the silver electrode layers and the I&C layer were  $15\ \mu\text{m}$  and  $30\ \mu\text{m}$ , respectively.

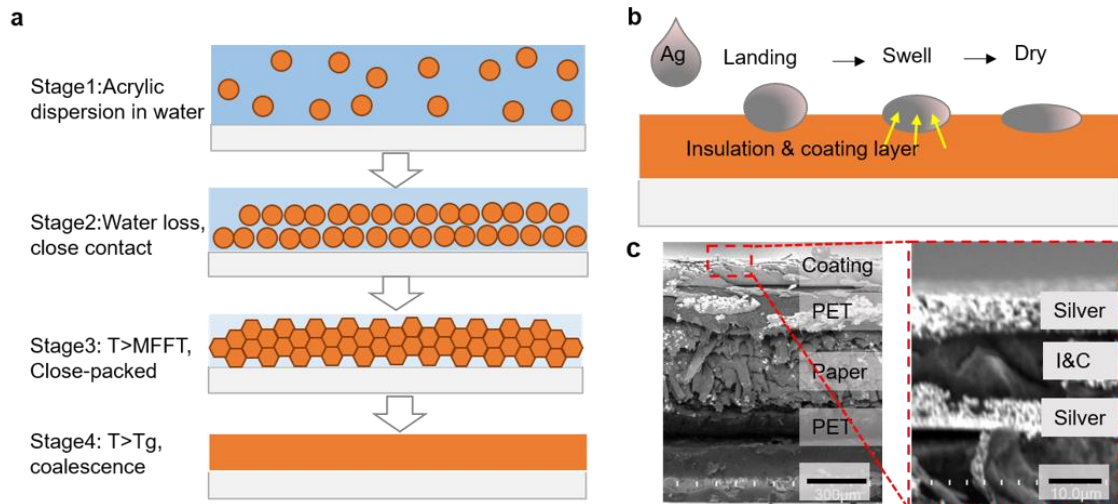


Fig.4.3 Microstructure analysis of I&C layer. a Film formation from acrylic dispersions. b Principle of ink absorption on the polymer-type coating layer. c Cross-sectional scanning electron microscopy (SEM) images of the photographic paper and the I&C layer. Scale bars are  $90\ \mu\text{m}$  (left panels) and  $30\ \mu\text{m}$  (right panels).

## 4.3 Results and discussion

### 4.3.1 Morphology and performance analysis of I&C layer

Experiments have shown that if the I&C layer was fabricated by direct dilution and printing of the MYX-2252 solution (Takamatsu Oil & Fat), the silver electrode printed on the I&C layer surface cannot conduct electricity. As Fig.4.4a shows, multiple cracks can be observed on the top silver electrode surface via SEM. This phenomenon can be explained using wettability. When silver ink drops on the I&C layer surface, the liquid will agglomerate on the solid surface because of its poor wettability. When the liquid is completely dry, cracks form. The wettability can be changed by adding polymers to the solution<sup>35</sup>. In this study, equal masses of PEG polymer and M-30 polymer were added to the solution and the silver electrode printed on the I&C layer surface was observed. The observation results are shown in Fig.4.4b and Fig.4.4c. Comparison shows that the I&C layer fabricated using insulating ink with M-30 has better wettability to the silver ink.

The insulating ink with added M-30 is selected for the relationship experiment between the number of printing times and the insulating effect. With increasing numbers of insulating ink printing times, the resistance of the silver electrodes on the bottom and top layers becomes increasingly high and the insulation effect improves accordingly, as shown in Fig.4.4d. When the insulating ink was printed six times, the resistance of the top and bottom layers reached 765 M $\Omega$ , which met the insulation requirements.

Three I&C layer types were fabricated using three different insulating inks. The insulating ink used to fabricate I&C layer<sub>1</sub> contained no additional polymers and the insulating inks used to fabricate I&C layer<sub>2</sub> and I&C layer<sub>3</sub> contained added PEG polymer and added M-30, respectively. Silver electrodes were printed on the surfaces of the three I&C layers and conductivity tests were performed, with results as shown in Fig.4.4e. Consistent with the SEM observations, the silver electrode print quality was better on the I&C layer made from insulating ink with added M-30.

During production of the sensor matrix, the I&C layer was produced by printing six layers of insulating ink with added M-30. After completion of printing of the top silver electrode on the I&C layer, the resistances of the six top silver electrodes and the six bottom silver electrodes in the sensor matrix were measured. The measurement results are shown in Fig.4.4f, and the uniformity of the resistance values for each electrode layer is good. Although the resistance value of the top silver

electrode is approximately three times that of the bottom silver electrode, this has no effect on the sensor performance.

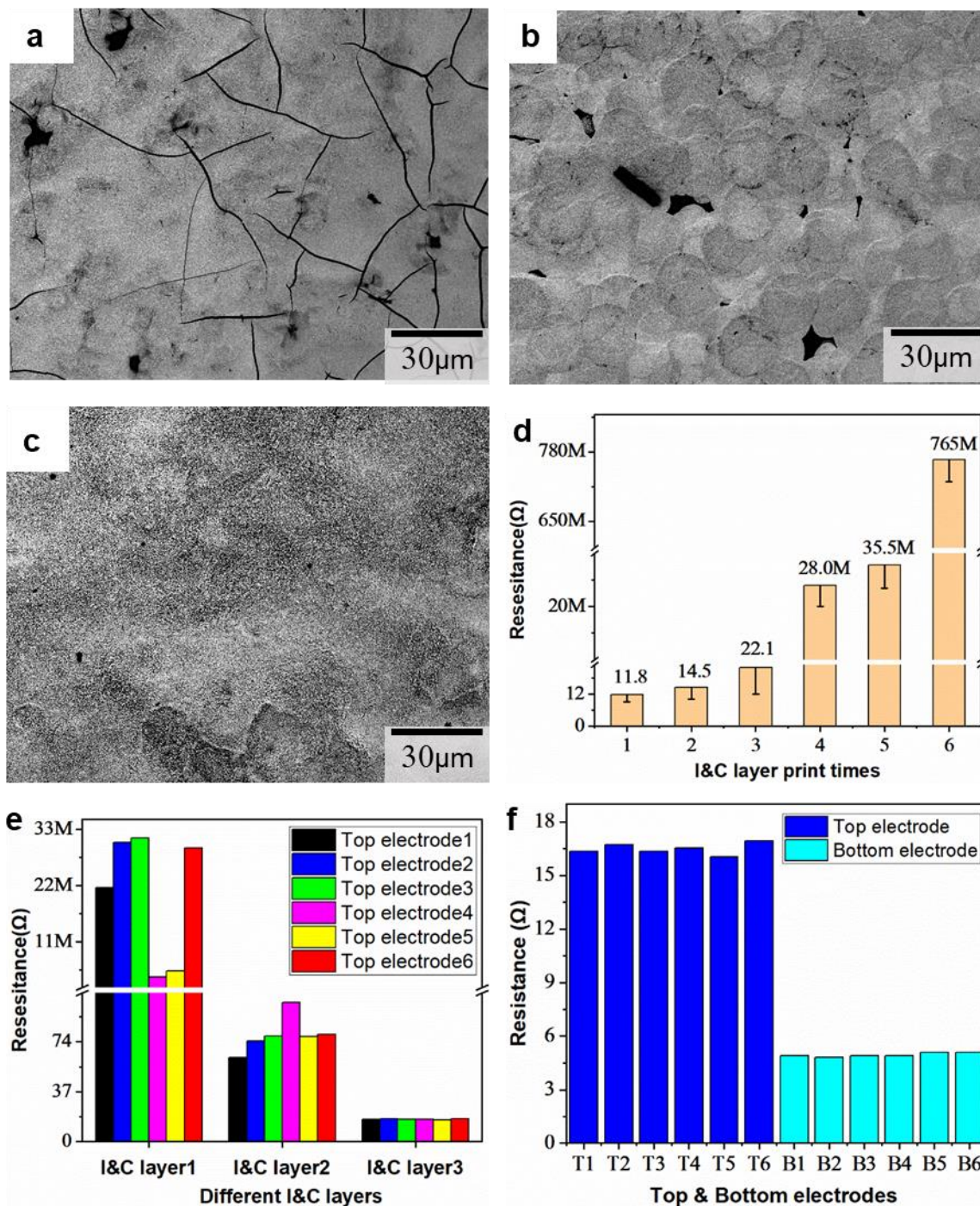


Fig.4.4 Insulation and ink fixing functions of I&C layer. **a** SEM images of top (column) silver electrode printing effects, **a** without adding other polymers, **b** with addition of polyethylene glycol (PEG), and **c** with addition of M-30 polymer to the insulating ink. **d** Change of resistance between row and column electrodes versus

the number of times I&C layers are printed using insulating ink with added M-30.

**e** Comparison of resistance values of top silver electrodes printed on three insulating layer types. **f** Comparison of resistance values of bottom (row) and top (column) silver electrodes of sensor matrix with I&C layers made from insulating ink with added M-30. Scale bars are 30  $\mu\text{m}$  for a–c.

#### 4.3.2 The selectivity of MIP films to the template molecules

I prepared four MIP solutions of saturated fatty acids and evaluated the selectivity of MIPs by SPME-GC-MS method. First of all, I prepared 25 aluminum cups for GC-MS analysis and divided them into 5 groups, respectively, as group 1, group 2, group 3, group 4 and group 5. Then the four MIP and NIP solutions were dropped 80  $\mu\text{L}$  into the 5 aluminum cups in each group. Secondly, aluminum cups containing the same solution in different groups were put into a vacuum drying oven in batches and dried at 40  $^{\circ}\text{C}$  for 8h, so as to completely remove the organic gas molecules and solvents in the sample. Thirdly, after all samples were dried, the GC-MS analysis experiment was performed according to the original group. In order to further determine whether the template molecules in the sample can be removed cleanly by vacuum drying, the 5 samples in group 1 need to be directly placed in the GC-MS instrument to quantitatively analyze the residual VOC after drying. By using the similarity search function on the analyzed data, there is no significant peak related to the template molecule. Therefore, it can be considered that the VOC in the sample can be removed by the vacuum drying method. Finally, the SPME-GC-MS method was used to quantitatively evaluate the amount of VOC absorbed by MIP in this study. The 5 samples in group 2 were placed in the gas chamber and 100ppm of PA gas was stably flowed for 4 hours and then put into the GC-MS instrument for analysis. The analysis results are shown in Fig. 4.5a. It can be seen from the TIC chromatogram that the PA-MIP sample has the largest absorption of PA vapor. As in group 2, the samples in group 3, group 4 and group 5 were also flowed with HA, HPA and OA vapor respectively, and analyzed by GC-MS instrument. In each group, the ratio IF of the TIC value of each MIP to the NIP was used as the standard for evaluating the amount of VOC absorbed by each MIP. That is, the normalized VOC absorption  $IF_{\text{MIP}} = \frac{TIC_{\text{MIP}}}{TIC_{\text{NIP}}}$ . The IF values of the four MIPs for the absorption of the four VOC gases are shown in Fig. 4.5b. The analysis of the results shows that the MIP sample has a stronger adsorption capacity for the corresponding template molecule, but it also has a certain adsorption effect for other gas molecules.

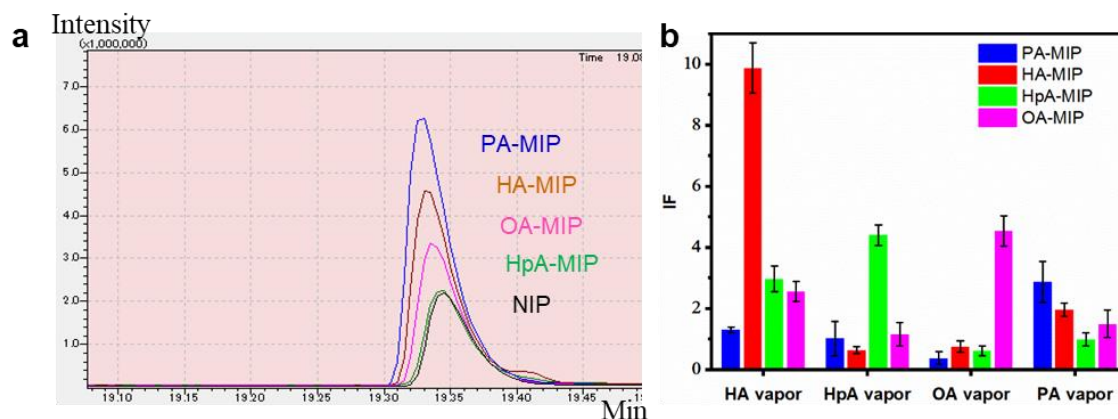


Fig.4.5 **a** GC-MS result of the 4 kinds of MIPs exposed to PA vapors at 100 ppm. **b** SPME-GC-MS result of the 4 kinds of MIPs exposed to 4 kinds of fatty acid vapors (PA/HA/OA/HpA) at 100 ppm.

### 4.3.3 Gas-sensing performance of sensor matrix

The CB layer produced by printer will be more uniform and repeatable. To verify this, I prepared 10 sensor matrices and divided them into 2 groups for experiments. There are five sensor matrices with the CB layer produced using a printer in the first group, which are labeled from P<sub>1</sub> to P<sub>5</sub>. There are five sensor matrices with the CB layer produced using a micropipette, which are labeled from M<sub>1</sub> to M<sub>5</sub>. The resistance value of 36 sensing units of each sensor matrix was measured and the average and standard deviation were calculated, as shown in Fig.4.6a. It can be seen from the calculation results that the standard deviation of the resistance value of the sensor matrix CB layer in group 1 is much smaller than that in group 2. This shows that the CB layer produced by the printer has better repeatability. By observing the CB layer made by the two methods with an optical microscope, it can be found that the texture of the CB layer made by the printer is more uniform, while there are many CB aggregations in the CB layer made by the micropipette, as shown in Fig.4.6b. This phenomenon can be explained as follows: the aggregation of CB in the solution takes a certain time. The ink droplets printed by the printer are at the picoliter level, while the ink droplets produced by the micropipette are at the micrometer level. Therefore, the CB ink printed by the printer dries faster, thereby reducing the aggregation of CB.

In this study, PA-MIP was used as an example to select the best CB layer printing times and MIP layer printing times using the controlled variable method. In order to determine the optimal number of CB layers, 6 sensor matrices were selected to

print the CB layer 1 time, 2 times, 3 times, ... 6 times. After the CB layer was printed, each sensor matrix was printed twice with the PA-MIP layer. Then the average resistance of each sensor matrix and the response to PA vapor at 6 ppm level were measured, as shown in Fig.4.6c. With the increase of the number of printing of the CB layer, the resistance value of the sensor matrix becomes smaller and smaller. The response of gas increases first and then decreases. When printing 3 layers of the CB layer, the gas response was the best. The reason why CB ink printing times can affect gas response can be explained by percolation effect. According to the percolation effect, CB polymer is divided into insulation state, percolation state and conductive state. When the amount of CB in the CB layer is in the percolation state, the response of CB polymer to gas is the best. In order to determine the best printing times of MIP layer, I selected 6 sensor matrices which were printed with 3 layers of CB layer, but PA-MIP layers were printed from 1 to 6 layers for comparative experiments. As shown in Fig.4.6d, when the PA-MIP layer was printed twice, the gas response intensity was the best. With the increase of the number of PA-MIP layers, the response intensity and speed of gas decreased gradually. The gas response principle of this study is that the gas is absorbed by MIP polymer to cause volume expansion, which makes the distance between CB particles farther. When the direct distance of CB particles increases, the conductivity of the CB layer decreases and the resistance increases. Therefore, gas detection can be realized by detecting the change of resistance. However, with the increase of MIP layer thickness, the micro change of volume after MIP layer absorbs gas is difficult to affect the CB layer, so both response intensity and response speed will gradually slow down with the increase of MIP layer number. When there is only one MIP layer, the sensor cannot produce a good response to the gas because of the MIP layer is too thin. In summary, 3 CB layers + 2 MIP layers can produce the best response effect.

In one sensor matrix, five sensing units were selected to print PA-MIP, HA-MIP, HpA-MIP, OA-MIP and NIP layers respectively. Then the experiment took PA gas at 6ppm as an example to test the gas response, and the experimental results were shown in Fig.4.6e. The sensor unit coated with PA-MIP had the best response to PA gas. Although the NIP layer also responds to PA gas, the response strength was relatively weaker than that of MIP. Finally, the HA, HpA, and OA vapor were respectively flowed, and the gas response difference between the printed MIP ink unit and the printed NIP ink unit was used as the normalized response intensity as shown in Fig.4.6f. The experimental results show that the MIP layer has the best

response to the VOC vapor consistent with the template molecules.

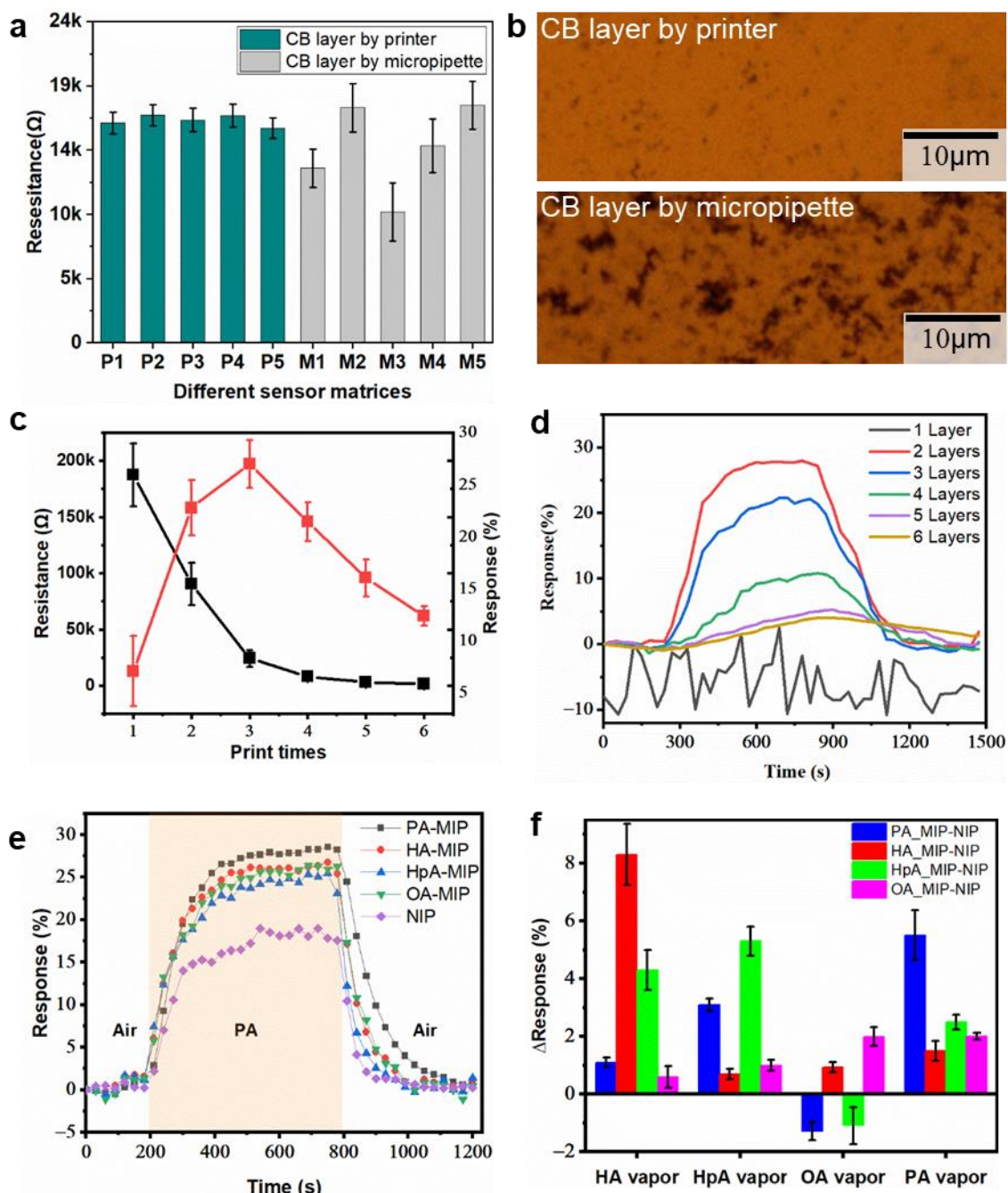


Fig.4.6 Uniformity and selective performance of gas sensor matrix. a Resistance average and standard deviation of different sensor matrices. b Micrographs of the CB layer (50  $\mu\text{m}$  scale) produced with an inkjet printer and a micropipette. c The relationship between CB printing times and the average value of sensor matrix resistance and the response to PA at 6 ppm level. d Changes in PA sensing response with the number of PA-MIP layers. e Real-time responses of sensor unit

coated with PA-MIP, HA-MIP, HpA-MIP, OA-MIP and NIP to PA vapor at 6 ppm level. f Sensitivity of MIP sensor matrix to same concentrations of PA, HA, HpA and OA vapor.

#### **4.3.4 Response characteristics of sensor unit coated with PA-MIP**

I took the sensor unit printed with PA-MIP ink as an example to conduct a gas response characteristic test. Fig.4.7a shows the sensing characteristics of the sensor unit printed with PA-MIP ink when exposed to PA vapor in the concentration range from 3 to 48 ppm. As the concentration of PA vapor increases, the rate of change of sensor resistance also increases. Through this positive correlation curve, the detection of unknown PA vapor concentration can be realized. Fig.4.7b shows the 5-cycle response of the PA-MIP sensing unit exposed to 3ppm PA vapor. From the experimental results, it can be found that the sensor not only has repeatability and recoverability, but also can detect relatively low concentrations of PA vapor.

The response and recovery characteristics of the sensor unit printed with PA-MIP ink to 3 ppm PA vapor were shown in Fig.4.7c. The response time was defined as the time taken to reach 80% of the total resistance change after the introduction of a corresponding organic vapor. The recovery time was defined as the time taken to return to 20% of the baseline resistance after the removal of the target analyte. Through calculation, the response time  $T_{80\%}$  and the recovery time  $T'_{80\%}$  to PA vapor are 200s and 180s respectively.

In addition, the sensor matrix was exposed to 3 ppm of PA vapor for one month. During this month, the response intensity of the sensor to the gas was measured by alternately introducing air and 3ppm PA vapor every 5 days. During this period, the gas response remained stable at around 22.5%, as shown in Fig.4.7d. The results of this experiment show that the sensor matrix has good long-term stability.

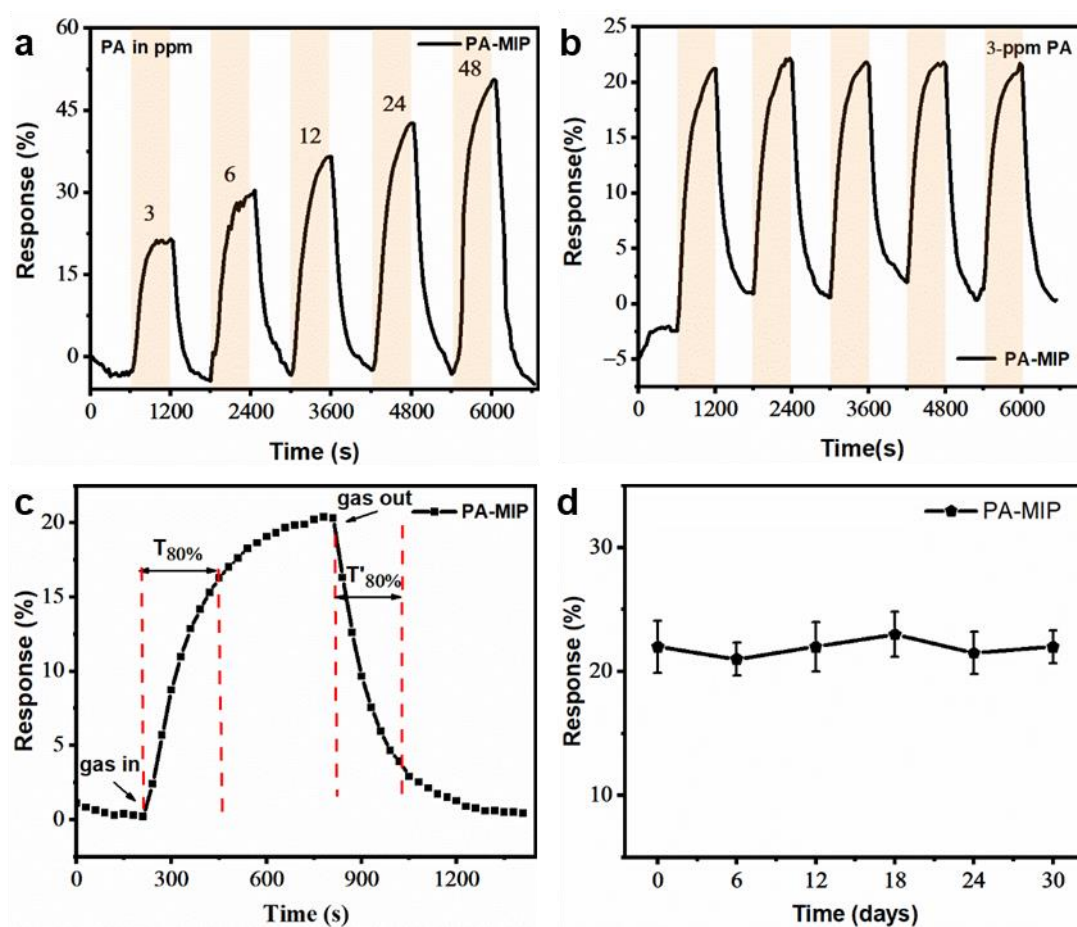


Fig.4.7 Response characteristics of sensor unit coated with PA-MIP. a Real-time sensing response of sensor unit coated with PA-MIP upon PA exposure with concentrations ranging from 3 to 48 ppm. b Cycling performance of sensor unit coated with PA-MIP in response to PA at 3 ppm level. c Response and recovery times calculated for 3 ppm of PA. d Long-term stability of response over a month under 3 ppm of propionic acid for sensor unit coated with PA-MIP.

#### 4.3.5 Mechanical stability of MIP-based sensor matrix

Finally, I characterized the full inkjet printed flexible sensor under the bending test to evaluate its flexibility and mechanical strength. Currently, there is no uniform standard to evaluate the flexibility of flexible devices. The most common method of characterizing flexible device is cyclic bending test by using a  $90^\circ$  bending angle<sup>36,37</sup>.

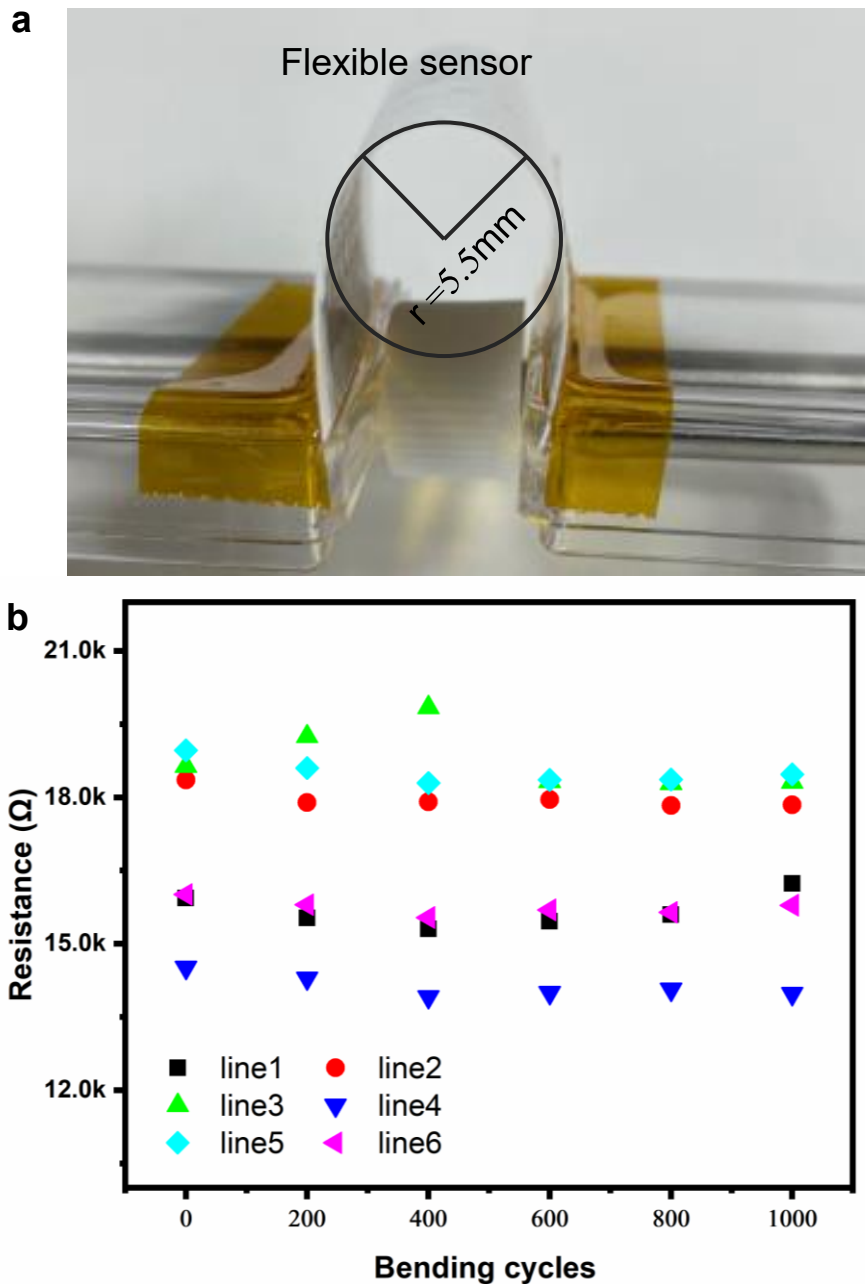


Fig.4.8 Characterization of the sensor matrix under bending tests. a Photograph of a flexible sensor matrix. b Changes in resistance as a function of bending cycles.

As shown in Fig.4.8a, this study conducted a cyclic bending test with a bending radius of 5.5 mm at a speed of 100 bends per minute by using a customized cyclic translational stage. After every 200 bending tests, the average resistance of each column of the sensor matrix is intermittently measured, and the result is shown in Fig.4.8b. The test results show that even after 1000 cycles, the resistance of the sensor matrix does not change by more than 5% at most, which is quite stable. This

shows that the sensor matrix has good flexibility and high mechanical strength. Maintaining the resistance level at the baseline of the sensor shows that extending the bending time will not have a negative impact on the sensing performance of the sensor matrix.

#### 4.4 Conclusion

In summary, a sensor matrix that can be used to detect different types of VOC has been developed using inkjet printing technology to print inks with different functions on a low-cost, environmentally-friendly and recyclable photo paper substrate. The key to this research lies in the development of functional inks such as CB ink, insulating ink, and MIP ink. In order to improve the printability of different inks, the surface tension, viscosity and other parameters of different inks have been optimized separately. The wettability of the film was changed by adding polymer to acrylic emulsion, so that the silver electrode could be printed on the surface of the I&C layer. The gas selectivity of MIP layer was verified by GC-MS analysis instrument and gas response method. I expect that the MIP ink production method of this work will be extended to the development of more VOC MIP materials. Bending and long-term dynamic sensing tests suggest that the sensor matrix has good stability and flexibility.

#### Reference

1. Ohura, T. *et al.* Comparative study on indoor air quality in Japan and China: Characteristics of residential indoor and outdoor VOCs. *Atmos. Environ.* **43**, 6352–6359 (2009).
2. Rostron, J. Sick building syndrome: A review of causes, consequences and remedies. *J. Retail Leis. Prop.* **7**, 291–303 (2008).
3. Chen, W. Y., Yen, C. C., Xue, S., Wang, H. & Stanciu, L. A. Surface Functionalization of Layered Molybdenum Disulfide for the Selective Detection of Volatile Organic Compounds at Room Temperature. *ACS Appl. Mater. Interfaces* **11**, 34135–34143 (2019).
4. Gallagher, M. *et al.* Analyses of volatile organic compounds from human skin. *Br. J. Dermatol.* **159**, 780–791 (2008).
5. Shirasu, M. & Touhara, K. The scent of disease: Volatile organic compounds of the human body related to disease and disorder. *J. Biochem.* **150**, 257–266

- (2011).
6. Mazzatenta, A., Pokorski, M. & Di Giulio, C. Real time analysis of volatile organic compounds (VOCs) in centenarians. *Respir. Physiol. Neurobiol.* **209**, 47–51 (2015).
  7. Boots, A. W. *et al.* Identification of microorganisms based on headspace analysis of volatile organic compounds by gas chromatography-mass spectrometry. *J. Breath Res.* **8**, (2014).
  8. Shang, L., Liu, C., Watanabe, M., Chen, B. & Hayashi, K. LSPR sensor array based on molecularly imprinted sol-gels for pattern recognition of volatile organic acids. *Sensors Actuators, B Chem.* **249**, 14–21 (2017).
  9. Jha, S. K., Liu, C. & Hayashi, K. Molecular imprinted polyacrylic acids based QCM sensor array for recognition of organic acids in body odor. *Sensors Actuators, B Chem.* **204**, 74–87 (2014).
  10. Viespe, C. & Grigoriu, C. Surface acoustic wave sensors with carbon nanotubes and SiO<sub>2</sub>/Si nanoparticles based nanocomposites for VOC detection. *Sensors Actuators, B Chem.* **147**, 43–47 (2010).
  11. Marikutsa, A., Novikova, A., Romyantseva, M., Khmelevsky, N. & Gaskov, A. Comparison of Au-functionalized semiconductor metal oxides in sensitivity to VOC. *Sensors Actuators, B Chem.* **326**, 128980 (2021).
  12. Ge, L. *et al.* Chemiresistor sensor matrix prepared by full-printing processes. *Flex. Print. Electron.* **6**, (2021).
  13. Nazemi, H., Joseph, A., Park, J. & Emadi, A. Advanced micro-and nano-gas sensor technology: A review. *Sensors (Switzerland)* **19**, (2019).
  14. Wohltjen, H., Barger, W. R., Snow, A. W. & Jarvis, N. L. Vapor-Sensitive Chemiresistor Fabricated With Planar Microelectrodes and a Langmuir-Blodgett Organic Semiconductor Film. *IEEE Trans. Electron Devices* **ED-32**, 1170–1174 (1985).
  15. Lange, U. & Mirsky, V. M. Chemiresistors based on conducting polymers: A review on measurement techniques. *Anal. Chim. Acta* **687**, 105–113 (2011).
  16. Briand, D. *et al.* Design and fabrication of high-temperature micro-hotplates for drop-coated gas sensors. *Sensors Actuators, B Chem.* **68**, 223–233 (2000).
  17. Chen, B. *et al.* Molecularly imprinted sol-gel/Au@Ag core-shell nano-urchin localized surface plasmon resonance sensor designed in reflection mode for detection of organic acid vapors. *Biosens. Bioelectron.* **169**, 112639 (2020).

18. Moon, S. E. *et al.* Low power consumption micro C<sub>2</sub>H<sub>5</sub>OH gas sensor based on micro-heater and screen printing technique. *Sensors Actuators, B Chem.* **187**, 598–603 (2013).
19. Rieu, M. *et al.* Fully inkjet printed SnO<sub>2</sub> gas sensor on plastic substrate. *Sensors Actuators, B Chem.* **236**, 1091–1097 (2016).
20. Khan, S. & Briand, D. All-printed low-power metal oxide gas sensors on polymeric substrates. *Flex. Print. Electron.* **4**, 0–8 (2019).
21. Yuan, Y. *et al.* Convenient CNT-Paper Gas Sensors Prepared by a Household Inkjet Printer. *ACS Omega* **5**, 32877–32882 (2020).
22. Mkhize, N., Murugappan, K., Castell, M. R. & Bhaskaran, H. Electrohydrodynamic jet printed conducting polymer for enhanced chemiresistive gas sensors. *J. Mater. Chem. C* **9**, 4591–4596 (2021).
23. Fioravanti, A. & Carotta, M. C. Year 2020: A snapshot of the last progress in flexible printed gas sensors. *Appl. Sci.* **10**, (2020).
24. Zhang, X. *et al.* Characteristics, reactivity and source apportionment of ambient volatile organic compounds (VOCs) in a typical tourist city. *Atmos. Environ.* **215**, 116898 (2019).
25. Drabińska, N. *et al.* A literature survey of all volatiles from healthy human breath and bodily fluids: The human volatilome. *Journal of Breath Research* (2021) doi:10.1088/1752-7163/abfido.
26. Shimizu, K. D. & Stephenson, C. J. Molecularly imprinted polymer sensor arrays. *Curr. Opin. Chem. Biol.* **14**, 743–750 (2010).
27. Janfaza, S. *et al.* A selective chemiresistive sensor for the cancer-related volatile organic compound hexanal by using molecularly imprinted polymers and multiwalled carbon nanotubes. *Microchim. Acta* **186**, (2019).
28. Bin, C., Chuanjun, L. & Kenshi, H. Selective Terpene Vapor Detection Using Molecularly Imprinted Polymer Coated Au Nanoparticle LSPR Sensor. *Ieee Sensors Journal*, **14**, 3458–3464 (2014).
29. Hu, Y. *et al.* The amino-terminal structure of human fragile X mental retardation protein obtained using precipitant-immobilized imprinted polymers. *Nat. Commun.* **6**, (2015).
30. Vasapollo, G. *et al.* Molecularly imprinted polymers: Present and future prospective. *Int. J. Mol. Sci.* **12**, 5908–5945 (2011).
31. Belbruno, J. J. Molecularly Imprinted Polymers. *Chem. Rev.* **119**, 94–119 (2019).
32. Alizadeh, T. & Rezaloo, F. A new chemiresistor sensor based on a blend of

- carbon nanotube, nano-sized molecularly imprinted polymer and poly methyl methacrylate for the selective and sensitive determination of ethanol vapor. *Sensors Actuators, B Chem.* **176**, 28–37 (2013).
33. Ruth, S. R. A. *et al.* Flexible Fringe Effect Capacitive Sensors with Simultaneous High-Performance Contact and Non-Contact Sensing Capabilities. *Small Struct.* **2**, 2000079 (2021).
  34. Keddie, J. L., Meredith, P., Jones, R. A. L. & Donald, A. M. Kinetics of Film Formation in Acrylic Latices Studied with Multiple-Angle-of-Incidence Ellipsometry and Environmental SEM. *Macromolecules* **28**, 2673–2682 (1995).
  35. Li, Z. *et al.* Microscale effects of polymer on wettability alteration in carbonates. *SPE J.* **25**, 1884–1894 (2020).
  36. Chen, W. Y., Jiang, X., Lai, S. N., Peroulis, D. & Stanciu, L. Nanohybrids of a MXene and transition metal dichalcogenide for selective detection of volatile organic compounds. *Nat. Commun.* **11**, 1–10 (2020).
  37. Trudeau, C., Beaupré, P., Bolduc, M. & Cloutier, S. G. All inkjet-printed perovskite-based bolometers. *npj Flex. Electron.* **4**, 1–5 (2020).

## Chapter 5 Conclusion and prospect

### 5.1 Conclusion

Common chemical resistance sensors can be divided into single sensor and sensor array according to the number of interdigital electrodes. Compared with single sensor, sensor array can add new dimensions to the observation, helping to estimate more parameters and improve the estimation performance. However, as the number of sensors in the sensor array increases, the area of the sensor array will also become very large, which is inconvenient for many application fields. In order to make more sensors in a limited area, a multi-layer sensor matrix was fabricated. As shown in Fig. 5.1, compared to the sensor array, the sensor density of the sensor matrix is greatly improved.

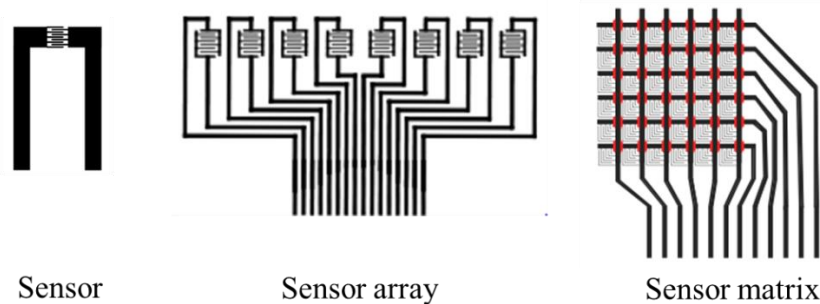


Fig.5.1 A comparison is about sensor, sensor array, and sensor matrix.

This novel stacked structure reduces the number of electrodes required for the measurements significantly and leads to easier sensor integration into an electronic data acquisition card. Additionally, in printed electronics, this stacked structure greatly increases the sensor density per unit area when compared with a single-layer sensor array structure.

### 5.2 Prospect

#### 5.2.1 Smart mask and human activity monitoring

To prevent the global spread of COVID-19, wearing masks during traveling is required by almost all countries. Masks block the droplets released when the wearer talks, coughs, or sneezes, making an essential contribution to slowing the spread of the virus. In addition, masks are necessary for surgeons, infectious disease doctors,

and infectious disease patients and have a wide range of use scenarios. If some intelligent improvements can be made to masks, masks can have more functions<sup>1,2</sup>.

Asthma is a common chronic inflammatory disease of the airways, with common symptoms such as wheezing, coughing, and difficulty breathing. About 300 million people worldwide have asthma, and all countries bear a severe economic burden for asthma-related diseases<sup>3</sup>. Asthma patients are more sensitive to smog weather, too humid or dry air; therefore, they need to wear masks often when they go out. These characteristics of asthma underscore the importance and necessity of continuous respiratory behavior monitoring. Through the constant detection of the breathing behavior of asthma patients, the influence of environmental factors on asthma can be judged according to the onset time and duration. Long-term data accumulation can provide the most appropriate advice to patients to avoid exposure to allergens.



Fig.5.2 The schematic of the smart mask.

In this study, a smart mask that can detect breathing behavior becomes possible by fabricating circuits and sensors on photo paper. The overall diagram of the system is shown in Fig. 5.2. The entire flexible measurement system is placed inside the mask. The system integrates a temperature sensor, humidity sensor, carbon dioxide sensor, and VOCs gas sensor. Through the data of these sensors, the breathing behavior of the person can be analyzed to determine the person's state.

Presently, three behavioral states of sitting, speaking, and fast running can be detected. The data collected by the smart mask can be transmitted to the mobile phone through the Bluetooth module for display and storage. In this experiment, the insulating ink I developed makes the fabrication of multi-layer circuit boards simpler and faster and provides the possibility for developing multi-layer sensors.

### A Design of measurement system

The schematic diagram and PCB (Printed Circuit Board) of the whole measurement system circuitry are designed using Altium Designer 22. Fig.5.3 shows the circuitry block diagram of the system and its interconnections. The circuitry comprises as main electronic components a strong anti-interference, high-speed, and low power consumption microcontroller unit (Shenzhen Guoxin AI Co., Ltd., STC8H1K08) for control and data processing purposes; a sensor matrix driver module including a 4x4 custom-designed sensor matrix for measurement of VOC's gas, two multiplexers (Analog Devices, ADG1608) for switching measurement channel, a Wheatstone bridge circuit for conversion of the resistance signal into the voltage signal, and an amplifier (Texas Instrument, INA337) for increasing measurement accuracy; a CO<sub>2</sub> sensor (Sensirion, SCD40/41) for measurement of CO<sub>2</sub>, temperature, and humidity through I<sup>2</sup>C (Inter-Integrated Circuit); a Bluetooth module for transferring data to mobile App through UART (Universal Asynchronous Receiver/Transmitter).

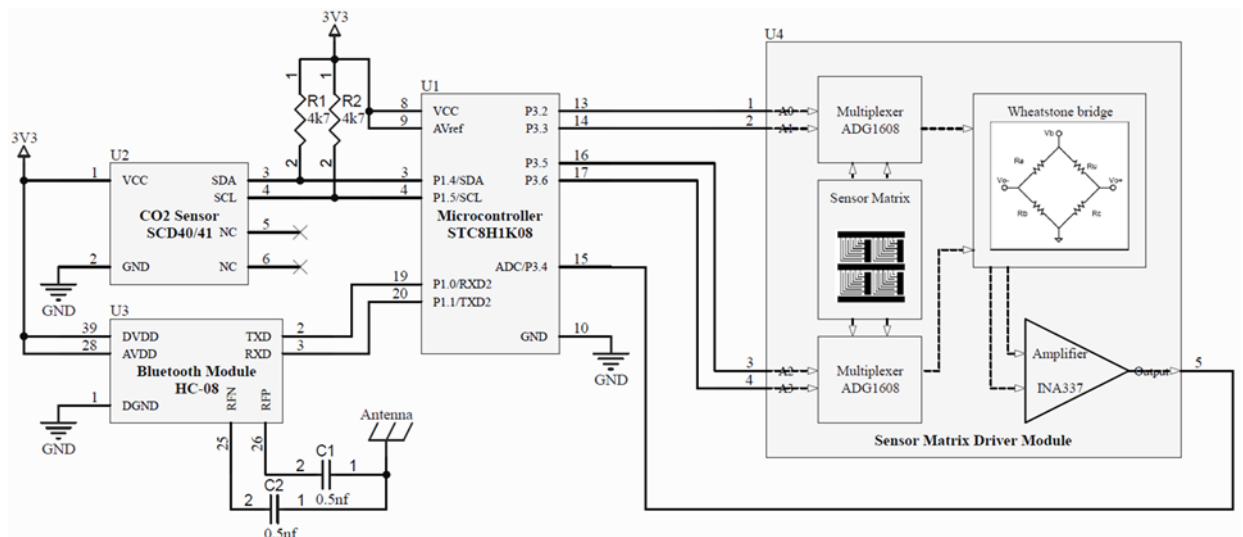


Fig.5.3 The schematic of the measurement circuitry.

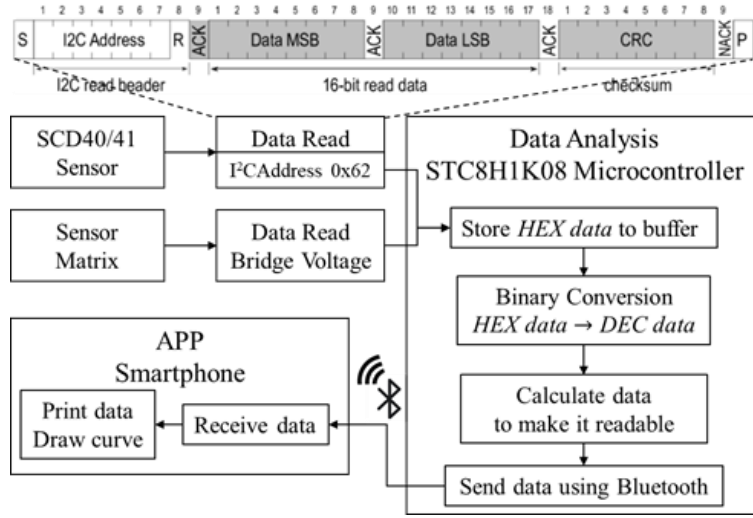


Fig.5.4 The process of data transfer.

The simplified schematic of the algorithm of the microcontroller and custom-designed app is shown in Fig. 5.4. The microcontroller receives the data from the CO<sub>2</sub> sensor and sensor matrix through I<sub>2</sub>C and ADC (Analog to Digital Converter). Data analysis contains main four steps. First, write hexadecimal data to the cache. Next, the data received in real-time is converted from hexadecimal to decimal for computational convenience. After the conversion is completed, different data needs to be calculated separately according to the following formula.

$$CO_2(\text{ppm}) = \text{Hexadecimal} \rightarrow \text{Decimal} \quad (2-1)$$

$$Temp.(^{\circ}C) = -45 + 175 \times \frac{Temp.Hex}{2^{16}-1} \quad (2-2)$$

$$RH(\%) = 100 \times \frac{RH_{Hex}}{2^{16}-1} \quad (2-3)$$

$$V_{Bridge} = \frac{\bar{V}_{BridgeHex}}{2^{10}-1} \times \bar{V}_{CC} \quad (2-4)$$

$$R_{Sensor} = \frac{R_{B2} \times R_{B3} + R_{B3} \times (R_{B1} + R_{B2}) \times \bar{V}_{Bridge} / \bar{V}_{CC}}{R_{B1} - (R_{B1} + R_{B2}) \times \bar{V}_{Bridge} / \bar{V}_{CC}} \quad (2-5)$$

Among them,  $Temp.Hex$  in (2-2),  $RH_{Hex}$  in (2-3), and  $\bar{V}_{BridgeHex}$  in (2-4) are data read by microcontroller;  $\bar{V}_{CC}$  in (2-4) and (2-5) are system voltage values equal to 3.3 volts;  $R_{B1}$ ,  $R_{B2}$ ,  $R_{B3}$  in (2-5) are resistance values of 5.1K, 1K, and 5.1K ohm in Whiston Bridge. Once the data is processed, it is sent to the mobile app via Bluetooth to display and draw curves.

## B Results

The sensor array is printed to evaluate the sensor, and the flexible PCB is made, as shown in Fig. 5.5. I use a blue block to show the custom-designed sensor matrix and

an orange block to show the sensor matrix driver circuit. Put the experimental setup into the mask and measure the human respiration for about 25 minutes, including resting state, talking state, and exercising state.

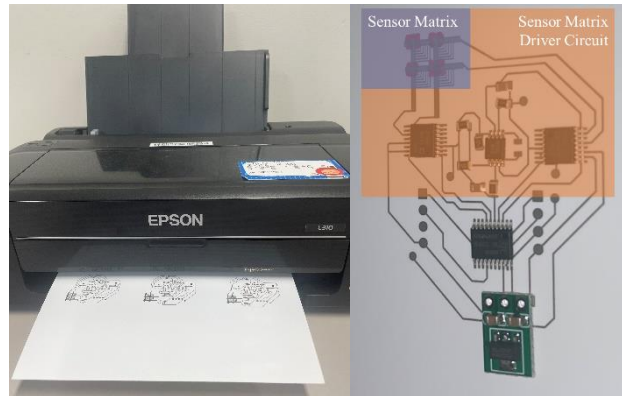


Fig.5.5 Sensor array printing and PCB fabrication.

Fig.5.6 shows the response of CO<sub>2</sub>, Temperature, and Relative Humidity. And Fig.5.7 shows the one channel response of VOCs gas from the sensor matrix. It can be seen from the figure that the CO<sub>2</sub> concentration, VOCs gas concentration, and humidity in the mask are significantly higher than those in the resting state when people are talking. However, during exercise, due to the acceleration of airflow caused by deep breathing, the CO<sub>2</sub> concentration, VOCs gas concentration, and temperature in the mask are slightly lower than those in the speaking state but also higher than those in the resting state.

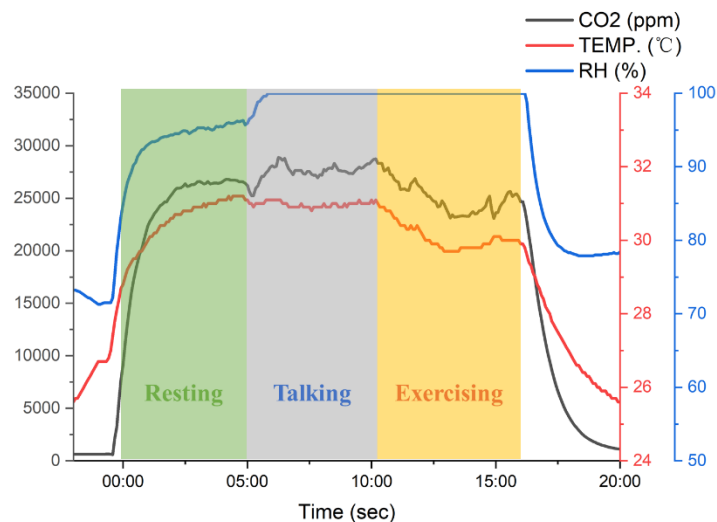


Fig.5.6 The response of CO<sub>2</sub>, Temperature, and Relative Humidity includes three human activity states which use the green, grey and yellow blocks to show.

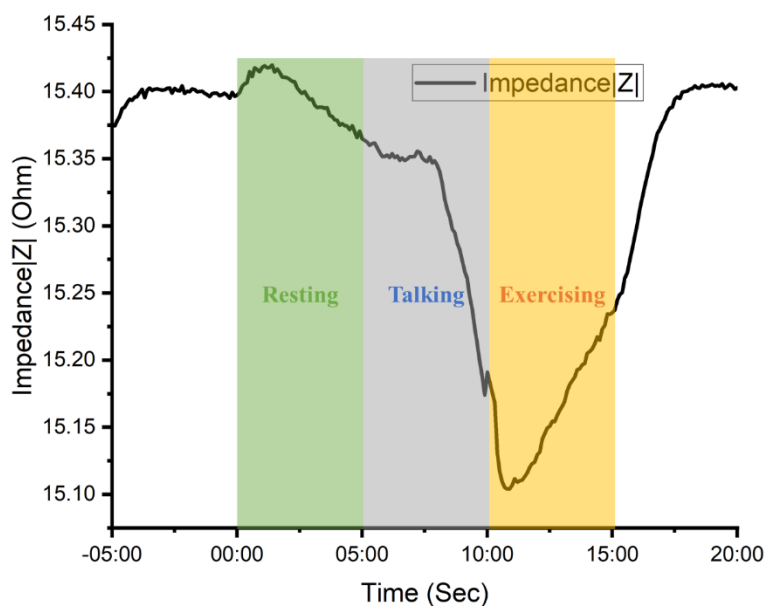


Fig.5.7 The response of the VOCs gas sensor includes three human activity states which use the green, grey, and yellow blocks to show.

### C Conclusion

The existing polymer solution is adjusted so that it can be used to make an insulating layer by inkjet printing. The conductive electrodes can continue to be printed on the insulation layer, making the fabrication of multi-layer sensors and printed circuit boards easier. In this study, temperature and humidity sensors, carbon dioxide sensors, and polymer sensors were added to the masks to detect respiratory behavior to a certain extent. Among them, the homemade polymer sensor has more obvious response strength and is flexible and inexpensive compared with the carbon dioxide module. These functions are expected to be used in future continuous monitoring of asthmatic patients to provide solutions for treating asthmatic patients.

### 5.2.2 Fabrication of multilayer sensor with heating electrode

For polymer gas sensors, the recovery time is longer. By heating the sensor when it needs to recover, the adhesion can be quickly resolved, returning the sensing material to its original state<sup>4</sup>. In addition to this, a certain degree of heating during the detection of gases such as ammonia can improve the sensitivity of the chemical reaction, making the sensor detection more sensitive. I have made it possible to make heater electrodes on the back of the sensor because I have developed insulating coating ink that can be used in inkjet printing. The heaters can be printed on the back of the photo paper or fabricated under the interdigitated electrodes.

Three views of the gas sensor with heater are shown in Fig.5.8.

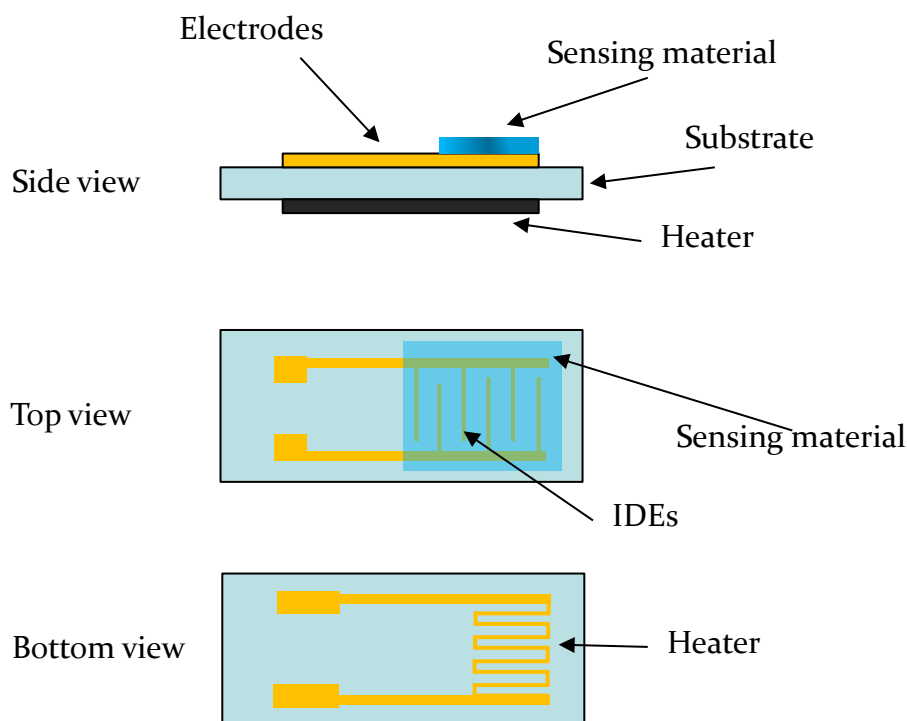


Fig.5.8 Three views of the sensor with heater.

### 5.2.3 Electronic nose based on sensor matrix

Combining increasingly sophisticated inkjet printing technologies with traditional gas-sensitive materials such as polymer semiconductors, metal oxides, carbon nanotubes, and emerging functional materials such as MXene and MOF to create sensing layers is driving the development of sensors toward portability, flexibility, and intelligence. However, current laboratory-developed sensors have been facing selectivity and stability problems with commercially available sensors<sup>5,6</sup>. Although selective materials such as MIP are available to improve the selectivity of sensors, in practice there are many types of gases, and developing MIP materials on a gas-by-gas basis is a less feasible approach. Multivariable sensors are expected to achieve improved selectivity and stability by utilizing a single sensing material with multiple responses to the target gas. Through the combination of multivariate sensors and related data analysis technologies such as machine learning, prediction and judgment of unknown situations can be realized. This cannot only enhance the data processing efficiency of the multivariate sensor, but also make up for the

limitations of the sensor itself.

The size of gas molecules, the permeability of gas molecules, and the physical adsorption capacity are different. I can control the thickness of the sensing film by adjusting the number of prints, and the concentration of carbon black and the type of polymer by adjusting the color of the print pattern. The combination of multiple ink preparations and a home printer allows for the creation of multi-channel sensors. The characteristics of the sensing film can be changed by controlling the difference in temperature of each channel. Combined with pattern recognition technology, miniaturized electronic noses can be produced.

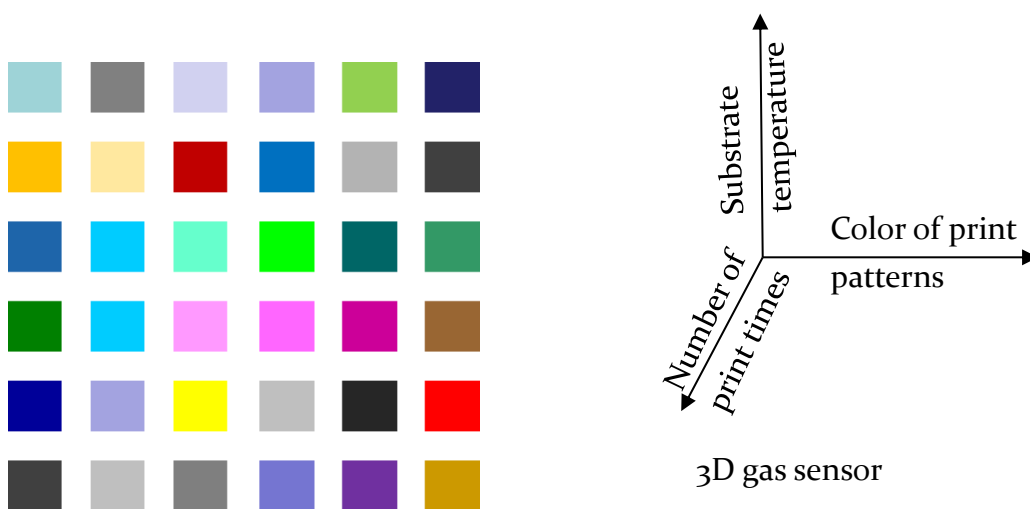


Fig.5.9 Schematic representation of the sensor matrix coated with different sensing materials and schematic diagram of the realization method of 3D gas sensor.

## Reference

1. Escobedo, P. *et al.* Smart facemask for wireless CO<sub>2</sub> monitoring. *Nature Communications* **13**, (2022).
2. Chen, A. *et al.* Wireless Wearable Ultrasound Sensor on a Paper Substrate to Characterize Respiratory Behavior. *ACS Sensors* **4**, 944–952 (2019).
3. Pitrez, P. M. C., Stein, R. T. & Martinez, F. D. The Global Burden of Asthma. *Pediatric Respiratory Medicine* **130**, 779–781 (2008).
4. Arshak, K., Moore, E., Lyons, G. M., Harris, J. & Clifford, S. A review of gas sensors employed in electronic nose applications. *Sensor Review* **24**, 181–198 (2004).
5. Lin, Y. *et al.* Printable Fabrication of a Fully Integrated and Self-Powered Sensor System on Plastic Substrates. *Advanced Materials* **31**, 1–9 (2019).
6. Dai, J. *et al.* Printed gas sensors. *Chemical Society Reviews* **49**, 1756–1789 (2020).

## Acknowledgements

I come from a remote and economically underdeveloped area of China. Since I have a younger brother and sister making family expenses relatively large, and my parents also only have elementary school education, resulting in parents no matter how hard they work, the income is very limited. I don't really believe I had the opportunity to study abroad and complete the relevant research during my PhD until now. The successful completion of my studies was partly the result of my own efforts, and partly the help from my professors and some friends.

First of all, I would like to appreciate my supervisor Prof. Kenshi Hayashi. I first met Prof. Kenshi Hayashi in March 2017 when he was invited by our undergraduate university to give a presentation on sensor related. I was deeply interested in the content of Prof. Kenshi Hayashi's report and took the initiative to get in touch with him. During my conversation with Prof. Kenshi Hayashi, I found him to be a very kind and enthusiastic professor, which made me determined to come to Japan to study.

Since I came to Japan, my English and Japanese skills were not very good, so I did not have a good time communicating with the Prof. Kenshi Hayashi at first. When Prof. Kenshi Hayashi introduced the sensor-related knowledge, if I didn't understand, he would often draw the diagram of the sensor to make me understand faster, which was very helpful to me. Despite being very busy, Prof. Kenshi Hayashi was still willing to spend a lot of time to guide my research, which made me very touched. Prof. Kenshi Hayashi not only gave me a lot of guidance in my research, but also gave me a lot of freedom in my time, which helped me a lot in my life in Japan and my future career planning.

Secondly, I am very grateful to my PhD thesis reviewers, Professors Yuji Oki and Junya Suehiro. They are experts in this field of inkjet printing and materials, and gave me a lot of valuable advice on revising my thesis. Even though they were very busy, they still read my thesis very carefully, which greatly improved the quality of my PhD thesis.

Thirdly, I sincerely appreciate Prof. Bin Chen who graduated from Hayashi lab. She was my undergraduate advisor, took me into scientific research, and introduced me to Prof. Kenshi Hayashi. During my Ph.D., Prof. Bin Chen worked as a researcher in Japan for two years. In the past two years, I often do experiments and chat together, making my research life full of joy.

Fourthly, I would like to give my thanks to Miss Maiko Moribe and Mr. Kaneko

Shigeru. Miss Maiko Moribe is the secretary and Mr. Kaneko Shigeru is the research assistant in our laboratory. They have given me a lot of help in my study and life. In particular, I am going through various procedures such as admission procedures, identity change procedures and phone card cancellation, etc. These seemingly simple things are very troublesome for a foreigner to deal with. Without their help, my research and life would not have gone so smoothly.

And I would like to express my grateful gratitude to Prof. Chuanjun Liu and Prof. Fumihiro Sassa for the precious advices in my research. Prof. Chuanjun Liu was a former assistant professor in our laboratory and now works for U.S.E company. Since my research topic is very similar to the research content of Prof. Chuanjun Liu's work, I often discussed some research problems with him and gave very valuable suggestions. Prof. Fumihiro Sassa has given me a lot of corrections and guidance on my manuscript for academic conferences and my slides for presentation. After each academic conference, he would help me to record the questions of others for my later revision and study, which helped me a lot.

I am very grateful to student members of Hayashi lab. They are very outgoing and fun, and doing research with them makes boring experiments interesting, and I treasure the time I spend with them.

At last, I am thankful for my roommates, we lived together for 5 years. Any difficulties or unhappiness during this time were spent together. This period of study abroad has been a valuable experience in my life, and I would like to thank once again the people who helped me during my study abroad.